Mechanistic Investigation of Coordinated Conformational Changes in Multisubunit Ion Channels and Enzymes

by

Kee-Hyun Choi

M.S. Chemistry
Korea University, 2001

Submitted to the Department of Chemistry
in Partial Fulfillment of the Requirements for the Degree of

Doctor of Philosophy in Biological Chemistry

at the
MASSACHUSETTS INSTITUTE OF TECHNOLOGY

February 2008

© 2008 Massachusetts Institute of Technology
All Rights Reserved

The author hereby grants to MIT permission to reproduce and to distribute publicly paper and electronic copies of this thesis document in whole or in part.

Signature of Author: _____
Department of Chemistry
November 13, 2007

Certified by: _____
Professor Stuart S. Licht
Thesis Supervisor

Accepted by: _____
Professor Robert W. Field
Chairman, Department Committee on Graduate Students

MASSACHUSETTS INSTITUTE OF TECHNOLOGY
MAR 2 5 2008
LIBRARIES

ARCHIVES

This doctoral thesis has been examined by a Committee of the Department of Chemistry as follows:

John M. Essigmann _____
William R. and Betsy P. Leitch Professor of Chemistry and Biological Engineering
Committee Chair

Stuart S. Licht _____
Samuel A. Goldblith Career Development Assistant Professor of Chemistry
Thesis Supervisor

Arup K. Chakraborty _____
Robert T. Haslam Professor of Chemical Engineering, Professor of Chemistry and
Professor of Biological Engineering

For My Parents

Mechanistic Investigation of Coordinated Conformational Changes in Multisubunit Ion Channels and Enzymes

by
Kee-Hyun Choi

Submitted to the Department of Chemistry on November 13, 2007
in Partial Fulfillment of the Requirements for the Degree of
Doctor of Philosophy in Biological Chemistry

ABSTRACT

Many enzymes and ion channels consist of multiple subunits and/or multiple distinct functional components. Coordinated conformational changes through allosteric interactions between subunits and/or between functional units can efficiently regulate protein activity. This dissertation describes investigations of coordinated conformational changes in two systems: the ATP-sensitive potassium (K_{ATP}) channel and the ATP-dependent bacterial protease, ClpAP.

K_{ATP} channels consist of two protein subunits: a pore-forming subunit, Kir6.2 and a regulatory subunit, SUR1. Kir6.2 is an inwardly rectifying potassium channel, and SUR1 belongs to the ATP-binding cassette (ABC) superfamily. Using patch clamp techniques, K_{ATP} channel activity was observed directly with single-channel resolution. The results indicate that noise from stochastic channel gating is significantly reduced compared to what would be observed for identical and independent channels, and provide evidence that negatively cooperative interactions between neighboring K_{ATP} channels are the source of the noise reduction. Simulations further suggest that negative coupling among K_{ATP} channels in pancreatic beta cells could be important for reliable signal transduction.

Energetic coupling between Kir6.2 and SUR1 subunits was also investigated. Single-channel records were analyzed to detect the violations of microscopic reversibility in channel gating that would occur if Kir6.2 conformational transitions were driven by the energy from ATP hydrolysis by SUR1. Although no violations of detailed balance in channel gating are detected on the time scale where ATP hydrolysis takes place, unexpected non-equilibrium gating is observed on longer time scales. These results imply that channel gating is coupled to non-equilibrium processes other than ATP hydrolysis by SUR1.

The second system studied for coordinated conformational change was ClpAP. ClpAP is composed of an ATPase, ClpA and a serine peptidase, ClpP. ClpA uses the free energy of ATP hydrolysis to unfold protein substrates and translocate them to ClpP, which proteolyzes them. To investigate how protein translocation by ClpA is coupled to proteolysis by ClpP, size distributions of peptide products were measured. The observation of non-exponential size distributions, in combination with simulations predicting how different mechanisms would influence the size distribution, supports the hypothesis that peptide product sizes are controlled by coordinated conformational changes of ClpA and ClpP.

Thesis Supervisor: Stuart S. Licht
Title: Samuel A. Goldblith Career Development Assistant Professor of Chemistry

TABLE OF CONTENTS

Chapter 1

Coordinated Conformational Changes of Multiprotein Complexes

1.1. Introduction

Many proteins are composed of multiple functional components. In particular, ATPases form diverse multiprotein complexes with a wide range of proteins such as other enzymes or ion channel proteins. The conformational cycles of ATPases driven by ATP hydrolysis can be coupled to conformational changes of other functional components. Such allosteric interactions between ATPases and other components within multiprotein complexes are important in protein activity regulation.

The AAA+ (ATPases associated with various cellular activities) family is a well-studied class of ATPases that appear in multiprotein complexes. Several review papers on AAA+ proteins provide a good overview of how ATPases work with other protein components as functional units and how coordinated conformational changes within multiprotein complexes regulate protein activity (1, 2). Complexes of ATPases and peptidases have been extensively investigated in *E. coli* (3). Bacterial ATPases such as ClpA and ClpX unfold their protein substrates and translocate them into the chamber of serine peptidases, such as ClpP, where the target proteins are hydrolyzed. ClpA and related ATPases undergo ATP hydrolysis-driven conformational changes, which are critical for unfolding and translocating the protein substrates. Without association with ClpA or ClpX, ClpP can only hydrolyze small peptide substrates.

The ATP-binding cassette (ABC) superfamily is another ATPase family where ATP hydrolysis-driven conformational changes are directly involved in protein functions (4, 5). Although most ABC proteins are active membrane transporters that carry small molecules across the cell membrane using the free energy of ATP hydrolysis, the sulfonylurea receptor (SUR), a unique ABC transporter in mammals, works with ion channel proteins as a functional unit (6). A major role of SUR in multiprotein complexes is in regulating ion channel activities, rather than transporting molecules. Conformational changes of SUR are controlled by ATP hydrolysis, presumably coordinated with conformational changes of ion channel proteins in the complex. However, the mechanism is unclear.

Conformational changes of multiprotein complexes could be also coordinated with those of neighboring complexes in the clusters that integral membrane proteins often form. Studies on allosteric regulation among membrane protein complexes in clusters, however, have been rarely reviewed, even though evidence of protein-protein interactions in these systems continues to grow, and the physiological significance of these interactions has been recognized. Previous work on interactions between clustered ion channel proteins is reviewed in this chapter: coordinated conformational changes between ion channels are discussed, mainly focusing on electrophysiological studies.

1.2. Coupled gating of ion channels

Regulation of transmembrane potential is a central part of cellular signaling pathways in excitable cells (7). Ion channel proteins play an essential role in electrical signaling since they control transmembrane potential by allowing permeation of ions across the cell membrane. To achieve rapid changes in transmembrane potential, ion channels utilize conformational changes, switching between a closed (non-conducting) state and an open (conducting) state in a signal-dependent manner. Conformational transitions of ion channels can be directly monitored in single-channel records using patch-clamp techniques (8). Because the channel opening/closing transitions are too fast to be resolved with the limited bandwidth of current techniques, only two discrete conformations (open and closed states) are observed in single-channel recordings.

In most cases, individual ion channels gate independently. Consequently, independent channel gating is often implicitly assumed in the statistical analysis of ion channel data. However, channel-channel interactions, i.e. the gating of one channel directly coupled to the gating of neighboring channels, have been observed at the single-channel level for a number of systems (9-25). The physiological significance of cooperative channel gating in signal transduction has been recognized in *in vivo* studies of several systems (26-29) although the molecular mechanisms by which such coupling between neighboring channels takes place still remain mostly unclear. Also, existing single-channel analysis methods to detect coupled gating are limited, necessitating the development of more explicit and easily-implemented methods.

1.3. Physiological functions of cooperativity

1.3.1. Positive cooperativity

Positively coupled gating, in which one channel is more likely to be open when the other channel is open than when it is closed, could serve as a strategy to enhance ion channel-mediated signaling in response to the cellular signals. In particular, positive cooperativity in the central nervous systems might be important for long-term potentiation, a cellular mechanism of synaptic strengthening for learning and memory. Cooperativity of α-amino-3-hydroxy-5-methylisoxazole-4-propionic acid (AMPA) receptors and *N*-methyl-D-aspartate (NMDA) receptors has been investigated to elucidate an underlying mechanism for long-term potentiation in the hippocampus (30, 31).

Cooperative gating of ryanodine receptors (RyRs), Ca^{2+} channels in rat cardiac myocytes has been shown to alter dynamic patterns of intracellular Ca^{2+} concentrations, such as Ca^{2+} spark duration, amplitude and frequency (27, 29), which is likely to influence Ca^{2+} signaling. Positively coupled gating between RyRs in cardiac muscle was also proposed as a mechanism for the termination of Ca^{2+} release (17). In this mechanism, the simultaneous channel closing reduces stochastic channel reactivation that would otherwise occur due to Ca^{2+} passing through neighboring channels.

Recently, cooperativity of voltage-gated Na^+ channels was suggested as an underlying mechanism for a rapid initiation of action potentials observed in cortical neurons (28). This abrupt initial rising phase was not described by the Hodgkin-Huxley model (7) that assumes independent channel gating. However, positive cooperativity among Na^+ channels accounts for the observed action potentials. Effects of positive coupling between neighboring Na^+ channels on action potentials were confirmed by computational modeling as well as *in vitro* experiments where the action potential initiation observed *in vivo* was reproduced by reducing the density of available Na^+ channels by applying tetrodotoxin, a Na^+ channel specific toxin. However, other alternative mechanisms are not excluded; an abrupt initiation of the action potential was also well-described by the modified Hodgkin-Huxley model that includes variability in

subthreshold potentials over the cortical neuronal membrane but not cooperativity between Na^+ channels (32).

1.3.2. Control of physiological noise due to channel gating: a possible physiological function for negative cooperativity

Negative coupling, i.e. an open state of one channel disfavors opening of the other channel, may effectively reduce channel gating noise produced by stochastic transitions between channel open and closed states. Random fluctuations in the number of open channels have been shown to be a dominant electrical noise source in excitable cells, affecting the membrane potential (33-35). The effects of gating noise from voltage-gated Na^+ and K^+ channels on action potentials in neurons have been extensively studied theoretically and experimentally (33-39). Membrane potential fluctuations generated by stochastic channel gating limit the reliability of neuronal responses to stimuli by altering neuronal dynamics, such as firing frequency and timing (35-39).

In a recent study (26), it was shown the stochastic gating of hyperpolarization-activated cation (I_h) channels in pyramidal neuron dendrites contributes to fluctuations in membrane potential, thereby damaging action potential fidelity: a 100-fold decrease in the ability to detect a signal and the temporal precision of firing. The small single-channel conductance of I_h channels (~0.7 pS) was suggested to play a role in reducing membrane noise from stochastic gating for reliable neuronal functions. However, minimizing gating noise through negative cooperativity between neighboring channels would be a more general and efficient way for reliable signal transduction in noisy cellular environments.

Although cooperative gating would possibly play a physiologically important role in other systems, it is challenging to study *in vivo* effects of channel coupling because the large numbers of proteins are involved in regulating/modulating channel activity inside the cells.

1.4. Electrophysiological evidence for gating cooperativity

Channel cooperativity has been found in patch-clamp studies of diverse channel types. Positively coupled gating has been reported in many types of ligand-gated channels: AMPA receptors (21, 22), RyRs (15, 17, 18), nicotinic acetylcholine receptors (nAChRs) (14, 23, 24), 1,4-dihydropyridine receptors (DHPRs) (12), $P2X_2$ receptors (11), and hyperpolarization-activated cyclic nucleotide-gated cation (HCN) pacemaker channels (10). In addition, bacterial voltage-gated K^+ channels (KcsA) (19) and gap junction channels (9, 16, 25) are other examples of positively coupled gating.

In contrast to positive coupling, negative coupling has been rarely observed in electrophysiological studies. Batrachotoxin-modified Na^+ channels are one example of negative coupling (13). Negative cooperativity was also observed in Na^+ channels in the nodal membrane of frog nerve fibers (20).

1.5. Analysis methods for cooperative gating

1.5.1. Binomial analysis

Once synchronous open/closed transitions are observed, which is highly suggestive of cooperativity, a binomial analysis on current amplitude histograms (distribution of the current levels) is an appropriate first step in test for gating cooperativity. The observed distributions of current amplitudes are compared with those predicted for independent channels, i.e., the binomial distributions. Deviations from a binomial distribution are indicative of cooperative gating; positive deviations (i.e., more simultaneous openings than expected from independent channel gating) are consistent with positive coupling, while negative deviations are consistent with negative cooperativity.

Positive deviations from a binomial distribution have been observed in reconstituted AMPA receptors from rat brain (21, 22), RyRs reconstituted into artificial lipid bilayers (15), native RyRs from both skeletal muscle and cardiac muscle (17, 18), nAChRs from embryonic chick myotubes (14), *Torpedo* nAChRs reconstituted in planar membranes (24), purified skeletal muscle DHPRs in planar lipid bilayers (12), mammalian $P2X_2$ receptors expressed in *Xenopus* oocytes (11), purified KcsA in giant liposomes (19), recombinant chick connexin45 gap junction channels (25), and native gap junction channels both from embryonic chick heart and from the earthworm axon septal membranes (9, 16). Negative deviations have been found in batrachotoxin-modified Na^+ channels in hybrid neuroblastoma NG108-15 cells (13).

Three assumptions must be made to interpret a binomial analysis in terms of cooperative interactions: that the channel record is stationary (i.e., no global changes in channel activity within a given record length), that the number of channels is correctly estimated, and that the channels are identical (40). If the channels do not have identical open probabilities, the observed variance will be less than the predicted variance for identical channels (41). A similar problem arises if channels are non-stationary and are varying on a timescale slower than the timescale of the recording since these channels will also appear non-identical. Finally, since the variance is linearly proportional to the

number of channels for the binomial distribution, an incorrect estimate of the number of channels will lead to an incorrect prediction for the variance.

The necessity for these assumptions often leads to complications in interpretations of the results from this method of analysis. First, reliable estimation of the number of channels in a patch is not always straightforward. This is likely the case when one estimates the number of active channels in the patch using the maximum number of simultaneous openings observed in channels with a low open probability. In this case, the number of channels in a patch is likely to be underestimated, resulting in an overestimation of positive deviations from the binomial distribution. In addition, non-identical but independent channels (independent channels with different open probabilities) show apparent negative deviations from a binomial distribution and are not distinguishable from negatively coupled channels are not distinguishable by a binomial analysis alone. Thus, binomial tests are often suggestive but not conclusive in the cases of both positive and negative cooperativity.

1.5.2. Variance analysis

Variance analysis is another way to detect cooperative gating (42). A mean-variance plot can be obtained by calculating the variance of the macroscopic current as a function of the mean current. The unitary current passed by one channel (single-channel current) can be estimated from the initial slope of a mean-variance plot based on the binomial theorem (42). If channels gate independently, the unitary current calculated from the initial slope of a mean-variance plot will be the same as the single-channel current. However, when channels are positively coupled, synchronous channel open/closed events will generate higher fluctuations in the mean macroscopic currents than those expected from independent channels. For negatively coupled channels, simultaneous opening/closing transitions are suppressed, generating lower fluctuations. Thus, the estimated unitary current from coupled channels will deviate from the single-channel current; positive cooperativity will increase the estimated unitary current whereas negative cooperativity will decrease it. More generally, when the experimentally

obtained variance in a mean-variance plot is higher or lower than expected from independent channel, these channels are not independent (43).

Mammalian HCN2 channels heterologously expressed in HEK-293 cells showed a larger unitary current calculated from variance analysis than expected from the single-channel current, suggesting positive cooperativity between neighboring channels (10). Variance analysis has also shown Na^+ channels in the nodal membrane of frog nerve fibers are negatively coupled (20).

However, a variance analysis has the same complications as a binomial analysis does, because it is also a binomial theorem-based method. In addition, steady-state (equilibrium) analyses like binomial and variance analyses do not include information about the kinetics of channel gating. Collective behaviors of coupled channels can be revealed in the kinetics of channel gating. Kinetic analysis can provide evidence for or against cooperativity in channel conformational transitions. Therefore, a further kinetic analysis of channel gating is often necessary to confirm coupled gating.

1.5.3. Conditional dwell-time density analysis

Although several ways to analyze gating kinetics to detect cooperativity between neighboring channels have been proposed (11, 13-15, 44, 45), they share a common basis: determining whether the dwell-time density of one channel is conditional on the other channel being either open or closed. Independent channels will have identical conditional dwell-time densities. In the case of coupled channels, however, the two conditional dwell-time densities will not be the same. For example, when the two interacting channels are present, the closed-time and/or open-time densities of one channel will depend on whether the other channel is open or closed. If channels are positively coupled, the opening rate will increase and/or the closing rate will decrease when neighboring channels are open. For negatively coupled channels, the presence of neighboring open channels will decrease the opening rate and/or increase the closing rate. Similarly, the channel opening and/or closing rates can be influenced by the closed state

of neighboring channels. That is, in the presence of neighboring closed channels, the opening rate will decrease and/or the closing rate will increase for positively cooperative channels, whereas the opening rate will increase and/or the closing rate will decease for negatively cooperative channels.

Experimental records obtained from embryonic chick myotube nAChRs showed that open-time densities are identical whether the neighboring channel is open or closed (14). However, closed-time densities showed that the mean closed time of one channel is longer when the other channel is closed than when it is open, suggesting positive interactions between neighboring channels affect channel opening but not channel closing. Similar results have been also found in RyRs reconstituted into artificial lipid bilayers (15). The opening rates were faster in the presence of open channels than in the absence of open channels, suggesting that channel opening depends on the presence of other open channels, i.e., positive coupling. Non-independent gating of $P2X_2$ receptors expressed in *Xenopus* oocytes was also studied using this kinetic analysis (11). The mean open time from single-channel patches is shorter than that from multichannel patches, suggesting the closing rate is influenced by positive interchannel interactions. The conditional dwell-time density analysis was also used to detect negative interactions between the two batrachotoxin-modified Na^+ channels (13). The existence of multiple closed states made the opening rate difficult to determine unambiguously; therefore, only the closing rate was calculated when the other channel was open and closed. The closing rates were identical in both cases, implying that negative interactions might influence the opening rate.

One clear advantage of this analysis over the previous studies is that one can get more mechanistic information about the coupling mechanism. The opening or closing transitions affected by channel-channel interactions can be identified by detecting any alteration of conditional open/closed time densities. However, conditional dwell-time analysis is not easy to implement. In particular, when more than two channels are present, more combinations of conditional dwell-time densities are generated, which makes this analysis more complicated. Finite length of records also limits the power of this analysis, because the number of dwells may be insufficient to generate statistically reliable dwell-

time densities. Clearly, this problem will be serious when multiple channels with a low open probability are present, because there will be a small number of multiple events. Finally, this analysis compares the mean open and closed times, i.e., mean closing and opening rates. However, more than one type of open/closed transition are likely to be present in a real gating mechanism. Thus, when the specific opening or closing transitions influenced by channel coupling are buried in all-point dwell-time densities, they might not be detectable and/or identifiable.

1.5.4. Maximum likelihood fitting analysis

Non-independent gating can be detected using a maximum likelihood fitting analysis with independent and cooperative models (11). When channels are independent, the channel opening and closing rates are not affected by whether the neighboring channels are open or closed. In a two-independent-channel system, for example, the opening rate from the two-channel closed state to the one-channel open state (k_{CO1}) is simply twice as fast as that from the one-channel open state to the two-channel open state (k_{O1O2}), i.e, $k_{CO1} = 2k_{O1O2}$. The closing rate from the two-channel open state to the one-channel open state (k_{O2O1}) is also twice as fast as that from the one-channel open state to the two-channel closed state (k_{O1C}), i.e, $k_{O2O1} = 2k_{O1C}$. Single-channel data can be fitted with the rate constraints ($k_{CO1} = 2k_{O1O2}$ and $k_{O2O1} = 2k_{O1C}$; independent model) and without those constraints (cooperative model). Using a maximum likelihood ratio test, the kinetic model that describes the experimental data better can be determined. This analysis was applied to single-channel records obtained from $P2X_2$ receptors expressed in *Xenopus* oocytes (11). The cooperative model fits $P2X_2$ receptor recordings better than the independent model, suggesting channel cooperativity. However, the maximum likelihood fitting method is model-dependent, which often causes ambiguity in results from data fitting due to the complex underlying kinetic mechanisms of channel gating.

1.6. Channel clustering

Colocalization of channels is prerequisite for functional channel coupling. Indeed, channel clustering has been observed in most ion channels where cooperative gating is observed, although the physical mechanisms of channel assembly mostly remain unclear.

1.6.1. Channel assembly *in vitro*

To detect physically assembled channels, analytical ultracentrifugation sedimentation velocity studies and native SDS-PAGE/Western blots can be used. Species with higher retention on native SDS-PAGE gels and higher sedimentation coefficients than the functional channel units are expected if the channels are clustered. These biochemical assays were carried out with purified KcsA channels, revealing the existence of KcsA supramolecular assemblies (19). Physically associated pairs of RyRs from skeletal and cardiac muscle were also observed in sucrose gradient centrifugation experiments and immunoblot analyses (17, 18). As another example, *Torpedo* nAChRs were purified as a mixture of monomers and dimers, which was evident in sucrose gradient experiments (24).

In vitro biochemical assays, however, are limited to channel proteins whose purifications are possible in large quantity and whose physical interactions are strong even under detergent-solublized conditions. Also, if other endogenous cellular molecules are involved in channel clustering, channel assemblies will not be detected with purified channel proteins alone.

1.6.2. Subcellular channel localization

Localization of HCN4 channels in caveolae, a membrane subdomain, was detected in rabbit sinoatrial (SAN) cells (46). Western blot analysis with caveolae isolated from SAN cells using discontinuous sucrose gradients provided the evidence of HCN4 channel localization. Chemical disruption of caveolae impaired HCN4

localization, affecting HCN4 channel kinetics. Freeze/fracture electron microscopy studies have revealed that gap junction channels aggregate into clusters in liver cells and earthworm septa (47, 48). RyR clusters in skeletal and cardiac muscle sarcoplasmic reticulum have been also observed *in situ* by electron microscopy (49-52).

1.6.3. Stimulation-induced channel clustering

Dimerization of *Torpedo* nAChRs in the postsynaptic membrane was transiently induced during synaptic stimulation (53). Changes in the populations of monomeric and dimeric AChRs as a result of electrical stimulus were observed *in situ* using rapid-freezing/cryofracture techniques. Intact electric organ tissues from *Torpedo* were rapidly frozen in the absence and presence of an electrical stimulus, fractured, and then observed using an electron microscope. Monomeric nAChRs (globular form, 9 nm in diameter) were the primary form found in the freeze-fracture replicas of unstimulated membranes. Following a single nerve impulse, however, nAChR dimers (elongated form, 18 nm in diameter) were momentarily formed; the decrease in the number of monomers was twice the increase in the number of dimers. The time course of an abrupt change in nAChR ultrastructures was comparable with that of the fast transient postsynaptic current evoked by the electric signal, implying that channel assemblies are associated with channel activation.

The inositol 1,4,5-triphosphate receptor (IP_3R), a ligand-gated Ca^{2+} channel is another example of stimulation-induced channel clustering (54). IP_3R in the endoplasmic reticulum (ER) membrane releases Ca^{2+} from the ER to cytoplasm upon IP_3 binding. Green fluorescence protein-fused IP_3Rs (GFP-IP_3Rs) expressed in COS-7 cells were assembled into clusters following application of IP_3-generating agents, which implies that IP_3-stimulation induces a channel conformational change to the open state, thereby initiating channel clustering. This hypothesis was further tested using mutant IP_3R channels that impair either IP_3 binding or channel activity without affecting ligand binding ability. Both IP_3R mutants failed to form clusters, supporting that ligand-stimulated channel conformational transitions are required for channel clustering.

1.6.4. Direct channel cross-linking

The direct evidence between physical channel linkage and coupled gating has been observed in RyRs (17, 18), AMPA receptors (21) and the cystic fibrosis transmembrane conductance regulator (CFTR), a Cl^- channel (55). Purified RyRs reconstituted in lipid bilayers exhibited coupled gating, which required FK506 binding protein, FKBP 12 and FKBP 12.6 for skeleton muscle and cardiac muscle type RyRs, respectively (17, 18). In addition, AMPA receptors isolated from rat brain showed positive cooperativity induced by dextran sulfate, a mimic of sulfated polysaccharides in synapses (21). Heparin, a synaptic polysaccharide, has been shown to modulate channel activities of AMPA receptors by linking them physically (56). Addition of dextran sulfate promoted simultaneous openings and closings of AMPA receptors, whose positive coupling was confirmed by a binomial analysis.

Lastly, interactions between CFTRs heterologously expressed in HEK-293 cells were facilitated by a multivalent CFTR binding protein, CAP70 (55). CAP70 linked CFTR channels by binding to the cytoplasmic C-terminus of CFTR through its four PDZ domains, stimulating the CFTR channel activity. Correlated physical and functional coupling between CFTRs was further tested using a bivalent monoclonal antibody that specifically recognizes the C-terminal residues of CFTR. Two CFTRs linked by a bivalent antibody also exhibited increased channel activity. CFTR current amplitude histograms became positively deviated from a binomial distribution upon addition of antibodies, indicating that positive coupling was induced by linking neighboring channels. However, it is not clear whether CFTR channel activation induced by CAP70 resulted from coupled gating, because no tests for cooperativity were carried out. The Na^+/H^+ exchanger regulatory factor (NHE-RF) was also shown to mediate CFTR channel interactions by cross-linking the C-terminal tails of CFTRs endogenously expressed in Calu-3 cells, increasing the CFTR channel activity (57). In this case, however, the gating was uncorrelated both before and after stimulation based on a binomial analysis even though multiple CFTR channels were simultaneously activated by NHE-RF.

1.7. Molecular basis of channel coupling

Although functional coupling correlated with physical clustering has been reported for several ion channels (17, 18, 21, 55), physical clustering of channels will not necessarily affect channel gating. Additional steps are required to link channel clustering to functional coupling that affects channel gating. Several molecular mechanisms have been proposed to account for coupled gating of multiple channels.

1.7.1. Permeant ions as a channel coupling mediator

One possible mechanism is that channels sense fluctuating local concentrations of permeant ions. Regulation of clustered Ca^{2+} channels by Ca^{2+}, its permeant ion has been studied in two types of Ca^{2+} channels (15, 58).

Ca^{2+}-mediated cooperative gating was proposed as a coupling mechanism for RyRs that release Ca^{2+} from the sarcoplasmic reticulum (SR) (15). The positive coupling between skeletal RyRs in lipid bilayers was dependent on luminal Ca^{2+} concentrations. Increased luminal Ca^{2+} concentrations resulted in increasing cytoplasmic Ca^{2+} via RyR channel openings, thereby simultaneously activating RyR channels through Ca^{2+} binding to the cytoplasmic activation sites of RyRs. The degree of positive coupling, defined as the difference between the channel opening rates in the absence and the presence of neighboring open channels, was decreased by reducing the luminal Ca^{2+} concentration. The dependency of coupled gating on luminal Ca^{2+} concentration suggests that sufficient luminal Ca^{2+} permeating one channel is necessary to diffuse from the pore so as to activate neighboring channels. Cooperative channel gating through luminal Ca^{2+} was abolished when the activation sites were saturated with cytoplasmic Ca^{2+} or when the Ca^{2+} flow was reversed (from the cytoplasm to the SR lumen) by applying a potential of opposite sign across the bilayer. Taken together, these results indicate that luminal Ca^{2+} induces coupled gating by increasing local cytoplasmic Ca^{2+} concentration that activates neighboring channels simultaneously.

A channel coupling process via Ca^{2+} influx through open channels was also observed for 1,4-dihydropyridine receptors (DHPRs) (58). Inactivation of DHPRs by prior Ca^{2+} influx has been shown to be an intrinsic negative feedback process that does not require cooperative interactions. However, the DHPR inactivation rate observed in two-channel patches from guinea pig ventricular myocytes was faster then that observed in one-channel patches, indicating the existence of interchannel interactions. Two-channel patches that contain one active and one inactive channel showed a reduced inactivation rate, indicating that Ca^{2+} influx from both channels are required for the inhibitory coupling rather than physical association of adjacent channels. When BAPTA (1,2-bis-(2-aminophenoxy)ethane-*N*,*N*,*N'*,*N'*-tetraacetic acid), a Ca^{2+} chelator, was applied into the cytoplasm, the inactivation process in two-channel patches slowed down more than that from one-channel patches, suggesting that Ca^{2+} mediates the interaction among DHPRs. Based on these results, two cytoplasmic Ca^{2+} inhibition sites were proposed: one located near to the pore and the other more distant from the pore. An inhibition site near the pore mediates Ca^{2+}-sensitive inactivation by Ca^{2+} flow through its own pore, accounting for channel inactivation even when bulk cytoplasmic Ca^{2+} was chelated. In contrast, the site distant from the pore is involved in coupled inhibition through local Ca^{2+} influx within overlapping domains of neighboring channels, which was diminished by Ca^{2+} chelators. Therefore, the inhibitory coupling between DHPRs arises from a shared and localized Ca^{2+} diffusion space from adjacent channels.

1.7.2. Concerted channel activation through the membrane

Interactions mediated by the cell membrane in which the channels are embedded provide another possible physical mechanism for coupled gating. In case of mechanosensitive (MS) channels, channel activities are regulated by relative movements of the channel and/or the membrane at the channel-membrane interface (59-61). Conformational changes of MS channels can be induced by membrane deformation (the bilayer model) or deformation of cytoskeletal or extracellular proteins that are directly connected to the channel (the tethered model). In any case, channel displacement with

respect to the membrane could produce hydrophobic mismatch between the lipid bilayer and the channel and trigger the channel conformational change. To the extent that gating conformational changes produce local changes in bilayer thickness, mechanosensitivity in channel gating will also lead to coupled gating.

The bilayer model is the dominant mechanism for prokaryotic MS channel gating (60). Purified bacterial MS channels reconstituted into artificial liposomes still exhibited mechanosensitivity, which indicates that MS channels can directly sense membrane deformation. Membrane movement (stretching or bending) can promote conformational transitions of MS channels via changes in the membrane geometry. Activation of *E. coli* MS channels was observed on insertion of lysophospholipids or amphipaths into the membrane, which perturb the local membrane curvature (62, 63).

In the tether mechanism, MS channels are directly linked to cytoskeletal or extracellular proteins that activate channels by pulling them from the membrane (61). The tether model has been proposed to describe MS channels in eukaryotic cells that have an extensive cytoskeletal network adjacent to the membrane. Direct evidence for the tether model has recently been obtained for two channels from the transient receptor potential (TRP) channel superfamily: zebrafish TRPN1 (also known as NompC) and *Drosophila* TRPA1 (also known as NompC) channels in the vertebrate sensory hair cells (64-66). Cadherin 23 proteins and the N-terminal ankyrin repeats of TRPA1 were identified as tethers for TRPN1 channels and TRPA1 channels, respectively. Cadherin 23 proteins link TRPN1 to the extracellular matrix, while the ankyrin domains of TRPA1 are attached to the cytoskeletons. Cytoskeleton/extracellular matrix deformation could displace the channel with respect to the lipid bilayer.

Mechanosensitivity has been also observed in voltage-gated and ligand-gated channels, including *Shaker*-IR voltage-gated K^+ channels (67), large conductance Ca^{2+}-activated K^+ (BK) channels (68), atrial ATP-sensitive K^+ channels (69), cardiac muscarinic K^+ channels (70), L-type and N-type Ca^{2+} channels (71, 72) and NMDA receptors in mouse neurons (73). The observation of mechanosensitivity in channels that are not classically gated by mechanical stress suggests that these channels will be

sensitive to perturbations that change the lipid bilayer thickness, including the conformational changes of other membrane proteins. Further studies will be required to determine whether this mechanosensitivity actually causes coupled gating in these systems.

1.7.3. Allosteric mechanisms

Neighboring channels might act as an allosteric modulator; i.e. the conformational state of one channel in clusters can influence conformational changes in neighboring channels, possibly by changing binding affinity of ligand in case of ligand-gated channels. Although direct visualization of allosteric conformational changes is limited by spatial and temporal resolution of current techniques, indirect evidence, such as Hill coefficients, can be obtained. Bacterial chemoreceptors are the best-studied model system for allostery in transmembrane receptors (74-76). Allosteric interactions between neighboring receptors have been proposed to account for the experimentally observed remarkable sensitivity of bacterial cells to their chemoeffectors. The signal amplification in *E. coli* cells was quantified using a fluorescence resonance energy transfer (FRET)-based *in vivo* assay, which provided evidence for allosteric interactions among receptors (77, 78). The receptors amplified the chemotactic signals (changes in chemoeffector concentrations) approximately 35-fold in a highly cooperative fashion (a Hill coefficient of ~10) that was well-described by the classical Monod-Wyman-Changeux (MWC) allosteric model. Allosteric protein interactions in clusters could also be an underlying mechanism for coupled gating of clustered ion channels.

1.8. Concluding remarks

Coupled gating has been observed in diverse channel types at the single-channel level. In spite of its potential physiological functions, however, the molecular basis of cooperative channel gating still remains to be investigated. Also, more unambiguous methods of biophysical analysis need to be developed to study coupled gating with single-channel recordings.

1.9. References

1. Erzberger, J. P., and J. M. Berger. 2006. Evolutionary relationships and structural mechanisms of AAA+ proteins. Annu Rev Biophys Biomol Struct 35:93-114.
2. Hanson, P. I., and S. W. Whiteheart. 2005. AAA+ proteins: have engine, will work. Nat Rev Mol Cell Biol 6:519-529.
3. Baker, T. A., and R. T. Sauer. 2006. ATP-dependent proteases of bacteria: recognition logic and operating principles. Trends Biochem Sci 31:647-653.
4. Biemans-Oldehinkel, E., M. K. Doeven, and B. Poolman. 2006. ABC transporter architecture and regulatory roles of accessory domains. FEBS Lett 580:1023-1035.
5. Linton, K. J., and C. F. Higgins. 2007. Structure and function of ABC transporters: the ATP switch provides flexible control. Pflugers Arch 453:555-567.
6. Alekseev, A. E., D. M. Hodgson, A. B. Karger, S. Park, L. V. Zingman, and A. Terzic. 2005. ATP-sensitive K+ channel channel/enzyme multimer: metabolic gating in the heart. J Mol Cell Cardiol 38:895-905.
7. Hille, B. 2001. Ion channels of excitable membranes. Sinauer Associates, Sunderland, MA.
8. Sakmann, B., and E. Neher. 1995. Single-channel recording. Plenum Press, New York, NY.
9. Chen, Y. H., and R. L. DeHaan. 1992. Multiple-channel conductance states and voltage regulation of embryonic chick cardiac gap junctions. J Membr Biol 127:95-111.
10. Dekker, J. P., and G. Yellen. 2006. Cooperative gating between single HCN pacemaker channels. J Gen Physiol 128:561-567.
11. Ding, S., and F. Sachs. 2002. Evidence for non-independent gating of P2X2 receptors expressed in Xenopus oocytes. BMC Neurosci 3:17.
12. Hymel, L., J. Striessnig, H. Glossmann, and H. Schindler. 1988. Purified skeletal muscle 1,4-dihydropyridine receptor forms phosphorylation-dependent oligomeric calcium channels in planar bilayers. Proc Natl Acad Sci U S A 85:4290-4294.
13. Iwasa, K., G. Ehrenstein, N. Moran, and M. Jia. 1986. Evidence for interactions between batrachotoxin-modified channels in hybrid neuroblastoma-cells. Biophys J 50:531-537.
14. Keleshian, A. M., R. O. Edeson, G. J. Liu, and B. W. Madsen. 2000. Evidence for cooperativity between nicotinic acetylcholine receptors in patch clamp records. Biophys J 78:1-12.
15. Laver, D. R., E. R. O'Neill, and G. D. Lamb. 2004. Luminal Ca2+-regulated Mg2+ inhibition of skeletal RyRs reconstituted as isolated channels or coupled clusters. J Gen Physiol 124:741-758.
16. Manivannan, K., S. V. Ramanan, R. T. Mathias, and P. R. Brink. 1992. Multichannel recordings from membranes which contain gap junctions. Biophys J 61:216-227.
17. Marx, S. O., J. Gaburjakova, M. Gaburjakova, C. Henrikson, K. Ondrias, and A. R. Marks. 2001. Coupled gating between cardiac calcium release channels (ryanodine receptors). Circ Res 88:1151-1158.

18. Marx, S. O., K. Ondrias, and A. R. Marks. 1998. Coupled gating between individual skeletal muscle Ca2+ release channels (ryanodine receptors). Science 281:818-821.
19. Molina, M. L., F. N. Barrera, A. M. Fernandez, J. A. Poveda, M. L. Renart, J. A. Encinar, G. Riquelme, and J. M. Gonzalez-Ros. 2006. Clustering and coupled gating modulate the activity in KcsA, a potassium channel model. J Biol Chem 281:18837-18848.
20. Neumcke, B., and R. Stampfli. 1983. Alteration of the conductance of Na+ channels in the nodal membrane of frog nerve by holding potential and tetrodotoxin. Biochim Biophys Acta 727:177-184.
21. Suppiramaniam, V., T. Vaithianathan, K. Manivannan, M. Dhanasekaran, K. Parameshwaran, and B. A. Bahr. 2006. Modulatory effects of dextran sulfate and fucoidan on binding and channel properties of AMPA receptors isolated from rat brain. Synapse 60:456-464.
22. Vaithianathan, T., K. Manivannan, R. Kleene, B. A. Bahr, M. P. Dey, A. Dityatev, and V. Suppiramaniam. 2005. Single channel recordings from synaptosomal AMPA receptors. Cell Biochem Biophys 42:75-85.
23. Yeramian, E., A. Trautmann, and P. Claverie. 1986. Acetylcholine receptors are not functionally independent. Biophys J 50:253-263.
24. Schindler, H., F. Spillecke, and E. Neumann. 1984. Different channel properties of Torpedo acetylcholine receptor monomers and dimers reconstituted in planar membranes. Proc Natl Acad Sci U S A 81:6222-6226.
25. Veenstra, R. D., H. Z. Wang, E. C. Beyer, and P. R. Brink. 1994. Selective dye and ionic permeability of gap junction channels formed by connexin45. Circ Res 75:483-490.
26. Kole, M. H., S. Hallermann, and G. J. Stuart. 2006. Single Ih channels in pyramidal neuron dendrites: properties, distribution, and impact on action potential output. J Neurosci 26:1677-1687.
27. McCall, E., L. Li, H. Satoh, T. R. Shannon, L. A. Blatter, and D. M. Bers. 1996. Effects of FK-506 on contraction and Ca2+ transients in rat cardiac myocytes. Circ Res 79:1110-1121.
28. Naundorf, B., F. Wolf, and M. Volgushev. 2006. Unique features of action potential initiation in cortical neurons. Nature 440:1060-1063.
29. Xiao, R. P., H. H. Valdivia, K. Bogdanov, C. Valdivia, E. G. Lakatta, and H. Cheng. 1997. The immunophilin FK506-binding protein modulates Ca2+ release channel closure in rat heart. J Physiol 500:343-354.
30. Malenka, R. C. 2003. Synaptic plasticity and AMPA receptor trafficking. Ann N Y Acad Sci 1003:1-11.
31. Malenka, R. C. 2003. The long-term potential of LTP. Nat Rev Neurosci 4:923-926.
32. McCormick, D. A., Y. Shu, and Y. Yu. 2007. Neurophysiology: Hodgkin and Huxley model--still standing? Nature 445:E1-2; discussion E2-3.
33. Diba, K., H. A. Lester, and C. Koch. 2004. Intrinsic noise in cultured hippocampal neurons: experiment and modeling. J Neurosci 24:9723-9733.

34. Jacobson, G. A., K. Diba, A. Yaron-Jakoubovitch, Y. Oz, C. Koch, I. Segev, and Y. Yarom. 2005. Subthreshold voltage noise of rat neocortical pyramidal neurones. J Physiol 564:145-160.
35. Schneidman, E., B. Freedman, and I. Segev. 1998. Ion channel stochasticity may be critical in determining the reliability and precision of spike timing. Neural Comput 10:1679-1703.
36. Chow, C. C., and J. A. White. 1996. Spontaneous action potentials due to channel fluctuations. Biophys J 71:3013-3021.
37. Kretzberg, J., M. Egelhaaf, and A. K. Warzecha. 2001. Membrane potential fluctuations determine the precision of spike timing and synchronous activity: a model study. J Comput Neurosci 10:79-97.
38. White, J. A., R. Klink, A. Alonso, and A. R. Kay. 1998. Noise from voltage-gated ion channels may influence neuronal dynamics in the entorhinal cortex. J Neurophysiol 80:262-269.
39. van Rossum, M. C., B. J. O'Brien, and R. G. Smith. 2003. Effects of noise on the spike timing precision of retinal ganglion cells. J Neurophysiol 89:2406-2419.
40. Kenyon, J. L., and R. J. Bauer. 2000. Amplitude histograms can identify positively but not negatively coupled channels. J Neurosci Methods 96:105-111.
41. Nedelman, J., and T. Wallenius. 1986. Bernoulli trials, Poisson trials, surprising variances, and Jensen inequality. Am Stat 40:286-289.
42. Traynelis, S. F., and F. Jaramillo. 1998. Getting the most out of noise in the central nervous system. Trends Neurosci 21:137-145.
43. Liu, Y., and J. P. Dilger. 1993. Application of the one-dimensional and two-dimensional Ising models to studies of cooperativity between ion channels. Biophys J 64:26-35.
44. Keleshian, A. M., G. F. Yeo, R. O. Edeson, and B. W. Madsen. 1994. Superposition properties of interacting ion channels. Biophys J 67:634-640.
45. Blunck, R., U. Kirst, T. Riessner, and U. Hansen. 1998. How powerful is the dwell-time analysis of multichannel records? J Membr Biol 165:19-35.
46. Barbuti, A., B. Gravante, M. Riolfo, R. Milanesi, B. Terragni, and D. DiFrancesco. 2004. Localization of pacemaker channels in lipid rafts regulates channel kinetics. Circ Res 94:1325-1331.
47. Goodenough, D. A. 1976. The structure and permeability of isolated hepatocyte gap junctions. Cold Spring Harb Symp Quant Biol 40:37-43.
48. Kensler, R. W., P. R. Brink, and M. M. Dewey. 1979. The septum of the lateral axon of the earthworm: a thin section and freeze-fracture study. J Neurocytol 8:565-590.
49. Block, B. A., T. Imagawa, K. P. Campbell, and C. Franzini-Armstrong. 1988. Structural evidence for direct interaction between the molecular components of the transverse tubule/sarcoplasmic reticulum junction in skeletal muscle. J Cell Biol 107:2587-2600.
50. Flucher, B. E., and C. Franzini-Armstrong. 1996. Formation of junctions involved in excitation-contraction coupling in skeletal and cardiac muscle. Proc Natl Acad Sci U S A 93:8101-8106.

51. Franzini-Armstrong, C., F. Protasi, and V. Ramesh. 1999. Shape, size, and distribution of Ca(2+) release units and couplons in skeletal and cardiac muscles. Biophys J 77:1528-1539.
52. Saito, A., M. Inui, M. Radermacher, J. Frank, and S. Fleischer. 1988. Ultrastructure of the calcium release channel of sarcoplasmic reticulum. J Cell Biol 107:211-219.
53. Dunant, Y., L. M. Garcia-Segura, D. Muller, and A. Parducz. 1989. Momentary alteration of the postsynaptic membrane during transmission of a single nerve impulse. Proc Natl Acad Sci U S A 86:1717-1720.
54. Tateishi, Y., M. Hattori, T. Nakayama, M. Iwai, H. Bannai, T. Nakamura, T. Michikawa, T. Inoue, and K. Mikoshiba. 2005. Cluster formation of inositol 1,4,5-trisphosphate receptor requires its transition to open state. J Biol Chem 280:6816-6822.
55. Wang, S., H. Yue, R. B. Derin, W. B. Guggino, and M. Li. 2000. Accessory protein facilitated CFTR-CFTR interaction, a molecular mechanism to potentiate the chloride channel activity. Cell 103:169-179.
56. Hall, R. A., V. Vodyanoy, A. Quan, S. Sinnarajah, V. Suppiramaniam, M. Kessler, and B. A. Bahr. 1996. Effects of heparin on the properties of solubilized and reconstituted rat brain AMPA receptors. Neurosci Lett 217:179-183.
57. Raghuram, V., D. O. Mak, and J. K. Foskett. 2001. Regulation of cystic fibrosis transmembrane conductance regulator single-channel gating by bivalent PDZ-domain-mediated interaction. Proc Natl Acad Sci U S A 98:1300-1305.
58. Imredy, J. P., and D. T. Yue. 1992. Submicroscopic Ca2+ diffusion mediates inhibitory coupling between individual Ca2+ channels. Neuron 9:197-207.
59. Kung, C. 2005. A possible unifying principle for mechanosensation. Nature 436:647-654.
60. Martinac, B. 2004. Mechanosensitive ion channels: molecules of mechanotransduction. J Cell Sci 117:2449-2460.
61. Sukharev, S., and D. P. Corey. 2004. Mechanosensitive channels: multiplicity of families and gating paradigms. Sci STKE 2004:re4.
62. Martinac, B., J. Adler, and C. Kung. 1990. Mechanosensitive ion channels of E. coli activated by amphipaths. Nature 348:261-263.
63. Perozo, E., A. Kloda, D. M. Cortes, and B. Martinac. 2002. Physical principles underlying the transduction of bilayer deformation forces during mechanosensitive channel gating. Nat Struct Biol 9:696-703.
64. Corey, D. P., J. Garcia-Anoveros, J. R. Holt, K. Y. Kwan, S. Y. Lin, M. A. Vollrath, A. Amalfitano, E. L. Cheung, B. H. Derfler, A. Duggan, G. S. Geleoc, P. A. Gray, M. P. Hoffman, H. L. Rehm, D. Tamasauskas, and D. S. Zhang. 2004. TRPA1 is a candidate for the mechanosensitive transduction channel of vertebrate hair cells. Nature 432:723-730.
65. Siemens, J., C. Lillo, R. A. Dumont, A. Reynolds, D. S. Williams, P. G. Gillespie, and U. Muller. 2004. Cadherin 23 is a component of the tip link in hair-cell stereocilia. Nature 428:950-955.
66. Sollner, C., G. J. Rauch, J. Siemens, R. Geisler, S. C. Schuster, U. Muller, and T. Nicolson. 2004. Mutations in cadherin 23 affect tip links in zebrafish sensory hair cells. Nature 428:955-959.

67. Gu, C. X., P. F. Juranka, and C. E. Morris. 2001. Stretch-activation and stretch-inactivation of Shaker-IR, a voltage-gated K+ channel. Biophys J 80:2678-2693.
68. Tang, Q. Y., Z. Qi, K. Naruse, and M. Sokabe. 2003. Characterization of a functionally expressed stretch-activated BKca channel cloned from chick ventricular myocytes. J Membr Biol 196:185-200.
69. Van Wagoner, D. R. 1993. Mechanosensitive gating of atrial ATP-sensitive potassium channels. Circ Res 72:973-983.
70. Pleumsamran, A., and D. Kim. 1995. Membrane stretch augments the cardiac muscarinic K+ channel activity. J Membr Biol 148:287-297.
71. Calabrese, B., I. V. Tabarean, P. Juranka, and C. E. Morris. 2002. Mechanosensitivity of N-type calcium channel currents. Biophys J 83:2560-2574.
72. Lyford, G. L., P. R. Strege, A. Shepard, Y. Ou, L. Ermilov, S. M. Miller, S. J. Gibbons, J. L. Rae, J. H. Szurszewski, and G. Farrugia. 2002. Alpha(1C) (Ca(V)1.2) L-type calcium channel mediates mechanosensitive calcium regulation. Am J Physiol Cell Physiol 283:C1001-1008.
73. Paoletti, P., and P. Ascher. 1994. Mechanosensitivity of NMDA receptors in cultured mouse central neurons. Neuron 13:645-655.
74. Kentner, D., and V. Sourjik. 2006. Spatial organization of the bacterial chemotaxis system. Curr Opin Microbiol 9:619-624.
75. Parkinson, J. S., P. Ames, and C. A. Studdert. 2005. Collaborative signaling by bacterial chemoreceptors. Curr Opin Microbiol 8:116-121.
76. Sourjik, V. 2004. Receptor clustering and signal processing in E. coli chemotaxis. Trends Microbiol 12:569-576.
77. Sourjik, V., and H. C. Berg. 2004. Functional interactions between receptors in bacterial chemotaxis. Nature 428:437-441.
78. Sourjik, V., and H. C. Berg. 2002. Binding of the Escherichia coli response regulator CheY to its target measured in vivo by fluorescence resonance energy transfer. Proc Natl Acad Sci U S A 99:12669-12674.

Chapter 2

Control of Channel Gating Noise in ATP-Sensitive Potassium Channels by Negative Coupling

2.1. Abstract

The ATP-sensitive potassium channel (K_{ATP}) helps control insulin secretion in pancreatic beta cells by sensing how the cell's metabolic state changes in response to glucose stimulation. Metabolic sensing by K_{ATP} is constrained by noise considerations. The noise due to stochastic K_{ATP} channel gating might disrupt the organization of bursts of electrical activity and the precision with which changes in ATP/ADP ratio are transduced to changes in membrane potential. Negatively cooperative interactions between K_{ATP} channels could reduce their noise output compared to identical and independent channels; however, it is unknown whether such interactions occur. Here we show that heterologously expressed K_{ATP} channels generate noise below the level possible for identical and independent channels. K_{ATP} activity exhibits correlated fluctuations, consistent with the existence of negatively cooperative dynamic interactions between K_{ATP} channels (i.e., an open K_{ATP} channel decreases the probability of its neighbors being open). Presence of the SUR1 subunit is necessary for robust collective fluctuations. If this mechanism of noise control is used *in vivo*, it might improve the precision of metabolic sensing, and help account for reliable signal transduction despite the relatively low expression level of K_{ATP} in pancreatic beta cells.

2.2. Introduction

ATP-sensitive potassium (K_{ATP}) channels control the membrane potential of pancreatic beta cells. These cells exhibit periodic bursts of electrical activity in response to glucose stimulation (1). K_{ATP} channels serve as a glucose sensor in beta cells: metabolism of glucose increases the ATP/ADP ratio, leading to closure of K_{ATP} channels, depolarization above the threshold of excitability, and secretion of insulin (Figure 2.1) (2). Although it has been well established and widely accepted that K_{ATP} channels couple metabolism to cell excitability by sensing the ATP/ADP ratio, K_{ATP} channel activity is also regulated by various proteins and small molecules. For instance, phosphorylation of K_{ATP} channels mediated by protein kinase A or by protein kinase C modulates channel activities (3-6). Small molecules like phosphatidylinositol-4,5-bisphosphate (PIP_2) are also important modulators of K_{ATP} channel activity (7, 8). In the context of a metabolic sensor, several metabolites other than nucleotides have been shown to regulate K_{ATP} channel activity: a fat metabolite, long-chain acyl-coenzyme A esters (9-11) and ketogenic metabolites (aromatic aldehydes and aromatic ketones) (12, 13) stimulate K_{ATP} channel activity.

Noise due to channel gating may also influence K_{ATP} channel functions in pancreatic beta cells. Noise is a fundamental property of cellular signaling pathways. Because cellular signaling pathways depend on molecular processes such as protein conformational changes and protein-protein interactions, they are subject to noise arising from thermally-induced stochastic fluctuations in the concentration or conformational state of signaling proteins. Noise has been shown to have a significant impact on biochemical pathways such as transcription and translation (14). Noise is also a relevant issue for electrical signaling in excitable cells such as neurons (15-18). Stochastic fluctuations in the number of open ion channels can have a significant effect on the membrane potential of excitable cells (19), particularly when a small number of channels (~10-1000) controls the membrane potential. Thus, channel gating noise may be important in the physiology of pancreatic beta cells because a relatively small number of K_{ATP} channels (~10^3-10^4) control the membrane potential (20). Isolated beta cells exhibit

regular bursts of electrical activity (21), indicating that their excitability is robust to the noise associated with K_{ATP} gating.

One possible contributor to the control of noise in pancreatic beta cells is control of the noise output of K_{ATP} channel gating. Noise from channel gating is usually assumed to arise through gating of identical and independent channels for which the variance in the number of channels open is described by the binomial distribution (18). However, if channels are non-identical in their open probabilities (e.g., due to differential phosphorylation (3-6)) or gate non-independently (e.g., the open probability of one depends on the open probability of its neighbors), the noise output will deviate from the prediction of the binomial distribution. In this study, we measure the noise output of heterologously expressed K_{ATP} channels and investigate the role of coupled gating in noise control using power spectrum analysis.

2.3. Methods

Molecular biology. Mouse pCMV-Kir6.2 and hamster pECE-SUR1 cDNA were provided by S. Seino (Chiba University, Chiba, Japan) and J. Bryan (Baylor College of Medicine, Houston, TX), respectively. A stop codon was introduced into the mouse Kir6.2 cDNA to delete the last 26 amino acids of the C-terminus (Kir6.2 ΔC1-26) using the QuikChange® Site-Directed Mutagenesis Kit (Stratagene, La Jolla, CA). All cDNA constructs were verified by DNA sequencing (MIT Biopolymers Lab, Cambridge, MA). Plasmids were prepared for transient transfection using the QIAfilter™ Plasmid Maxi Kit (QIAGEN Inc., Valencia, CA).

Cell culture. Human embryonic kidney (HEK) 293 cells (American Type Culture Collection, Manassas, VA) were cultured in Dulbecco's modified Eagle's medium containing 10% (v/v) fetal bovine serum in humidified 5% CO_2 at 37°C. Cells were passaged every three days by treatment with trypsin.

DNA transfection. HEK 293 cells were transiently transfected with either mouse Kir6.2 plus hamster SUR1 or with Kir6.2 ΔC1-26 cDNA. pEGFP-N1 vector (BD Biosciences, San Jose, CA) was co-transfected as a marker with the cDNA of interest using the FuGENE 6 Transfection Reagent (Roche Applied Science, Indianapolis, IN). Transfection was performed according to the manufacturer's instructions with total 1 μg of cDNA per 35-mm culture dish (2:3:5 ratio of Kir6.2, SUR1, and pEGFP-N1 or 1:4 ratio of Kir6.2 ΔC1-26 and pEGFP-N1). Some recordings were carried out on cells transfected with ~twofold greater amounts of cDNA; the amount of cDNA used did not affect apparent open probability, N_{max}, or the current variance. Transfected cells were incubated in humidified 5% CO_2 at 37°C. Approximately 36 to 72 hr after transfection, the cells were used for single-channel recordings.

Electrophysiology. Micropipettes were pulled from borosilicate glass capillaries (MTW 1B150F-4; World Precision Instruments Inc., Sarasota, FL) on a puller (PP-830; Narishige Group, Tokyo, Japan) with resistance typically ~5-12 MΩ. Pulled pipettes were coated with Sylgard (Dow Corning Corporation, Midland, MI) and fire-polished using a microforge (MF-830; Narishige Group, Tokyo, Japan) to reduce the noise level.

Single-channel recordings were performed at room temperature with an Axopatch 200B patch clamp amplifier (Axon Instruments Inc., Union City, CA) and were low-pass filtered (10 kHz) with a 4-pole Bessel filter. Single-channel data were acquired and digitized at 20 kHz using QuB software (www.qub.buffalo.edu) (22, 23). Single-channel currents were recorded using the inside-out patch clamp configuration (24, 25) at a membrane potential of –80 mV, with the pipette (extracellular) solution containing (in mM): 140 KCl, 10 NaCl, 1.1 $MgCl_2$, and 10 K-HEPES, pH to 7.3 and with the bath (intracellular) solution containing (in mM): 140 KCl, 10 NaCl, 1.1 $MgCl_2$, 0.5 $CaCl_2$, 5 K-EGTA, and 10 K-HEPES, pH to 7.3 (5). 1 mM MgATP (ATP magnesium salt; Sigma, St. Louis, MO) and 5 μM PIP_2 (Calbiochem, San Diego, CA) were directly added to the bath solution (26).

Single-channel data analysis and simulations. Digitized single-channel records were filtered at 5 kHz and analyzed using QuB software. Stationary segments of 100-sec duration were idealized using the half-amplitude method.

When n_o consecutive single openings have been observed, the probability of observing more single openings before the first multiple opening occurs is $P(r \geq n_o) = \pi^{(no - 1)}$, where r is a total number of consecutive single openings and π is the probability that one open channel is closed before a second channel is open (27). The probability π can be estimated as $(1 - P_{open}) / (1 - P_{open} / N)$, where N is the actual number of independent channels in the patch. An observed K_{ATP} channel record contains $\sim 3 \times 10^4$ consecutive single openings with P_{open} of ≥ 0.50. The probability of a run this long, $P(r \geq 3 \times 10^4)$, therefore, would be < 0.0001 if there were two channels present, so it is very likely that exactly one channel is present.

The rate constants of the best-fit model (Scheme 1) were obtained by fitting the duration histograms using the maximum interval likelihood (MIL) function of QuB.

$$C_f \underset{k_{-f}}{\overset{k_f}{\rightleftharpoons}} O \underset{k_{-s}}{\overset{k_s}{\rightleftharpoons}} C_s \qquad \text{(Scheme 1)}$$

where O is the open state, C_f is the short closed state within a burst in which the channel rapidly opens and closes, and C_s represents the long closed state determining the interburst duration.

Markov models with the rate constants obtained from the experimental records were used to simulate records of the same length as the experimental records, but with the constraint that the channels were identical and independent. The simulated records were analyzed to estimate the uncertainty in the prediction of current variance due to the finite length of records. Analysis of 11 simulated records indicates that the mean deviation of the variance from the predicted binomial variance is 0.6 ± 0.3%.

Variance analysis. The mean and variance in the number of open channels were calculated as previously described (18). For a patch containing N channels, the mean number of open channels is:

$$NP_{open} = \sum_{n=0}^{N} O_n \cdot n \tag{1}$$

where P_{open} is the open channel probability and O_n is the mean occupancy of an n state (open channel).

The variance (σ^2) is defined as:

$$\sigma^2 = \sum_{n=0}^{N} O_n \cdot (n - NP_{open})^2 \tag{2}$$

In the case of identical and independent channels, the relationship between the variance and the mean can be derived from the binomial theorem:

$$\sigma^2 = NP_{open}(1 - P_{open}) = NP_{open} - (NP_{open})^2 / N \tag{3}$$

Although the variance (σ^2) cannot be predicted unless the number of channels in the patch (N) is known, we can set a lower bound on the predicted variance using the maximum number of simultaneous channel openings (N_{max}):

$$\sigma^2 = NP_{open} - (NP_{open})^2 / N_{max} \quad (4)$$

Power spectrum analysis. The spectrum histograms were generated using QuB software. In detail, a short-time fast Fourier transformation (FFT) was performed on idealized single-channel records with a window size of 262144 sampling points. The sliding window overlapped with the previous and next window by half, and each window was multiplied by a Hanning window function to limit edge effects. The resulting FFT bins are grouped into 100 histogram bins. The power spectrum was fitted with the sum of three Lorentzian functions:

$$S(f) = S_1 / (1 + (f/f_1)^2) + S_2 / (1 + (f/f_2)^2) + S_3 / (1 + (f/f_3)^2) \quad (5)$$

where S(f) is the power spectral density at the frequency f. S_1, S_2 and S_3 are the zero-frequency asymptotes, and f_1, f_2 and f_3 are the corner frequencies (fc) of the Lorentzian components 1, 2 and 3, respectively. The power spectrum was also fitted with power law, α / f^{β}, where α is the amplitude and β is the exponent.

Randomization of dwells was carried out while preserving the constraint (observed experimentally) that more than one channel does not open or close simultaneously. To synthesize randomized records that obeyed this constraint, the record was randomized dwell by dwell, with each subsequent dwell chosen at random from the group of dwells separated by one conductance level from the dwell under consideration (e.g., a dwell with one channel open would always be followed by a zero-channel or two-channel dwell).

Modeling of variability in membrane potential. The Goldman-Hodgkin-Katz equation (28) (Eq. 6) was used to calculate the average membrane potential (V) of a cell

containing two conductances: an ATP-sensitive hyperpolarizing conductance, G_H (reversal potential of –90 mV, V_H), and an ATP-insensitive depolarizing conductance, G_D (reversal potential of 0 mV, V_D):

$$V = (G_H V_H + G_D V_D) / (G_H + G_D) \quad (6)$$

G_H, which corresponds to K_{ATP} channel conductance in pancreatic beta cells, can be expressed as a function of intracellular ATP concentration, $[ATP]_i$:

$$G_H = G_O / [1 + ([ATP]_i / K_i)^{\alpha}] \quad (7)$$

where G_O is the total ATP-sensitive potassium conductance (set at 10,000 pS (29, 30)) and K_i is the half-maximal inhibitory ATP concentration (set at 15 μM (20, 29)). The Hill coefficient, α, is set at 1 for independent channels and 0.8 for negatively coupled channels.

The number of open K_{ATP} channels (N_{open}) was obtained from the ATP-sensitive conductance (G_H) divided by the single K_{ATP} channel conductance of 15 pS. Fluctuations in the number of open K_{ATP} channels (σ^2) can be calculated from the first derivative of the dependence of N_{open} on the chemical potential of ATP (31):

$$\sigma^2 = \langle (N_{open})^2 \rangle - \langle N_{open} \rangle^2 = kT \cdot \delta \langle N_{open} \rangle / \delta \mu \quad (8)$$

where k is Boltzmann's constant, T is absolute temperature, and μ is the chemical potential of ATP, defining intracellular ATP concentration at –75 mV (resting potential) as the standard concentration.

Fluctuations in the membrane potential (υ^2) were calculated using variability in the number of open channels (σ^2) (32):

$$\upsilon^2 = (I_H / (G_H + G_D))^2 (\sigma^2 / N_{open}^2) \quad (9)$$

where I_H is the ATP-sensitive hyperpolarizing current, $(G_H G_D / (G_H + G_D))$ $(V_H - V_D)$.

Signal-to-noise ratios (SNRs) are calculated using the membrane potential and fluctuation as the signal and noise, respectively, $(V / \upsilon)^2$.

The probability density function (PDF) of a Gaussian distribution was used to calculate the probability that a cell at rest (resting potential, V_r of –75 mV) becomes electrically active due to fluctuations in membrane potential (υ):

$$PDF(\upsilon) = \frac{1}{\upsilon\sqrt{2\pi}}\exp(-\frac{(X-V_r)^2}{2\upsilon^2}) \qquad (10)$$

where X is the threshold potential leading to electrical activity in pancreatic beta cells (set at –60 mV).

Statistical analysis. Values are listed as mean ± S.E.M. The Kolmogorov-Smirnov test was used for comparison of non-normal distributions while the *t*-test was used for normal distributions (as evaluated using the Shapiro-Wilk test). Differences were considered significant at a level of $P < 0.05$.

2.4. Results

Noise properties of patches with two channels open simultaneously. In order to determine whether K_{ATP} channels gate as identical and independent units, we examined membrane patches where a maximum of two simultaneous openings were observed, and determined the distribution of occupancies in the possible states (Figure 2.2). Deviations from the binomial distribution were quantified using the parameter *r*, which is negative if channels are non-identical or negatively coupled (33). The average *r* is –0.03 ± 0.007 (n = 5) (Figure 2.2.B), corresponding to what would be observed for two independent channels with open probabilities differing by ~twofold (33).

Noise properties of multichannel patches. To generalize the analysis of noise output to records containing multiple channels open simultaneously, we measured the current variance as a function of the mean current. Using the maximum number of channels open simultaneously (N_{max}), a lower bound on the variance expected for identical and independent channels can be calculated (see Methods). In most membrane patches (7/11 records), the observed variance was less (14 ± 2%, n = 7, P = 0.0006, two-tailed paired *t*-test) than expected from identical and independent channels (Figure 2.3.B). Analysis of all the patches indicates that the noise output is significantly less (9 ± 3%, n = 11, P = 0.01, two-tailed paired *t*-test) than predicted for identical and independent channels.

Patch-to-patch variability in noise output is correlated with variability (34, 35) in N_{max} and in apparent open probability (NP_{open}/N_{max}, where NP_{open} is the average number of channels open) (Table 2.1). Patches with apparent $P_{open} < 0.1$ generate noise consistent with identical and independent channels and typically exhibit $N_{max} > 2$. These observations are consistent with the presence of two forms of K_{ATP}: a high-P_{open} form in which gating heterogeneity decreases noise output and a low-P_{open} form that exhibits more homogeneous gating and higher noise output. Suppression of multiple openings by negative coupling between the high-P_{open} channels might account for the observation of smaller N_{max} for high-P_{open} channels than for low-P_{open} channels.

As a complementary method of testing for identical and independent gating, we compared mean/variance plots for observed records with simulated records where gating was constrained to be identical and independent. Compared to the simulated data, probability density in the observed records is more highly concentrated in the regions associated with non-identical/non-independent channels (Figure 2.3.C).

Dynamic conformational coupling in control of K_{ATP} noise output. Decreased noise output might arise from two mechanisms: static heterogeneity (non-identicality) in channel P_{open} (e.g., due to differences in post-translational modifications such as phosphorylation (3-6)) or dynamic conformational coupling between channels that causes non-independent gating. To distinguish between these alternatives, we first determined whether fluctuations in gating vary dynamically over time. An absence of dynamic variations would be consistent with static heterogeneity in gating. Current records from multichannel patch exhibit dynamic heterogeneity in the form of transitions between discrete states of characteristic open probability (Figure 2.4.A). Dynamic heterogeneity of this kind might arise from modal gating of channels without any coupling between channels, i.e., each channel undergoes transitions among states with different open probabilities. In that case, however, the variance in the number of channels open would still be expected to follow the binomial distribution (36). Thus, the observation of both decreased noise and dynamic heterogeneity is not consistent with purely static heterogeneity in channel open probability but is consistent with the hypothesis that the channels are coupled.

To distinguish between coupled gating and non-identicality of channels, power spectrum analysis was carried out on K_{ATP} channel currents. Gating of single channels is widely accepted as a stochastic process that can be described with Markov models (25). In that case, the power spectrum of the current record can be described as the sum of Lorentzian components, with each distinct component representing a Markovian step in a given gating process (37). Power spectra are expected to be similar for one-channel records and multichannel records as long as the channels gate independently.

Power spectra can be used to investigate whether there are correlations within the record. To accomplish this, power spectra can be compared for experimental records and the same records after the order of the dwells had been randomized. If the dwells are uncorrelated, randomization of the dwells will not affect the power spectrum. However, if dwells are correlated, randomization will remove the correlation, changing the appearance of the power spectrum.

To determine kinetic components of individual K_{ATP} channel gating, a power spectrum of records from one-channel patches (as defined in Methods) was obtained first. The power spectrum of single K_{ATP} channel currents exhibits at least three components: one distinct fast component and two components in the lower frequency range (Figure 2.4.B). This observation is consistent with previous single-channel kinetic studies and the results of the current work, which have shown that K_{ATP} exhibits bursts with opening and closing rate constants ~10^3 sec^{-1} and burst/interburst transitions with a broad range of rate constants (~1-100 sec^{-1}). The fast component (corner frequency, f_c = ~800 Hz) in the power spectrum can be assigned to intraburst transitions. The intermediate component (f_c = ~15 Hz) can be attributed to interburst transitions, and may include several poorly resolved Lorentzian components. The slowest component (f_c < 1 Hz) is difficult to measure accurately due to the finite length of records. The power spectrum of one-channel records is unaffected by randomization of dwells (Figure 2.4.B), as expected if one-channel gating does not exhibit correlations.

The power spectra of records from multichannel patches with noise below the binomial limit did not exhibit the same features as power spectra from one-channel records (Figure 2.4.C). The presence of a fast component at ~800 Hz corresponding to intraburst events was distinct as in one-channel records. In the low frequency region of the spectra, however, power increased monotonically without the appearance of distinct components; the power decays approximately as $1/f^{\beta}$ ($\beta = 0.96 \pm 0.05$, fitting the linear region at f < 10 Hz). These data indicate that when the noise output is low, multiple channels are not behaving simply as the superposition of multiple single-channel events; rather, their kinetics displays a unique low-frequency component, which might arise from correlated activity of multiple channels.

For multichannel patches with noise at or above the binomial limit, the $1/f^{\beta}$ component is not always observed. Some records appear to be well-described by a sum of multiple Lorentzian components; their power spectra are essentially flat below 10 Hz (Figure 2.4.D). Because of the contribution of these records, the average β is less for the high-noise records than for the low-noise records ($\beta = 0.60 \pm 0.03$).

Analysis of randomized dwells is consistent with the hypothesis that multiple channel patches can exhibit correlations not observed in one-channel patches. Randomization of the dwells from records of one-channel patches has little effect on the appearance of the spectra (Figure 2.4.B). However, for randomized records from multichannel patches, the $1/f^{\beta}$ component is no longer observed. Power spectra from the randomized records appear to be the sum of Lorentzian components, dominated by features at ~10 and ~500 Hz (Figure 2.4.C), which is qualitatively similar to spectra from one-channel patches. If the difference between one-channel patches and multichannel patches were due to static heterogeneity in the multichannel patches, randomizing the dwells would not be expected to have an effect on the appearance of the multichannel patch power spectra. The observation that randomizing the dwells removes the $1/f^{\beta}$ features of the multichannel records thus suggests that the multichannel records exhibit correlations that are absent in one-channel records.

Role of the SUR1 subunit in negative coupling. Cooperative interactions between SUR1 subunits of neighboring channels might mediate coupled gating of K_{ATP}. To determine whether SUR1 is required for negative coupling between channels, we examined current records of Kir6.2 ΔC1-26, a truncation mutant that can be expressed at the plasma membrane in the absence of SUR1 (38). Previous studies indicate that the C-terminal truncation affects channel trafficking without affecting channel gating (38). Fluctuations in Kir6.2 ΔC1-26 channel activity were measured to distinguish between static heterogeneity and coupled gating. SUR1-free mutant channels exhibit reduced collective fluctuations in gating compared to the wild-type channels. For the mutant, shifts between discrete modes were less pronounced than for the wild-type (Figure 2.5.B), suggesting a decreased role for dynamic conformational coupling.

Analysis of the power spectra from records of mutant channels suggests that the correlations observed with wild-type channels are not present for the mutant. The power spectra of mutant records from low-noise patches are qualitatively similar to those of the wild-type ($\beta = 0.76 \pm 0.03$, Figure 2.5.C). However, for Kir6.2 ΔC1-26 in the absence of SUR1, randomized records exhibit power spectra that are almost identical to the original experimental records (Figure 2.5.C). These observations suggest that for the mutant channels, multichannel records do not exhibit any correlated activity. The similarity between low-noise mutant and wild-type records in the low frequency region of the power spectrum may be due to static heterogeneity in the mutant patches.

If the mutant channels exhibit static heterogeneity, they might exhibit noise reduction even in the absence of negatively cooperative interactions. In half of the multichannel patches examined (6 of 12), noise is at the binomial limit (deviation from the binomial limit = 2 ± 1%) (Table 2.1). In the remaining patches, noise is significantly below the binomial limit (ratios ranging from 5 to 107%) (Table 2.1). Overall, any increase in noise output for the SUR1-free mutant compared to the wild-type (a median noise output of 3% less than the binomial limit for the mutant, compared to 10% less than the binomial limit for the wild-type) was not statistically significant ($n = 12$, $m = 11$, $P = 0.14$, one-tailed Kolmogorov-Smirnov test) (Figure 2.6.A).

An analysis of the noise output as a function of open probability supports the hypothesis that static heterogeneity is the major contributor to the decreased noise output observed for the SUR1-free mutant. The largest deviations in noise output occur for records with P_{open} in the middle of the observed range, which will be observed when both high-P_{open} and low-P_{open} channels are present in one patch (Figure 2.6.B). Since this static heterogeneity is not observed for the wild-type channels, its specific physiological relevance is unclear. However, phosphorylation of Kir6.2 has been shown to affect P_{open} (3-6), indicating that heterogeneous phosphorylation could affect noise control *in vivo*.

2.5. Discussion

Noise in multichannel patches is below the lower limit predicted for identical and independent channels. The observation that the noise is less than the binomial prediction indicates that heterologously expressed K_{ATP} channels are either non-identical or non-independent.

A kinetic analysis favors the non-independent mechanism. If channels are independent, the power spectra of records from patches containing multiple channels would be similar to those from patches containing only one channel. The corner frequency of the slow component would be expected to increase with an increasing number of channels in the patch, since more channels would produce a faster burst-to-interburst transition. However, the number of kinetic components is expected to be independent of the number of channels in the patch for independent channels. In fact, the multichannel power spectra contain a feature at low frequencies that is not observed in the one-channel spectra. This feature is well-fitted with a $1/f^{\beta}$ dependence. Although the $1/f^{\beta}$ component is only apparent over a range of one decade in frequency, the observation that multiple channels in the patch affect the kinetic features in the power spectrum supports the hypothesis that the channels are interacting.

The $1/f^{\beta}$ feature is present in all of the patches exhibiting noise reduction, but also in some of the patches where no noise reduction is observed. It is possible that the observation of the $1/f^{\beta}$ feature in high noise patches is due to the conservative criterion used here to define noise reduction. The binomial limit is calculated from the maximum number of channels observed to be open simultaneously in the patch. If more channels are present in the patch than the maximum number observed, the calculated noise reduction underestimates the true value. Thus, an underestimate of the number of channels would lead to a record being classified as "high noise" even though channels were non-identical and/or non-independent.

Analysis of randomized records also supports the non-independent mechanism. Static heterogeneity might also give rise to a $1/f^{\beta}$ component in multichannel patches if

the channels in the patch are sufficiently heterogeneous. The presence or absence of correlations in the data can be used to distinguish between static heterogeneity and non-independent gating. If the channels are non-independent, there will be correlations in the records of multichannel patches that are not present in one-channel patches. For one-channel patches, randomization of the dwells has no discernible effect on power spectra, suggesting that correlations associated with the gating mechanism of individual channels are minimal. Although a simple bursting mechanism has some degree of correlation (long interburst closed times are likely to be followed by short intraburst closed times), the vast majority of events occur within bursts, and are expected to be uncorrelated, as observed. In contrast, randomization of multichannel records leads to a marked change in the appearance of the power spectrum, eliminating the $1/f^{\beta}$ feature in the low-frequency region of the spectrum. The results are thus consistent with the interpretation that the $1/f^{\beta}$ feature is the result of correlated fluctuations associated with non-independent channel activity: it is only present when multiple channels are present in the patch, and randomization eliminates it.

Results obtained with a Kir6.2 mutant in the absence of SUR1 suggest that the SUR1 subunit participates in negative coupling between K_{ATP} channels. For the Kir6.2 mutant alone, deviations from the binomial variance prediction are observed, but appear to be largely due to non-identicality of channels. The correlations observed in wild-type multichannel records are not present in the mutant data. One possibility is that heterogeneous phosphorylation or other post-translational modifications of the mutant channels introduces static heterogeneity; the absence of the SUR1 subunit might, for example, expose normally inaccessible phosphorylation sites. Biochemical studies will be required to answer this question.

Taken together, these observations suggest a novel role for SUR1 as a mediator of interchannel interactions. This subunit may thus have a third important role in K_{ATP} physiology in addition to its well-established functions as a trafficking chaperone (38-40) and a mediator of nucleotide sensitivity (38, 39). Clustering of K_{ATP} channels has previously been proposed based on electron microscopic (41) and pharmacological (42) studies. Further work is needed to determine the molecular basis for interchannel

interactions. One speculative mechanism for interchannel coupling is heterodimerization of nucleotide binding folds (43, 44) on adjacent channels. Such an interaction could, in principle, link multiple channels both spatially and functionally into a single unit. Protein-lipid-protein interactions might also contribute to coupled channel gating. Any change in the cross-sectional area of the channel due to gating of one channel (as previously observed for potassium (45) and sodium (46) channels) will also affect lipid bilayer tension (47), possibly affecting the ability of neighboring channels to open/close.

Effects of negative cooperativity on transduction of a metabolic signal to an electrical signal. It remains to be seen whether the noise suppression observed in heterologously expressed channels also occurs *in vivo*. As a first step in ascertaining whether the effects observed *in vitro* may have physiological consequences, the effects of K_{ATP} noise on metabolic signaling can be estimated. Noise due to K_{ATP} gating may have deleterious effects on the ability of pancreatic beta cells to act as metabolic sensors. K_{ATP} transduces a metabolic signal into an electrical signal through its effect on the transmembrane electrical potential. Because potassium channels hyperpolarize the cell under physiological conditions, ATP-induced closure of K_{ATP} causes depolarization. Depolarization from resting ~ –75 mV to ~ –60 mV leads to action potential-like spikes of activity and/or more complex patterns of electrical activity (20).

When a cell contains a small number of K_{ATP} channels, noise due to stochastic gating can significantly affect the fraction of channels open. Variability in the number of open channels affects how precisely the metabolic state of the cell determines the membrane potential. However, energy considerations limit the number of channels that can be expressed; increasing the total ionic current also increases the energy cost of maintaining ion homeostasis via ATP-dependent pumps. Previous measurements of ionic currents and ATP metabolism in pancreatic beta cells indicate that the energy costs of ionic signaling are substantial: ~10% of the ATP produced by glucose metabolism is consumed to maintain ionic homeostasis (see below). Increasing the precision of metabolic signaling by a large increase in channel expression is not feasible since the increased ATP hydrolysis required to support the extra channels would act as a shunt for

the ATP produced by glucose metabolism, diminishing the metabolic signal that the channels measure.

Estimated energy production by glucose metabolism in pancreatic beta cells compared to energy cost of ionic signaling. The maximum change in intracellular ATP due to glucose metabolism in pancreatic beta cells can be estimated from the rate of glucose consumption. The rate of glucose consumption is $\sim 10^0$ pmol islet^{-1} hr^{-1} at sub-stimulating glucose concentrations and $\sim 10^1$ pmol islet^{-1} hr^{-1} at glucose concentrations high enough to stimulate insulin secretion (48). Using a value of 38 ATP molecules synthesized/glucose molecule consumed (49), rates of $\sim 10^0$ and 10^1 pmol ATP islet^{-1} min^{-1} can be calculated for resting and stimulated beta cells. The increase in ATP production due to glucose metabolism can thus be estimated to be $\sim 10^1$ pmol ATP islet^{-1} min^{-1}.

The energetic cost of maintaining ionic homeostasis can be estimated from steady-state ionic currents. At rest, pancreatic beta cells exhibit $\sim 10^0$ pA leak current mainly due to K_{ATP} channels (34, 35). At the plateau potential of bursts of activity, inward current due to voltage-gated calcium channels is $\sim 10^1$ pA (34, 35). Maintaining ionic homeostasis would thus require hydrolysis of $\sim 10^{-1}$ pmol ATP islet^{-1} min^{-1} for a potassium leak current at rest and $\sim 10^0$ pmol ATP islet^{-1} min^{-1} during the plateau phase of the burst (using values of $\sim 10^3$ cells/islet (34, 35, 48) and 0.5 ATP hydrolyzed per potassium or calcium ion pumped (49)). Thus, while increasing concentrations of glucose stimulate rates of ATP production, the rate of ATP depletion due to ionic currents remains constant at ~10% of the rate of ATP production.

An alternative method of estimating the relative energy cost of maintaining ionic homeostasis comes from measurements of heat production by beta cells. The increase in heat production associated with high glucose concentrations is $\sim 10^0$ pW/cell (34, 35). Using the estimates derived above for currents at rest (–70 mV) and at the plateau potential (–30 mV), the glucose-induced change in heat dissipation associated with ionic currents is $\sim 10^{-1}$ pW/cell. These estimates suggest that ionic currents dissipate ~10% of the extra energy generated by beta cells at high glucose concentrations.

Estimates of the energy cost associated with electrical signaling in beta cells thus support the idea that significant increases in the ATP hydrolysis required for ionic homeostasis would interfere with the ability of the cell to increase the ATP/ADP ratio in response to glucose metabolism. The energy cost of electrical signaling depends on the density of ion channels in the membrane. If the number of channels in the cell were much greater than it is, the rate of ATP hydrolysis associated with ionic homeostasis would be comparable to the rate of ATP production via glucose metabolism. ATP hydrolysis would then act as an effective shunt, preventing accumulation of ATP in response to glucose metabolism. Shunting of ATP in this way would interfere with the ability of the cell to detect glucose, since metabolism of glucose would be less tightly linked to the ATP/ADP ratio.

Measurements of the decrease in K_{ATP} noise output due to coupled gating allow estimation of its possible effects on energy consumption in metabolic signaling. The observed noise due to stochastic gating is ~10% less than expected for identical and independent channels. A comparable effect operating *in vivo* would thus enable the cell to operate with ~20% fewer K_{ATP} channels without increasing the noise output relative to identical and independent channels (18). Because the membrane potential depends on relative ionic conductances (28), decreasing the number of K_{ATP} channels would allow the expression of other channels to be scaled down proportionately, thereby decreasing the total energy cost of ionic signaling. Because the metabolic cost of K_{ATP}-initiated electrical signaling in vivo is significant compared to the metabolic fluctuations that this system must measure, decreasing the energy cost of ionic signaling by ~20% is likely to be physiologically relevant.

Modeling of fluctuations in membrane potential. A simple quantitative model suggests that channel gating noise can have a substantial effect on the precision of metabolic signaling. In this model, the cell is approximated as a compartment containing K_{ATP} and a non-selective cation channel (a depolarizing conductance) (Figure 2.7.A). The number of open K_{ATP} channels is modeled as a simple binding isotherm with a Hill coefficient of 1 for identical and independent channels and < 1 for negatively coupled

channels. Fluctuations in the number of open K_{ATP} channels are calculated (31) and used to determine the magnitude of fluctuations in the membrane potential.

This quantitative model shows that negative coupling between K_{ATP} channels increases the precision of metabolic signaling. Negative coupling of moderate strength (a Hill coefficient of 0.8) decreases the variability in membrane potential by ~10-15% (Figure 2.7.B). Defining the signal as the change in membrane potential from the resting potential (i.e., at a sub-stimulating glucose concentration), the signal-to-noise ratio is thus increased ~25-40% by negative coupling (Figure 2.7.C). This increase in signal-to-noise ratio comes at the expense of signal gain: negative coupling decreases the change in membrane potential induced by a small perturbation in chemical potential (i.e., it decreases $dN_{open} / d\mu$).

A decrease in noise due to negative coupling can also decrease the probability that a cell at rest will become electrically active due to random fluctuations in membrane potential. The model indicates that while this probability is low for identical and independent channels (~0.2%, assuming a threshold potential of –60 mV and normally distributed membrane potential fluctuations), it is high enough to be non-negligible in a pancreatic islet containing ~10^3 beta cells. Negative coupling decreases this probability by a factor of two (Figure 2.7.D).

2.6. Conclusions

The kinetic behavior of K_{ATP} suggests that K_{ATP} channel activity could be negatively coupled. The SUR1 subunit in particular appears to have a role in coordinating interactions between intact channels in the membrane, which is a novel mechanistic role for SUR1 (Figure 2.8). It is not yet clear whether this phenomenon occurs *in vivo*. However, the ability to reconstitute this activity *in vitro* without exogenous factors and the observation that K_{ATP} channels are present in puncta at the plasma membrane (41) suggest that the channels may self-assemble into functionally coupled units *in vivo*. In addition, effects of the magnitude observed *in vitro* are not negligible compared to the magnitude of channel noise expected to affect insulin signaling. Simplified models of metabolic signaling support the idea that negative coupling of the magnitude observed *in vitro* could have a significant effect on beta cell physiology. Negative coupling between K_{ATP} channels might affect signaling in other cells expressing this channel in its various isoforms, such as the brain and the heart. Decreased stochastic gating fluctuations might also enhance energy efficiency in other ion channel-based signaling systems that are under both noise and energy constraints. In general, considerations of noise, energy consumption, and signal gain may help determine when ion channels gate as identical and independent units and when their gating is positively (50, 51) or negatively (52) coupled.

2.7. Figures and Table

Figure 2.1. K_{ATP} channel has an important role in insulin secretion in pancreatic β-cells. The increased ATP/ADP ratio induced by high glucose levels causes the K_{ATP} channel to close. This depolarizes the cell membrane, thereby increasing entry of calcium through voltage-gated calcium channels. The increased calcium level, in turn, triggers insulin secretion.

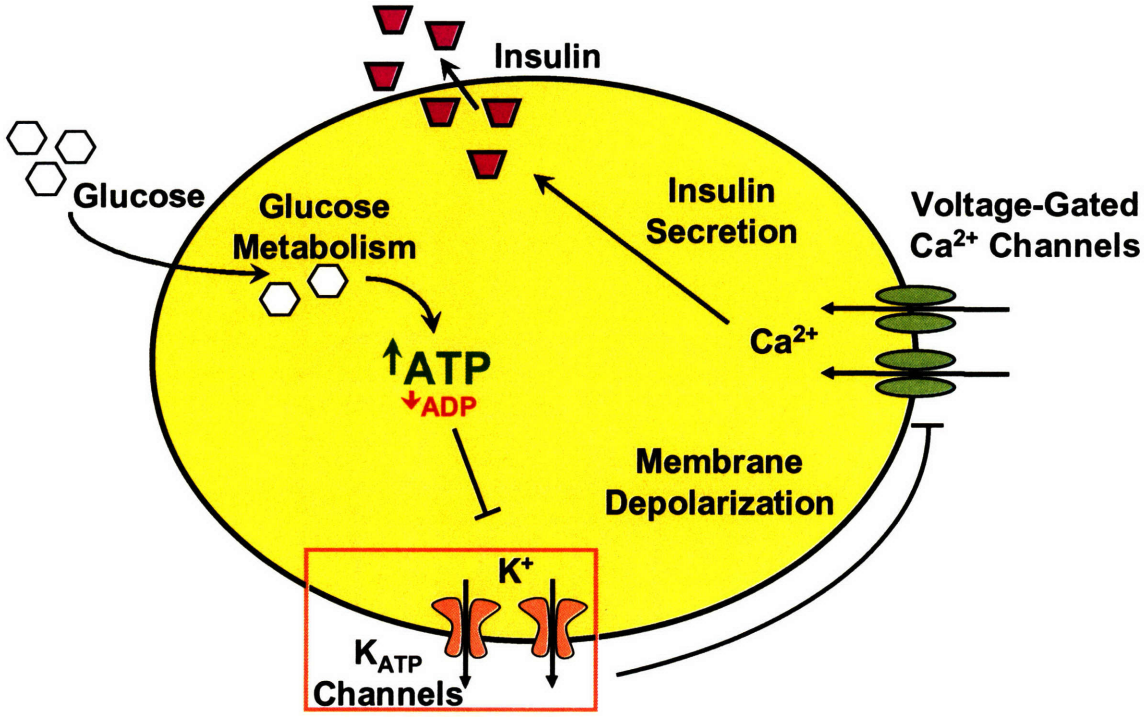

Figure 2.2. K_{ATP} channels exhibit less noise than expected for identical and independent channels. (A) A representative patch clamp recordings of individual K_{ATP} channels from a patch containing no more than two simultaneously open channels. (B) Deviation of observed occupancies in states with zero, one, or two simultaneously open channels from the occupancies predicted by the binomial distribution, which assumes identical and independent channels (error bars, S.E.M., n = 5).

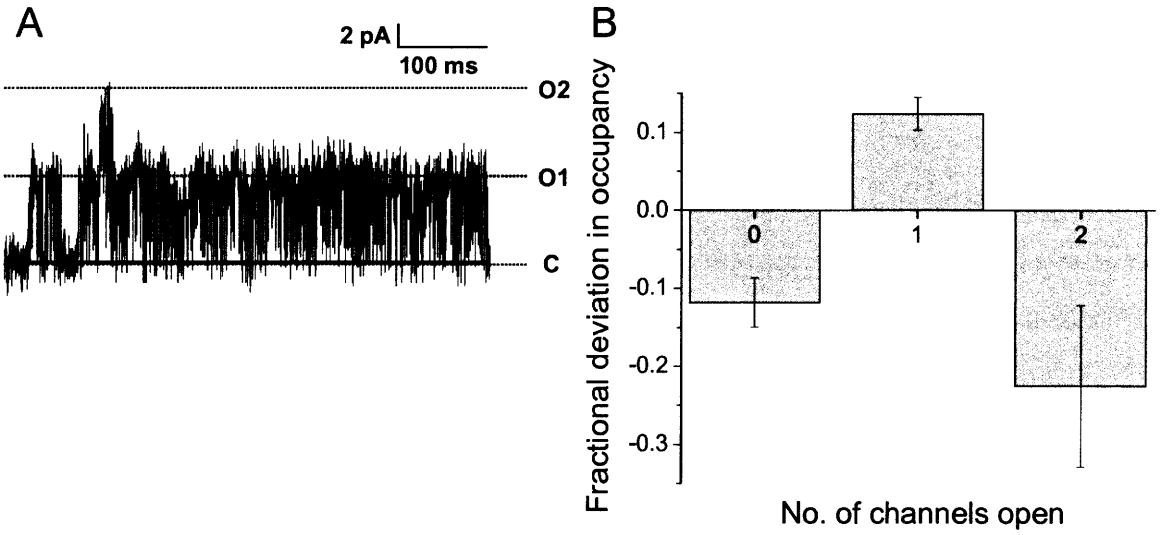

Figure 2.3. Patches containing multiple K_{ATP} channels exhibit decreased noise. (A) A representative patch clamp recording of individual K_{ATP} channels from a multichannel patch. (B) Cumulative probability histograms for deviations from identical and independent behavior (red circles, experimental records; black squares, simulated records for identical and independent channels; see Methods). (C) The normalized difference of mean/variance plots between observed records and simulated identical/independent records ($(m/v)_{obs.} - (m/v)_{sim.}$, n = 5) (black solid line, expected curve for one channel open; red dashed line, expected curve for two negatively coupled/non-identical channels; blue dashed line, expected curve for two identical and independent channels).

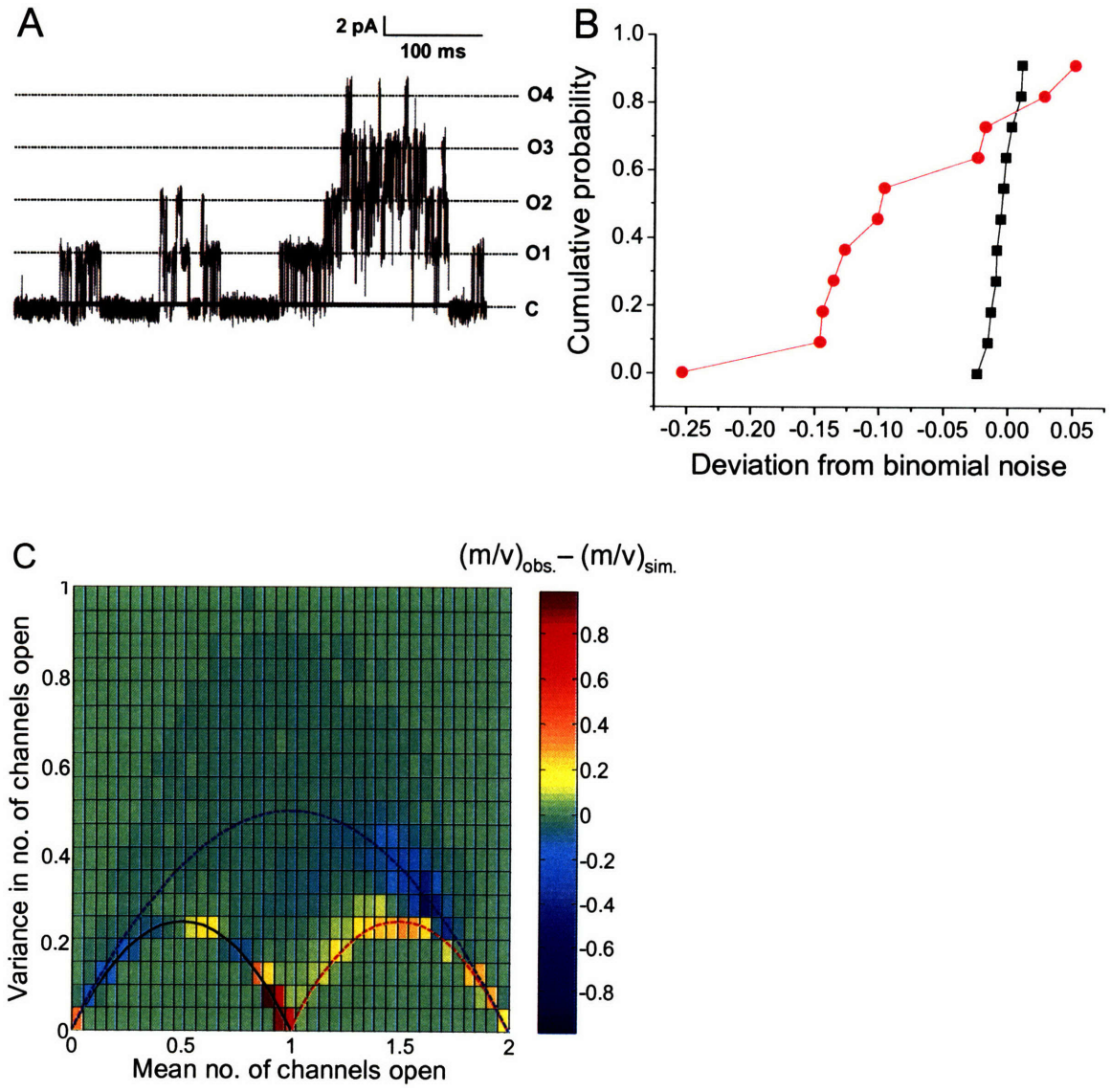

Figure 2.4. Dynamic heterogeneity in K_{ATP} gating. (A) K_{ATP} currents shift between high- and low-activity modes. The number of open channels was averaged for every 5 ms. (B) Power spectral density from the records of one-channel patches (red open circles, observed records; black open circles, randomized records; red solid line, a fit with three-Lorentzian functions for observed records; black solid line, a fit with three-Lorentzian functions for randomized records). (C) Power spectral density from the records of multichannel patches with low noise (red open circles, observed records; black open circles, randomized records; red solid line, a $1/f^{\beta}$ fit for observed records; black solid line, a fit with three-Lorentzian functions for randomized records). (D) Power spectral density from the records of multichannel patches with high noise (red open circles, observed records; black open circles, randomized records; red solid line, a fit with three-Lorentzian functions for observed records; black solid line, a fit with three-Lorentzian functions for randomized records).

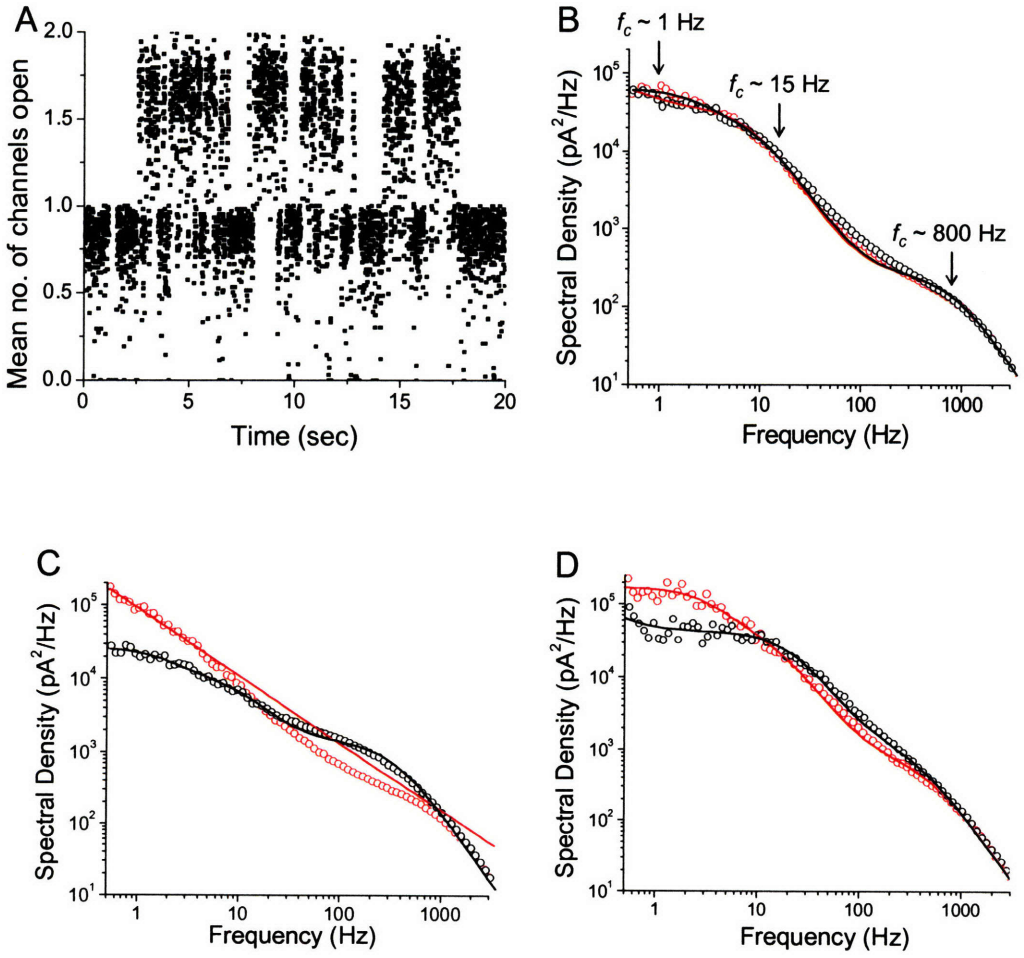

Figure 2.5. SUR1 is required for robust negative coupling in K_{ATP} gating. (A) Representative patch clamp recordings of individual Kir6.2 ΔC1-26 channels from a multichannel patch. (B) Dynamic heterogeneity in currents is weak in the absence of SUR1. The number of open channels was averaged for every 5 ms. (C) Power spectral density from the records of multi-channel patches of Kir6.2 ΔC1-26 channels with low noise (red open circles, observed records; black open circles, randomized records; red solid line, a $1/f^{\beta}$ fit for observed records).

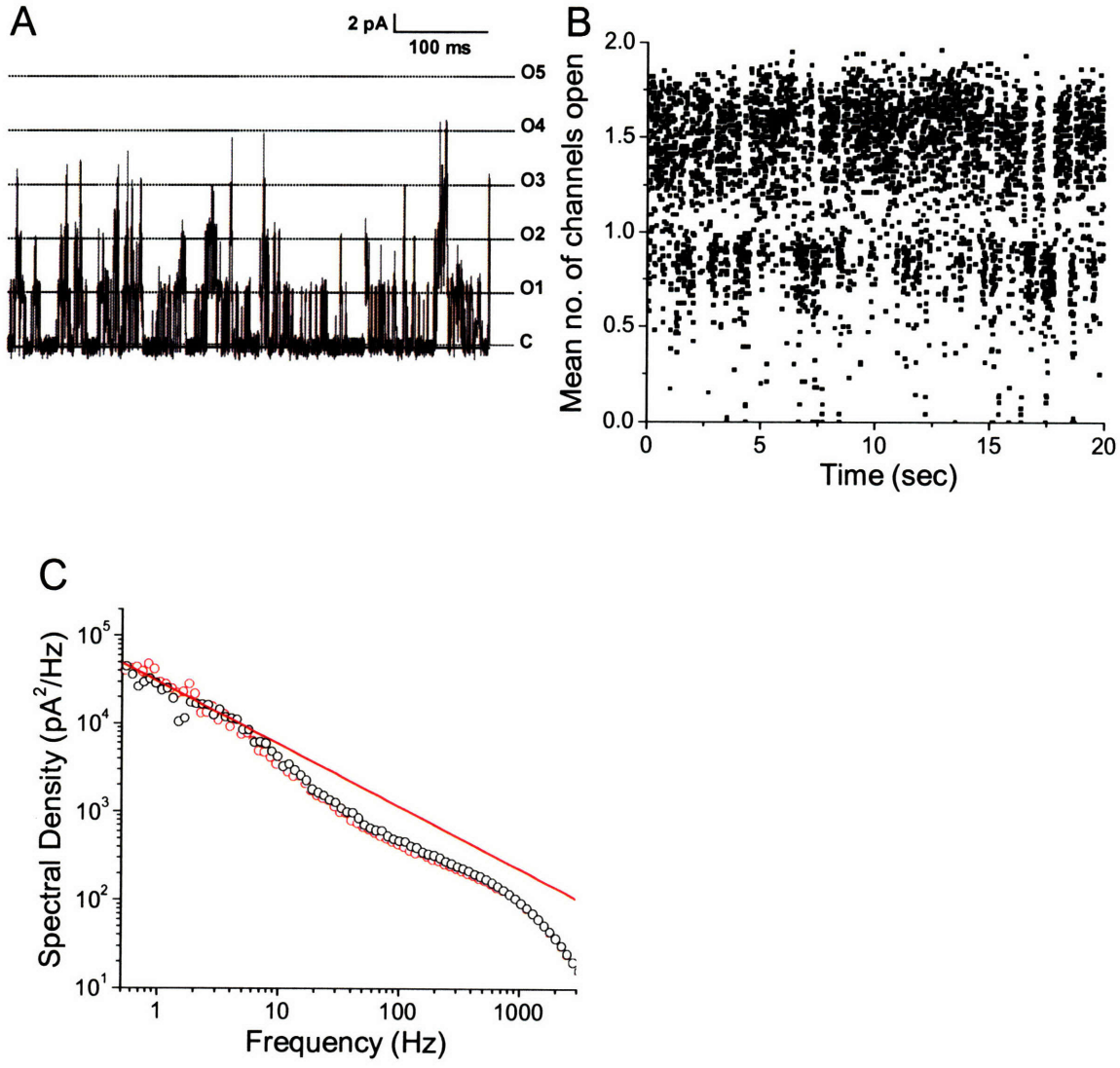

Figure 2.6. Decreased noise output observed for the SUR1-free mutant is attributed to static heterogeneity. (A) Cumulative probability histograms for deviations from identical and independent behavior (red circles, SUR1 + Kir6.2; black squares, Kir6.2 ΔC1-26). (B) Static mixtures of high-P_{open} and low-P_{open} channels account for decreased noise in the absence of SUR1 (red circles, SUR1 + Kir6.2; black squares, Kir6.2 ΔC1-26).

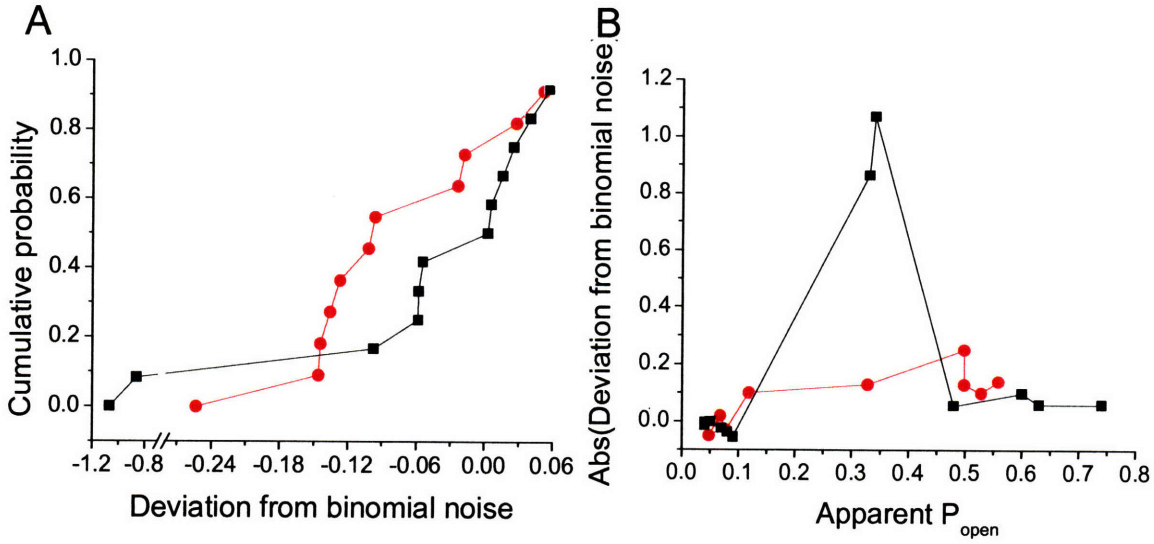

Figure 2.7. Modeling of fluctuations in membrane potential. (A) Schematic of model cell containing an ATP-sensitive hyperpolarizing conductance (red) and a depolarizing conductance (green). (B) Fluctuations (standard deviation, υ) in the membrane potential are reduced ~10-15% by negative interactions (red solid line, negatively coupled channels; black dotted line, identical and independent channels). (C) The signal-to-noise ratio (SNR) is increased ~25-40% by negative coupling (red solid line, negatively coupled channels; black dotted line, identical and independent channels). (D) Negative coupling decreases the probability that a cell at rest will become excited due to noise in the membrane potential by ~50% (red solid line, negatively coupled channels; black dotted line, identical and independent channels).

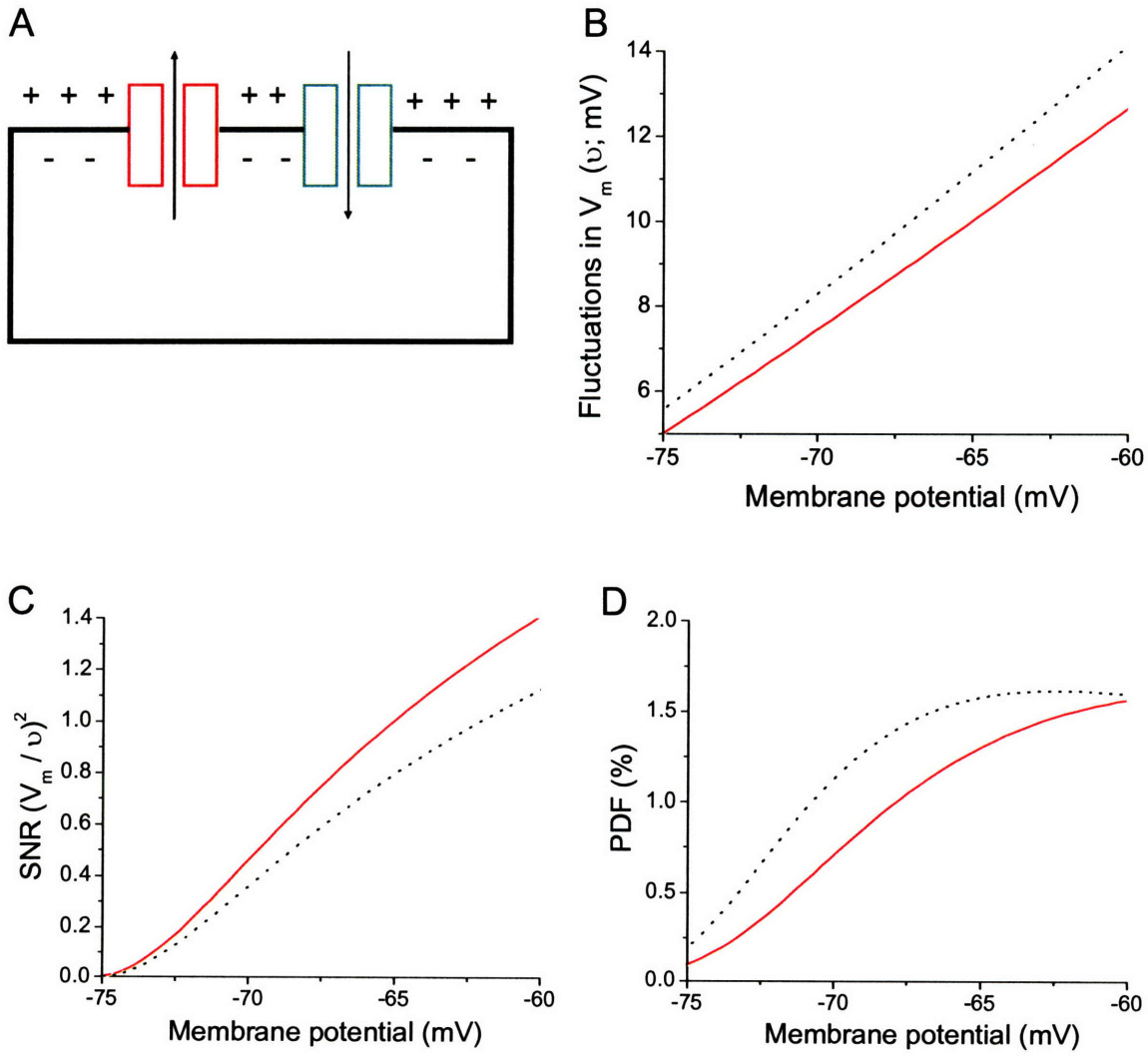

Figure 2.8. Proposed mechanism for noise control in K_{ATP} gating. K_{ATP} channels (sectors, SUR1; circles, Kir6.2) are linked (transiently or stably) via interactions between SUR1 subunits. Occupancy of one channel in the open state (yellow/orange) disfavors open state occupancy of its neighbors (blue/purple), mitigating large fluctuations in channel activity and decreasing the total noise output.

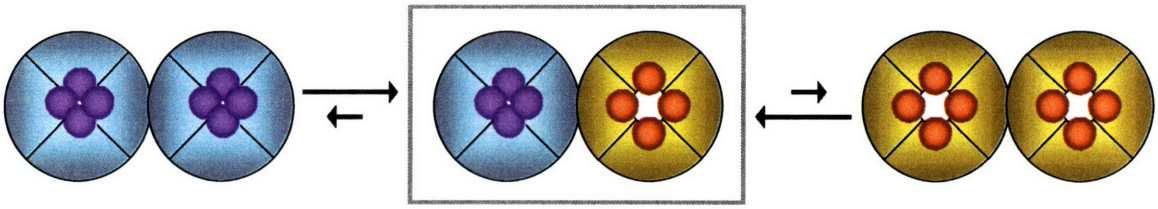

Table 2.1. Patch properties of K_{ATP} and Kir6.2 ΔC1-26 channels

	Patch	Decrease in noise output	Apparent P_{open}	Exponent, β
K_{ATP}	Low-noise (n = 7)	14 ± 2%	0.40 ± 0.06	0.96 ± 0.05
	High-noise (n = 4)	1 ± 2%	0.09 ± 0.03	0.60 ± 0.03
Kir6.2 ΔC1-26	Low-noise (n = 6)	37 ± 19%	0.52 ± 0.07	0.76 ± 0.03
	High-noise (n = 6)	2 ± 1%	0.06 ± 0.01	0.35 ± 0.04

* Results are means ± S.E.M.

2.9. References

1. Satin, L. S., and P. D. Smolen. 1994. Electrical bursting in beta-cells of the pancreatic islets of langerhans. Endocrine 2:677-687.
2. Nichols, C. G. 2006. K_{ATP} channels as molecular sensors of cellular metabolism. Nature 440:470-476.
3. Beguin, P., K. Nagashima, M. Nishimura, T. Gonoi, and S. Seino. 1999. PKA-mediated phosphorylation of the human K_{ATP} channel: separate roles of Kir6.2 and SUR1 subunit phosphorylation. EMBO J 18:4722-4732.
4. Lin, Y. F., Y. N. Jan, and L. Y. Jan. 2000. Regulation of ATP-sensitive potassium channel function by protein kinase A-mediated phosphorylation in transfected HEK293 cells. EMBO J 19:942-955.
5. Ribalet, B., S. A. John, and J. N. Weiss. 2000. Regulation of cloned ATP-sensitive K channels by phosphorylation, MgADP, and phosphatidylinositol bisphosphate (PIP_2). A study of channel rundown and reactivation. J Gen Physiol 116:391-409.
6. Light, P. E., C. Bladen, R. J. Winkfein, M. P. Walsh, and R. J. French. 2000. Molecular basis of protein kinase C-induced activation of ATP-sensitive potassium channels. Proc Natl Acad Sci U S A 97:9058-9063.
7. Baukrowitz, T., U. Schulte, D. Oliver, S. Herlitze, T. Krauter, S. J. Tucker, J. P. Ruppersberg, and B. Fakler. 1998. PIP2 and PIP as determinants for ATP inhibition of K_{ATP} channels. Science 282:1141-1144.
8. Shyng, S. L., and C. G. Nichols. 1998. Membrane phospholipid control of nucleotide sensitivity of K_{ATP} channels. Science 282:1138-1141.
9. Branstrom, R., B. E. Corkey, P. O. Berggren, and O. Larsson. 1997. Evidence for a unique long chain acyl-CoA ester binding site on the ATP-regulated potassium channel in mouse pancreatic beta cells. J Biol Chem 272:17390-17394.
10. Liu, G. X., P. J. Hanley, J. Ray, and J. Daut. 2001. Long-chain acyl-coenzyme A esters and fatty acids directly link metabolism to K_{ATP} channels in the heart. Circ Res 88:918-924.
11. Manning Fox, J. E., C. G. Nichols, and P. E. Light. 2004. Activation of adenosine triphosphate-sensitive potassium channels by acyl coenzyme A esters involves multiple phosphatidylinositol 4,5-bisphosphate-interacting residues. Mol Endocrinol 18:679-686.
12. Ma, W., J. Berg, and G. Yellen. 2007. Ketogenic diet metabolites reduce firing in central neurons by opening K_{ATP} channels. J Neurosci 27:3618-3625.
13. Fan, Z., K. Nakayama, T. Sawanobori, and M. Hiraoka. 1992. Aromatic aldehydes and aromatic ketones open ATP-sensitive K+ channels in guinea-pig ventricular myocytes. Pflugers Arch 421:409-415.
14. Raser, J. M., and E. K. O'Shea. 2005. Noise in gene expression: origins, consequences, and control. Science 309:2010-2013.
15. Diba, K., H. A. Lester, and C. Koch. 2004. Intrinsic noise in cultured hippocampal neurons: experiment and modeling. J Neurosci 24:9723-9733.
16. Faber, D. S., W. S. Young, P. Legendre, and H. Korn. 1992. Intrinsic quantal variability due to stochastic properties of receptor-transmitter interactions. Science 258:1494-1498.

17. Franks, K. M., C. F. Stevens, and T. J. Sejnowski. 2003. Independent sources of quantal variability at single glutamatergic synapses. J Neurosci 23:3186-3195.
18. Traynelis, S. F., and F. Jaramillo. 1998. Getting the most out of noise in the central nervous system. Trends Neurosci 21:137-145.
19. Nimchinsky, E. A., R. Yasuda, T. G. Oertner, and K. Svoboda. 2004. The number of glutamate receptors opened by synaptic stimulation in single hippocampal spines. J Neurosci 24:2054-2064.
20. Ashcroft, F. M., and P. Rorsman. 1989. Electrophysiology of the pancreatic beta-cell. Prog Biophys Mol Biol 54:87-143.
21. Kinard, T. A., G. de Vries, A. Sherman, and L. S. Satin. 1999. Modulation of the bursting properties of single mouse pancreatic beta-cells by artificial conductances. Biophys J 76:1423-1435.
22. Qin, F., A. Auerbach, and F. Sachs. 1997. Maximum likelihood estimation of aggregated Markov processes. Proc R Soc Lond B Biol Sci 264:375-383.
23. Qin, F., A. Auerbach, and F. Sachs. 2000. A direct optimization approach to hidden Markov modeling for single channel kinetics. Biophys J 79:1915-1927.
24. Hamill, O. P., A. Marty, E. Neher, B. Sakmann, and F. J. Sigworth. 1981. Improved patch-clamp techniques for high-resolution current recording from cells and cell-free membrane patches. Pflug Arch Eur J Phy 391:85-100.
25. Sakmann, B., and E. Neher. 1995. Single-channel recording. Plenum Press, New York, NY.
26. Lin, Y. W., T. Jia, A. M. Weinsoft, and S. L. Shyng. 2003. Stabilization of the activity of ATP-sensitive potassium channels by ion pairs formed between adjacent Kir6.2 subunits. J Gen Physiol 122:225-237.
27. Colquhoun, D., and A. G. Hawkes. 1995. The principles of the stochastic interpretation of ion-channel mechanisms. In Single-channel recording. B. Sakmann, and E. Neher, editors. Plenum Press, New York, NY. 397-482.
28. Hille, B. 2001. Ion channels of excitable membranes. Sinauer, Sunderland, MA.
29. Cook, D. L., L. S. Satin, M. L. J. Ashford, and C. N. Hales. 1988. ATP-sensitive K+ channels in pancreatic beta-cells. Spare-channel hypothesis. Diabetes 37:495-498.
30. Rorsman, P., and G. Trube. 1985. Glucose dependent K+ channels in pancreatic beta-cells are regulated by intracellular ATP. Pflug Arch Eur J Phy 405:305-309.
31. Liu, Y., and J. P. Dilger. 1993. Application of the one-dimensional and two-dimensional Ising models to studies of cooperativity between ion channels. Biophys J 64:26-35.
32. Oosawa, F. 2001. Spontaneous signal generation in living cells. B Math Biol 63:643-654.
33. Kenyon, J. L., and R. J. Bauer. 2000. Amplitude histograms can identify positively but not negatively coupled channels. J Neurosci Meth 96:105-111.
34. Enkvetchakul, D., G. Loussouarn, E. Makhina, S. L. Shyng, and C. G. Nichols. 2000. The kinetic and physical basis of K_{ATP} channel gating: toward a unified molecular understanding. Biophys J 78:2334-2348.
35. Loussouarn, G., L. J. Pike, F. M. Ashcroft, E. N. Makhina, and C. G. Nichols. 2001. Dynamic sensitivity of ATP-sensitive K+ channels to ATP. J Biol Chem 276:29098-29103.

36. Manivannan, K., S. V. Ramanan, R. T. Mathias, and P. R. Brink. 1992. Multichannel recordings from membranes which contain gap junctions. Biophys J 61:216-227.
37. Neher, E., and C. F. Stevens. 1977. Conductance fluctuations and ionic pores in membranes. Annu Rev Biophys Bioeng 6:345-381.
38. Tucker, S. J., F. M. Gribble, C. Zhao, S. Trapp, and F. M. Ashcroft. 1997. Truncation of Kir6.2 produces ATP-sensitive K+ channels in the absence of the sulphonylurea receptor. Nature 387:179-183.
39. Babenko, A. P., G. Gonzalez, L. Aguilar-Bryan, and J. Bryan. 1999. Sulfonylurea receptors set the maximal open probability, ATP sensitivity and plasma membrane density of K_{ATP} channels. Febs Lett 445:131-136.
40. Zerangue, N., B. Schwappach, Y. N. Jan, and L. Y. Jan. 1999. A new ER trafficking signal regulates the subunit stoichiometry of plasma membrane K_{ATP} channels. Neuron 22:537-548.
41. Geng, X. H., L. H. Li, S. Watkins, P. D. Robbins, and P. Drain. 2003. The insulin secretory granule is the major site of K_{ATP} channels of the endocrine pancreas. Diabetes 52:767-776.
42. Hehl, S., and B. Neumcke. 1993. Negative cooperativity may explain flat concentration-response curves of ATP-sensitive potassium channels. Eur Biophys J Biophy 22:1-4.
43. Campbell, J. D., M. S. P. Sansom, and F. M. Ashcroft. 2003. Potassium channel regulation. Structural insights into the function of the nucleotide-binding domains of the human sulphonylurea receptor. Embo Rep 4:1038-1042.
44. Mikhailov, M. V., J. D. Campbell, H. de Wet, K. Shimomura, B. Zadek, R. F. Collins, M. S. P. Sansom, R. C. Ford, and F. M. Ashcroft. 2005. 3-D structural and functional characterization of the purified K_{ATP} channel complex Kir6.2-SUR1. EMBO J 24:4166-4175.
45. Gu, C. X., P. F. Juranka, and C. E. Morris. 2001. Stretch-activation and stretch-inactivation of *Shaker*-IR, a voltage-gated K+ channel. Biophys J 80:2678-2693.
46. Lundbaek, J. A., P. Birn, A. J. Hansen, R. Sogaard, C. Nielsen, J. Girshman, M. J. Bruno, S. E. Tape, J. Egebjerg, D. V. Greathouse, G. L. Mattice, R. E. Koeppe, 2nd, and O. S. Andersen. 2004. Regulation of sodium channel function by bilayer elasticity: the importance of hydrophobic coupling. Effects of micelle-forming amphiphiles and cholesterol. J Gen Physiol 123:599-621.
47. Andersen, O. S., and R. E. Koeppe, 2nd. 2007. Bilayer thickness and membrane protein function: an energetic perspective. Annu Rev Biophys Biomol Struct 36:107-130.
48. Erecinska, M., J. Bryla, M. Michalik, M. D. Meglasson, and D. Nelson. 1992. Energy metabolism in islets of Langerhans. Biochim Biophys Acta 1101:273-295.
49. Voet, D., and J. G. Voet. 2004. Biochemistry. J. Wiley & Sons, New York, NY.
50. Marx, S. O., K. Ondrias, and A. R. Marks. 1998. Coupled gating between individual skeletal muscle Ca2+ release channels (ryanodine receptors). Science 281:818-821.
51. Yeramian, E., A. Trautmann, and P. Claverie. 1986. Acetylcholine receptors are not functionally independent. Biophys J 50:253-263.

52. Iwasa, K., G. Ehrenstein, N. Moran, and M. Jia. 1986. Evidence for interactions between batrachotoxin-modified channels in hybrid neuroblastoma-cells. Biophys J 50:531-537.

Chapter 3

Testing for Violations of Microscopic Reversibility in ATP-Sensitive Potassium Channel Gating

3.1. Abstract

In pancreatic beta cells, insulin secretion is tightly controlled by the cells' metabolic state via the ATP-sensitive potassium (K_{ATP}) channels. ATP is a key mediator in this signaling process, where its role as an inhibitor of K_{ATP} channels has been extensively studied. Since the channel contains an ATPase as an accessory subunit, the possibility that ATP hydrolysis mediates K_{ATP} channel opening has also been proposed. However, a rigorous test of coupling between ATP hydrolysis and channel gating has not previously been performed. In the present work, we examine whether K_{ATP} channel gating obeys detailed balance in order to determine whether ATP hydrolysis is strongly coupled to the gating of the K_{ATP} channel. Single-channel records were obtained from inside-out patches of transiently transfected HEK-293 cells. Channel activity in membrane patches with exactly one channel shows no violations of microscopic reversibility. Although K_{ATP} channel gating shows long closed times on the timescale where ATP hydrolysis takes place, the time symmetry of channel gating indicates that it is not tightly coupled to ATP hydrolysis. This lack of coupling suggests that channel gating operates close to equilibrium; although detailed balance is not expected to hold for ATP hydrolysis, it still does so in channel gating. Based on these results, the function of the ATPase active site in channel gating may be to sense nucleotides by differential binding of ATP and ADP, rather than to drive a thermodynamically unfavorable conformational change.

3.2. Introduction

K_{ATP} channels mediate coupling between the transmembrane electrical potential of cells and their metabolic state (1). ADP, present in larger quantities than ATP when the cell has depleted its energy stores, stimulates channel opening, while ATP inhibits it. These channels are the first component in the signal transduction pathway leading to insulin secretion from pancreatic beta cells, and they are the target of the clinically important sulfonylurea class of diabetes medications (2).

Native K_{ATP} channels consist of two functionally distinct gene products (3, 4). One, called Kir6.2, is a potassium channel. It provides the pore for conduction of ions, switching between a "closed" non-conducting state and an "open" conducting state in a nucleotide-dependent manner and thereby mediating rapid changes in transmembrane potential. It has an ATP-binding site and a phosphatidylinositol-4,5-bisphosphate (PIP_2)-binding site. The other, called the sulfonylurea receptor (SUR1), is homologous to the ATP-binding cassette (ABC) family of transporters, which use the free energy of hydrolysis of ATP to transport small molecules and peptides across the cell membrane (5). SUR1 contains the binding site for sulfonylureas (6), as well as two nucleotide binding domains (NBDs), which can bind ATP or ADP (7, 8). In this work, we investigate the possible role of ATP hydrolysis in K_{ATP} gating (i.e., the protein conformational changes that open and close the channel). Measurements of channel gating kinetics at the single-molecule level are used to determine whether channel gating exhibits the violations of microscopic reversibility expected if it is tightly coupled to ATP hydrolysis.

Several lines of evidence point to a role for ATP hydrolysis in control of K_{ATP} gating. First, MgADP binding to NBD2 of SUR1 has a stimulatory effect on channel gating (7-9). Second, NBD2 of SUR1 hydrolyzes ATP in the presence of Mg^{2+} with a turnover number of ~1.5 sec^{-1} per SUR1 tetramer (10). Finally, use of inorganic ions (orthovanadate and beryllium fluoride) to stabilize the putative pre-hydrolytic and post-hydrolytic conformations of the cardiac channel (Kir6.2/SUR2A) shows that the pre-hydrolytic state favors channel closing, while the post-hydrolytic state favors channel opening (11). In suggesting that SUR1's catalytic cycle drives Kir6.2's gating

conformational change, these studies raise the question of whether ATP hydrolysis is strongly coupled to the gating of the K_{ATP} channel.

However, other lines of evidence suggest that ATP hydrolysis is not tightly coupled to channel gating. The turnover number for ATP hydrolysis by NBD2 of SUR1 is much smaller than the rate constants associated with K_{ATP} channel gating (10, 12, 13). This observation suggests that most Kir6.2 gating events occur independently of conformational transitions in SUR1. In addition, active site mutations in NBD2 of SUR1 expected to impair ATPase activity have modest effects on K_{ATP} gating (13). One complicating factor in interpreting these results is the possibility that ATPase rates in the native SUR1-Kir6.2 complex are greater than those observed in the purified, detergent-solublized preparation.

In this work, we examine coupling of ATP hydrolysis to channel opening using single-channel kinetic experiments carried out on intact SUR1-Kir6.2 complexes in cell membranes. If the gating conformational change is an equilibrium process, microscopic reversibility will be obeyed, meaning that the statistical properties of the single-channel record will not depend on time direction used to measure them; that is, they are the same whether the record is "played forwards" or "played in reverse." However, if channel gating is coupled to an irreversible reaction, the characteristics of the single-channel record will not be time direction-invariant: its statistical properties will be different when it is "played in reverse." Thus, if channel gating is tightly coupled to an irreversible process such as ATP hydrolysis, the gating reaction will not exhibit microscopic reversibility (14).

Several methods were previously used to test microscopic reversibility in single-channel experiments. One method is to obtain maximum likelihood estimates of rate constants from single-channel data either with or without the constraint of detailed balance, and compare the maximum likelihoods from each estimate (15). If channel gating does not obey microscopic reversibility, the maximum likelihood will be greater without the detailed balance constraint than with it. A number of ion channels, including the muscle-type nicotinic acetylcholine receptor (nAChR) (16) and *N*-methyl-*D*-aspartate

(NMDA) receptors (NR1-NR2A, NR2B, or NR2C) (17, 18) have been analyzed using this method. The resulting likelihood ratios suggested that gating transitions between fully-open states and closed states of these channels is time-reversible. A second method is to compare two-dimensional distributions of pairs of adjacent open and closed dwell-times in forward and reverse time directions; these distributions will differ if gating violates microscopic reversibility (19). This method was used for analysis of the gating of a large conductance Ca^{2+}-activated potassium (BK) channel (19). The difference between the two distributions was not statistically significant, consistent with the hypothesis that BK channel gating obeys microscopic reversibility. Cross-correlation functions of open and closed dwell-times were also used to test time reversibility in channel gating (20, 21). This approach was applied to single-channel records from the locust muscle glutamate receptor (GluR) (20). Cross-correlation functions in the forward/reverse time directions appeared to be identical, suggesting that GluR gating is an equilibrium process.

Only a few ion channels to date have been shown to be driven by external energy sources. The cystic fibrosis transmembrane conductance regulator (CFTR), a chloride channel, exhibits non-equilibrium gating (22). This channel is an ATPase and a member of the ATP-binding cassette superfamily (23). A one-dimensional dwell-time distribution analysis was used to test violations of microscopic reversibility of CFTR gating. When gating takes place at thermodynamic equilibrium, dwell-time distributions will be a sum of decaying exponential components with their maxima at $t = 0$ (24). For CFTR, however, closed time distributions for CFTR have maxima at times greater than zero; the paucity of short closed events constitutes strong evidence that an irreversible step must precede channel opening. The ATP concentration dependence of CFTR gating rate constants suggests that ATP hydrolysis is this irreversible step (22).

For several channels, non-equilibrium transitions are observed among subconductance states (states with conductances intermediate between fully closed and fully open). This type of non-equilibrium gating is observed in the *Torpedo* ClC-0 chloride channels (25, 26), nAChRs (27), both recombinant and native NMDA receptors (NR1-NR2D) (28-30), and mutant NMDA receptors (NR1 N598Q-NR2A) (31). Non-equilibrium transitions between subconductance states were also observed in curare-

activated nAChR gating (32) and the Ba^{2+}-induced BK channel gating (33). The external energy sources for gating asymmetry are unclear in some cases. However, irreversible gating of the ClC-0 chloride channels and the NMDA receptors appeared to be driven by flow of the permeant ions down the transmembrane electrochemical gradient (25, 26, 31).

3.3. Methods

Molecular biology. Mouse pCMV-Kir6.2 and hamster pECE-SUR1 cDNA were provided by S. Seino (Chiba University, Chiba, Japan) and J. Bryan (Baylor College of Medicine, Houston, TX), respectively. A stop codon was introduced into the mouse Kir6.2 cDNA to delete the last 26 amino acids of the C-terminus (Kir6.2 ΔC1-26) using the QuikChange® Site-Directed Mutagenesis Kit (Stratagene, La Jolla, CA). All cDNA constructs were verified by DNA sequencing (MIT Biopolymers Lab, Cambridge, MA). Plasmids were prepared for transient transfection using the QIAfilter™ Plasmid Maxi Kit (QIAGEN Inc., Valencia, CA).

Cell culture. Human embryonic kidney (HEK) 293 cells (American Type Culture Collection, Manassas, VA) were cultured in Dulbecco's modified Eagle's medium containing 10% (v/v) fetal bovine serum in humidified 5% CO_2 at 37°C. Cells were passaged every three days by treatment with trypsin.

DNA transfection. HEK 293 cells were transiently transfected with either mouse Kir6.2 plus hamster SUR1 or with Kir6.2 ΔC1-26 cDNA. pEGFP-N1 vector (BD Biosciences, San Jose, CA) was co-transfected as a marker with the cDNA of interest using the FuGENE 6 Transfection Reagent (Roche Applied Science, Indianapolis, IN). Transfection was performed according to the manufacturer's instructions with total 1 μg of cDNA per 35-mm culture dish (2:3:5 ratio of Kir6.2, SUR1, and pEGFP-N1 or 1:4 ratio of Kir6.2 ΔC1-26 and pEGFP-N1). Transfected cells were incubated in humidified 5% CO_2 at 37°C. Approximately 36 to 72 hr after transfection, the cells were used for single-channel recordings.

Electrophysiology. Micropipettes were pulled from borosilicate glass capillaries (MTW 1B150F-4; World Precision Instruments Inc., Sarasota, FL) on a puller (PP-830; Narishige Group, Tokyo, Japan) with resistance typically ~5-12 MΩ. Pulled pipettes were coated with Sylgard (Dow Corning Corporation, Midland, MI) and fire-polished using a microforge (MF-830; Narishige Group, Tokyo, Japan) to reduce the noise level. Single-channel currents were recorded using the inside-out patch clamp configuration at a

membrane potential of –80 mV, with the pipette (extracellular) solution containing (in mM): 140 KCl, 10 NaCl, 1.1 $MgCl_2$, and 10 K-HEPES, pH to 7.3 and with the bath (intracellular) solution containing (in mM): 140 KCl, 10 NaCl, 1.1 $MgCl_2$, 0.5 $CaCl_2$, 5 K-EGTA, and 10 K-HEPES, pH to 7.3 (34). 1 mM MgATP (ATP magnesium salt; Sigma, St. Louis, MO) and 5 μM PIP_2 (Calbiochem, San Diego, CA) were directly added to the bath solution (35). Single-channel recordings were performed at room temperature with an Axopatch 200B patch clamp amplifier (Axon Instruments Inc., Union City, CA) and were low-pass filtered (10 kHz) with a 4-pole Bessel filter. Single-channel data were acquired and digitized at 20 kHz using QuB software (www.qub.buffalo.edu) (36, 37).

Single-channel data analysis. K_{ATP} channel recordings where only single openings but no double openings (i.e., two channels open simultaneously) were observed for 10 min were analyzed. Digitized single-channel records were filtered at 5 kHz and idealized using the half-amplitude method with the QuB software. The observed open probability (P_o) is 0.46 ± 0.09 (N = 5, S.D.) with a lowest P_o observed of 0.39. Dwell-time distributions were fitted using the maximum interval likelihood (MIL) function in the QuB software suite, which provides maximum likelihood estimates for rate constants in a specified model. A dead time of 0.1 ms was used for missed event correction (24).

When n_o consecutive single openings have been observed, the probability of observing more single openings before the first multiple opening occurs is $P(r \geq n_o) = \pi^{(no-1)}$, where r is a total number of consecutive single openings and π is the probability that one open channel is closed before a second channel is open (24). The probability π can be estimated as $(1 - P_o) / (1 - P_o/N)$, where N is the actual number of independent channels in the patch. An observed K_{ATP} channel record contains ~2 x 10^5 consecutive single openings with P_o of ≥0.39. The probability of a run this long, $P(r \geq 2 \times 10^5)$, therefore, would be < 0.0001 if there were two channels present, so it is very likely that exactly one channel is present.

3.4. Results

To test for violations of microscopic reversibility due to ATP hydrolysis, single-channel currents were recorded from inside-out membrane patches of transiently transfected HEK-293 cells in the presence of 1 mM MgATP and 5 μM PIP_2 in the bath solution (Figure 3.1). These conditions are expected to allow both channel opening and ATP hydrolysis (10, 38). PIP_2 has been identified as a modulator that binds to Kir6.2 subunits and adjusts the apparent inhibition constant (K_i) for ATP to within the range of cytosolic [ATP]; K_is of ATP for K_{ATP} inhibition in the absence or presence of 5 μM PIP_2 are 10.5 μM and 3.6 mM, respectively (38, 39). ATP concentration in the millimolar range is expected to support SUR1-catalyzed ATP hydrolysis since K_M for ATP hydrolysis by the purified K_{ATP} channel is 0.4 mM (10). Membrane patches containing exactly one channel were analyzed (see Methods), and an open probability (P_o) of 0.46 ± 0.09 (N = 5, S.D.) was observed.

Kinetically distinct states of K_{ATP} have been observed in previous single-channel electrophysiological studies (40-43). Binding of MgATP drives the K_{ATP} complex into a long-lived closed state. Binding of MgADP, on the other hand, drives the channel into a bursting state in which the channel rapidly opens and closes. If channel gating is tightly coupled to ATP hydrolysis, these kinetically defined states of K_{ATP} – a bursting state and an interburst closed state – might correspond to intermediates in the ATP hydrolysis cycle. Single-channel records were analyzed to determine whether transitions between the bursting and interburst states exhibit detailed balance violations.

Dwell-time distribution analysis. If an irreversible step is present in K_{ATP} channel gating, the characteristic dwell time on the interburst closed state or the bursting state will be determined by the ATP hydrolysis rate at SUR1. A paucity of short events in the probability density function of the dwell-time distribution is predicted if an irreversible enzymatic step precedes channel gating since the "hidden" enzymatic step acts to introduce a lag time into observed transitions (24). The probability density functions of burst lengths and interburst closed dwell-times pooled from the five membrane patches (distributions were calculated for ~6.0×10^4 events using a bin size of 1 ms; a critical time

of 1 ms was used for assigning burst lengths (24)) were determined. These distributions were exponential, having maxima at time zero as judged by dwell-time histograms (Figure 3.2). The one-dimensional dwell-time distributions are therefore consistent with channel gating occurring independently of ATP hydrolysis.

Maximum likelihood analysis. As another test for non-equilibrium gating, correlations in time between observations of kinetically defined states were measured. Violations of microscopic reversibility would correspond to excursions through a cyclic mechanism in one direction (e.g., clockwise) occurring more frequently than excursions in the other direction (e.g. counterclockwise); in other words, detailed balance would not be obeyed. Thus, violations of microscopic reversibility in channel gating can be detected by determining whether imposing the detailed balance constraint decreases the maximum likelihood (44). The significance of the increase in the maximum likelihood by removing the detailed balance constraint can be statistically evaluated using the likelihood ratio test. The difference between the log likelihoods (LLs) multiplied by a factor of 2 is asymptotically distributed as the χ^2 statistic. Thus, one can assess for statistical significance using χ^2 significance levels. Since detailed balance imposes one constraint, the χ^2 has 1 degree of freedom. When the twofold likelihood ratio ($2\Delta LL$) is greater than 3.84, the observed increase in the maximum log likelihood is significant at the 5% level.

For maximum likelihood fitting, a kinetic scheme containing the two open states (O_1 and O_4), the intraburst closed state (C_f) and the two interburst closed states (C_2 and C_3) was used (Figure 3.3.A). Although more complex models have also been proposed for K_{ATP} channel gating (41, 42, 45), the two-open-three-closed-states model is widely accepted and used for wild-type K_{ATP} channel in the presence of ATP and PIP_2 (34, 45). Since bursting kinetics is an intrinsic property of Kir6.2 channel (42, 46), intraburst open and closing events are presumably not affected by ATP hydrolysis by SUR1. In this model, thus, the intraburst closed state (C_f) is placed out of the cycle so that only the burst/interburst transitions are subject to the detailed balance constraint. The open and closed dwell-time distributions were fitted to the kinetic model in Figure 3.3.A either without or with the constraint of detailed balance ($O_1 \rightarrow C_2 \rightarrow C_3 \rightarrow O_4$) (Figure 3.3.B and 3.3.C). LL/event calculated from the maximum likelihood fitting of each file (~2.1×10^5

events) is 6.5 ± 0.1 (N = 5, S.D.) with absolute LLs of ~1.3×10^6. The difference in maximum log likelihoods obtained for the constrained and unconstrained fitting is not statistically significant for any of the five recordings (2ΔLL of 0.1 ± 0.1 < 3.84), consistent with an absence of microscopic reversibility violations.

Two-dimensional dwell-time distribution analysis. As a further test for microscopic reversibility violations, two-dimensional (2D) dwell-time distributions were obtained from single-channel recordings in the forward and in the reverse directions in time. The 2D distributions of pairs of adjacent burst and interburst dwell-times represent the frequency of occurrence and correlation between adjacent dwell times (47). If detailed balance is obeyed, there will be no difference between the 2D distributions in the forward/reverse time directions (14). A χ^2 test can be performed to determine whether differences between the two distributions are significant. If the Z-score, defined as $(2\chi)^{1/2} - (2D - 1)^{1/2}$, from a χ^2 test is higher than 1.96 with more than 100 degrees of freedom (D), violations of microscopic reversibility are significant at the 5% level, i.e., microscopic reversibility is violated (48). The 2D dwell-time distributions calculated in forward and reverse time directions from K_{ATP} single-channel recordings (> 10,000 events with 1 ms critical time) are identical within experimental uncertainty (Figure 3.4); Z-score of 1.7 ± 0.1 (N = 5, S.E.M.) with > 200 degrees of freedom.

Cross-correlation function analysis. Cross-correlation functions have also been used to test for violations of microscopic reversibility (20). Cross-correlation functions for kinetically distinguishable states will be non-symmetric with respect to the sign/direction of time if microscopic reversibility is violated (49). The dwell-time cross-correlation function is defined by $G_{oc}(k) = \text{Cov}\,[O(i), C(i+k)] / (\text{Var}\,[O(i)]\ \text{Var}\,[C(i)])^{0.5}$, where Cov is covariance, $O(i)$ is the ith open time, $C(i)$ is the ith closed time, k is the lag (0, 1, ...) and Var is variance. The same holds for cross-correlation function in the opposite time direction, defined by $G_{co}(k) = \text{Cov}\,[C(i), O(i+k)] / (\text{Var}\,[C(i)]\ \text{Var}\,[O(i)])^{0.5}$. Non-null cross-correlation functions can be observed when the minimum (N_p) of the number of open gateway states and closed gateway states (i.e., states directly linked to a state of the opposite class, such as an open state linked to a closed state (50)) is larger than 1 (51, 52), as is the case for the cyclic models considered here. At thermodynamic

equilibrium, the open-closed and closed-open cross-correlations ($G_{oc}(k)$ and $G_{co}(k)$) are identical. Inequality of $G_{oc}(k)$ and $G_{co}(k)$, on the other hand, would be consistent with irreversibility in channel gating.

Open and closed dwell-times from five K_{ATP} single-channel records (~1.3×10^6 events) were pooled to generate cross-correlation functions. Obtained cross-correlation functions revealed a weak, negative correlation between closed times and preceding and following open times up to a lag ~k = 10 (Figure 3.5). Non-zero cross-correlations indicate multiple gateway states ($N_p > 1$) in the underlying mechanism of the K_{ATP} channel gating. The negative correlation indicates that the long closed state is linked to the relatively short open state (16). These are consistent with the previously proposed kinetic mechanism of K_{ATP} channel gating (34, 45). There was no significant difference between $G_{oc}(k)$ and $G_{co}(k)$ obtained from K_{ATP} single-channel data (Figure 3.5). The cross-correlation analysis is therefore consistent with gating of K_{ATP} occurring as an equilibrium process.

Detection limit of each method. Because no significant violations of microscopic reversibility were detected using any of the tests employed, it is important to establish lower limits for the magnitude of detailed balance violations detectable by these methods. To examine what extent of irreversibility is detectable by each method, single-channel data were first simulated with the best fit model for the observed K_{ATP} channel recordings (Figure 3.3.A) with the same record length as the experimental records (10 min) using the following rate constants (sec^{-1}): k_{21} = 100, k_{23} = 100, k_{32} = 100, k_{43} = 100, k_{41} = 100, k_{14} = 100, k_{15} = 5000, k_{51} = 5000. Single-channel data with detailed balance violations of varying magnitude were generated by varying k_{12} and k_{34}. The magnitude of detailed balance violations can be quantified by calculating the asymmetry in the transition frequencies, which can be expressed by $(f_{AB} - f_{BA}) / (f_{AB} + f_{BA})$ when the transition frequency f_{AB} from state A to state B is given by the product of the equilibrium occupancy p_A times the rate constant for the transition k_{AB} (53). The equilibrium state occupancies were calculated using the Q-matrix method (54).

A 2.7% violation of detailed balance (k_{12} and k_{34} = 90 sec^{-1}) was not detectable using any of the methods; 2ΔLL of 3.1 (< 3.84) and Z-score of 0.7 (< 1.96). When the detailed balance violation was increased to 4.2% (k_{12} and k_{34} = 85 sec^{-1}), it was detectable by the maximum likelihood analysis but not by the 2D dwell-time distribution analysis; 2ΔLL of 16.7 and Z-score of 0.7. Finally, a detailed balance violation of 5.9% (k_{12} and k_{34} = 80 sec^{-1}) was detected both by the 2D dwell-time distribution analysis and the maximum likelihood analysis; 2ΔLL of 15.0 and Z-score of 2.9.

ATP-independent violations of microscopic reversibility on timescales longer than burst/interburst transitions. K_{ATP} also appears to undergo changes in activity on timescales longer than those associated with the predominant transition between bursting and non-bursting states. As previously observed (41, 46, 55), the closed time distribution for K_{ATP} exhibits a number of closed components longer than the predominant interburst interval of ~10 ms. Qualitatively, large shifts in average channel activity are observable on the timescale of seconds and above (Figure 3.6.A).

To determine whether the slow changes in average channel activity obey microscopic reversibility, third-order correlation functions, defined as $G_2(\tau_1, \tau_2) = < A(0)A(\tau_1)A(\tau_1 + \tau_2) >$ (49), were calculated for records in which activity $A(t)$ was averaged over 100 ms (Figure 3.6.B). For thermodynamically reversible processes, the third-order correlation function is symmetric with respect to the sign/direction of time, and equal to its transpose when expressed as a matrix. The difference between the third-order correlation function and its transpose ($G_2 - G_2^T$) therefore provides a way to measure violations of microscopic reversibility.

Third-order correlation functions for average K_{ATP} activity are not symmetric, consistent with violations of microscopic reversibility (Figure 3.7.A). The experimentally observed maximum relative asymmetry ($G_2 - G_2^T$ = 0.015 ± 0.002; N = 7, S.E.M.) is comparable to that observed in simulated records of comparable length in which detailed balance is violated ($G_2 - G_2^T$ = 0.01 ± 0.001; N = 5, S.E.M.) (Figure 3.8.B). In the simulated data, asymmetry in the third-order correlation functions is apparent at timescales > 1 sec, as expected from the mechanism used, in which transitions through the cycle

occur on the timescale of seconds. Asymmetry in the experimental data is pronounced only on timescales > 1 sec as well, indicating that if it is associated with bursting/non-bursting transitions, it can only be associated with the slowest of these transitions. For both simulated and experimental data, decay in the third-order correlation function is evident on timescales > 1 sec (Figure 3.9), indicating that the observed asymmetry is not simply due to random fluctuations in uncorrelated channel activity.

The SUR1 subunit is necessary for violations of microscopic reversibility to occur. Channel activity for a mutant Kir6.2 channel that can be expressed in the absence of SUR1 (56) exhibits a symmetric third-order correlation function (Figure 3.7.B) ($G_2 - G_2^T$ = 0.003 ± 0.001; N = 5, S.E.M., comparable to simulated records for a gating reaction at equilibrium where $G_2 - G_2^T$ = 0.006 ± 0.001; N = 5, S.E.M.; Figure 3.8.C). However, ATP is not required for violations of microscopic reversibility to be observed (Figure 3.7.C). Recordings obtained in the absence of bath-applied ATP exhibit asymmetric third-order correlation functions ($G_2 - G_2^T$ = 0.012 ± 0.002; N = 6, S.E.M.), indistinguishable from those observed in the presence of ATP. These observations indicate that slow conformational changes of K_{ATP} are coupled to an irreversible process other than ATP hydrolysis.

Kinetic identifiability in detection of microscopic reversibility violations. For ion channel systems that lack subconductance states (conformations with conductance intermediate between open and closed), distinguishing between equilibrium and non-equilibrium mechanisms can be difficult. Irreversible transitions may not be detected if they connect states that cannot be distinguished. However, kinetic criteria are also valid for identifying states.

A cyclic mechanism with three different bursting states (Figure 3.10.A) provides an example of a mechanism that contains kinetically identifiable states. For this mechanism, the bursting states differ in their opening rate constants, and are linked by irreversible transitions. Rate constants are as follows (sec^{-1}): k_{12}, k_{23}, k_{31} = 1, k_{13}, k_{32}, k_{21} = 0.001, k_{41}, k_{52}, k_{63} = 1000, k_{14} = 100, k_{25} = 400 and k_{36} = 1600. Simulations indicate that the open probability varies in a regular, cyclic fashion; open probabilities shift from low to medium

to high, and then back to low (Figure 3.10.B). The third-order correlation function calculated from this record (averaged over 50 ms windows) is asymmetric (Figure 3.10.C). Thus, even though this mechanism contains only two classes of conductance states (open and closed), the kinetic identifiability of states allows violations of microscopic reversibility to be observed. A similar result is observed when only two of the bursting states exhibit different open probabilities, i.e., $k_{14} = k_{25} = 400$ sec^{-1} and $k_{36} = 1600$ sec^{-1} (Figure 3.11).

In contrast, violations of microscopic reversibility are not detectable for a non-equilibrium cyclic mechanism in which the bursting states have identical kinetic properties, i.e., $k_{14} = k_{25} = k_{36} = 400$ sec^{-1}. Simulations of this mechanism indicate that the open probability does not vary with time (Figure 3.12.A), and the third-order correlation function is symmetric (Figure 3.12.B). In this case, there are not enough kinetically identifiable states for microscopic reversibility violations to be detected.

These simulations illustrate that a channel with only two conductance states may still have a sufficient number of kinetically identifiable states to detect violations of microscopic reversibility. However, a non-equilibrium process may not exhibit observable violations of microscopic reversibility due to a lack of kinetically identifiable states as shown in present simulations. As for other tests of microscopic reversibility, the absence of detectable microscopic reversibility violations thus does not rule out a non-equilibrium mechanism. Nonetheless, the detection of microscopic reversibility violations indicates that a sufficient number of kinetically identifiable states are present, and channel gating is not an equilibrium process.

3.5. Discussion

Lack of evidence for violations of detailed balance in the dominant mode of K_{ATP} channel gating. The four dwell-time-based analyses used to test for deviations from microscopic reversibility provide no evidence for such deviations. Each method, however, has a limit on the magnitude of microscopic reversibility violations that it can detect. For records of the length used in this study, 2D dwell-time distribution analysis has the detection limit of ~6% irreversible opening and closing transitions. One could detect up to ~4% irreversible gating using the maximum likelihood analysis. Thus, even if there is a small excess of flux through one direction of a gating cycle, it is less than ~4-6% of the total gating transitions.

In addition to the detection limit on the magnitude of detailed balance violations, there are unique issues of interpretation associated with each of the analyses. The maximum likelihood analysis is most sensitive in detecting violations and statistically straightforward because the log likelihood ratio distribution follows a χ^2 distribution (44). However, unlike the other analyses, the maximum likelihood analysis is model-dependent, since it assumes a specific gating mechanism. Unambiguous assignment of detailed gating mechanisms is generally difficult since multiple mechanisms often provide comparably good fits to the data when the underlying kinetics is complex. In addition, the maximum likelihood analysis is performed based on the aggregated Markov models where the estimation of the transition rates is burdened by the issue of the non-identifiability in certain models (44). If transition rates from two formally distinct states are equal, dwell times arising from those states may not be experimentally identifiable as arising from separate states, lowering the power to detect violations of microscopic reversibility. Dwell-time distribution analysis is limited by uncertainties associated with finite record length. These uncertainties are greatest in the tails of histograms, i.e., the longer timescales, where bins have the lowest counts. Long recordings are thus required to minimize these uncertainties. Finally, cross-correlation function analysis is more general and easy to carry out. However, cross-correlation functions may also be of insufficient magnitude to be interpreted for time reversibility. Omission of short dwell-times (bursting events) due to the finite bandwidth of records may decrease the apparent magnitude of

correlations (20), as would be the case if there is a correlation between the occurrence of long closed dwells and short open dwells. Also, when the rates of the open-open and closed-closed transitions are fast compared to the rates of open-closing transitions, the degree of cross-correlation could be reduced (20).

Time-asymmetric slow activity changes do not require ATP hydrolysis. Although analyses of the relatively fast (1-100 ms) gating conformational changes of K_{ATP} provide no evidence for violations of microscopic reversibility, slower changes in activity do violate microscopic reversibility as determined by the observation of time-asymmetric third-order correlation functions. The observed time-asymmetry in third-order correlation functions might arise from a slow increase or decrease in open probability, i.e., non-stationary records could manifest itself as apparent violations of microscopic reversibility. To investigate this possibility, a test for stationarity of channel activity was performed by calculating the linear trend in channel activity (averaged over 10 ms). Channel activity of wild-type and mutant channels changes globally at a rate of 5×10^{-4} and 7×10^{-4} channel openings/sec (0.2-0.3% of the mean activity per second), respectively. The global trends are comparable for the mutant, which exhibits negligible asymmetry in its third-order correlation function, as for the wild-type, which exhibits measurable asymmetry; global trends in channel activity therefore appear not to account for the observed asymmetry in the third-order correlation function.

As for the dwell-time-based methods described above, third-order correlation functions will fail to detect microscopic reversibility violations if the mechanism does not have a sufficient number of identifiable states. In previous work (21, 49), it has been noted that ion channel systems often fail to meet this criterion because the open and closed states are the only states of distinguishable conductance. However, states that are identifiable kinetically rather than through conductance also produce time asymmetric third-order correlation functions. For K_{ATP}, the multiple non-bursting states (observed as multiple kinetic components in the closed time distribution) are likely to be the kinetically identifiable states that allow time-asymmetric third-order correlation functions to be observed.

Coupling to some irreversible processes appears to require the presence of the SUR1 subunit since the recordings of the Kir6.2 subunit alone exhibit time-symmetric third-order correlation functions. However, the deviations from microscopic reversibility are independent of the presence of ATP. The lack of ATP dependence supports the conclusion that ATP hydrolysis by SUR1 is not directly coupled to conformational changes of Kir6.2. However, the observation of SUR1-dependent time-asymmetric behavior suggests that K_{ATP} gating is coupled to some other irreversible processes. One potential candidate is PIP_2 hydrolysis. PIP_2 is present in HEK-293 membranes, and phospholipase C (the enzyme that hydrolyzes PIP_2) may be retained in membrane patches since it is membrane-associated (57). Modulation of K_{ATP} activity coupled to ongoing PIP_2 hydrolysis might account for the violations of microscopic reversibility observed on the timescale of seconds. If PIP_2 is depleted slowly over the course of the experimental record, but individual hydrolysis events take place on the timescale of seconds, microscopic reversibility violations might be observed due to local depletion of PIP_2 without being accompanied by substantial macroscopic rundown. Slow PIP_2-dependent rundown (on the timescale of hours at submicromolar Ca^{2+}) has been reported previously for K_{ATP} (58); at the higher calcium concentrations used in the current experiments, this process might still be sufficiently slow to account for the observed microscopic reversibility violations without causing large decreases in open probability. Previous studies indicate that the C-terminal truncation affects channel trafficking without affecting channel gating (56); differences between mutant and wild-type channels are thus not likely to be due to the lack of the C-terminus in the mutant. Allosteric interactions between SUR1 and phospholipase C might facilitate PIP_2 hydrolysis by phospholipase C, which may account for SUR1-depedent non-equilibrium processes. Further studies will be required to resolve these issues.

Implications for the physiological role of the SUR1 ATPase active site. The lack of observed microscopic reversibility violations associated with ATP hydrolysis suggests that the physiological role of SUR1 is not to couple ATP hydrolysis to gating of Kir6.2. However, previous work has clearly shown that binding of nucleotides to the SUR1 NBDs affects channel activity (7-9). One possibility that accommodates all of the kinetic data is that ATP hydrolysis is much slower than channel gating in the intact, native channel. In

that case, MgATP and MgADP would act much like classical allosteric inhibitors/activators of channel activity. Binding of MgATP or MgADP to the SUR1 NBDs would shift the conformational equilibrium to the non-bursting and bursting conformations, respectively. However, direct transitions between MgATP-bound and MgADP-bound states via ATP hydrolysis would be rare compared to indirect transitions via dissociation of one nucleotide and binding of the other nucleotide (Figure 3.13). In this mechanism, the NBDs can be thought of as sensing relative nucleotide concentration through equilibrium binding rather than as motors driving a cycle of gating conformational changes.

3.6. Conclusion

Coupling of the K_{ATP} channel gating reaction to the thermodynamically irreversible ATP hydrolysis reaction has been proposed. Using single-channel kinetics, the microscopic reversibility of gating reactions was quantitatively characterized to address the question of whether K_{ATP} carries out non-equilibrium gating. Based on consistent results from several independent analyses, the dominant mode of channel gating does not violate microscopic reversibility, implying that ATP hydrolysis is not directly coupled to channel gating. Signatures of irreversibility are observed at longer timescales, but these are not associated with ATP hydrolysis. Thus, SUR1 might act as a sensor of ATP/ADP ratio in the presence of saturating ATP physiologically, rather than act as a motor to drive the gating conformational change.

3.7. Figures

Figure 3.1. A representative recording of a single K_{ATP} channel in an excised inside-out patch. (A) Open probability (P_o) of K_{ATP} channel in the presence of 1 mM ATP and 5 μM PIP_2 is 0.46 ± 0.09 (N = 5, S.D.). (B) The expanded single-channel trace of K_{ATP} channel shows closed and open states.

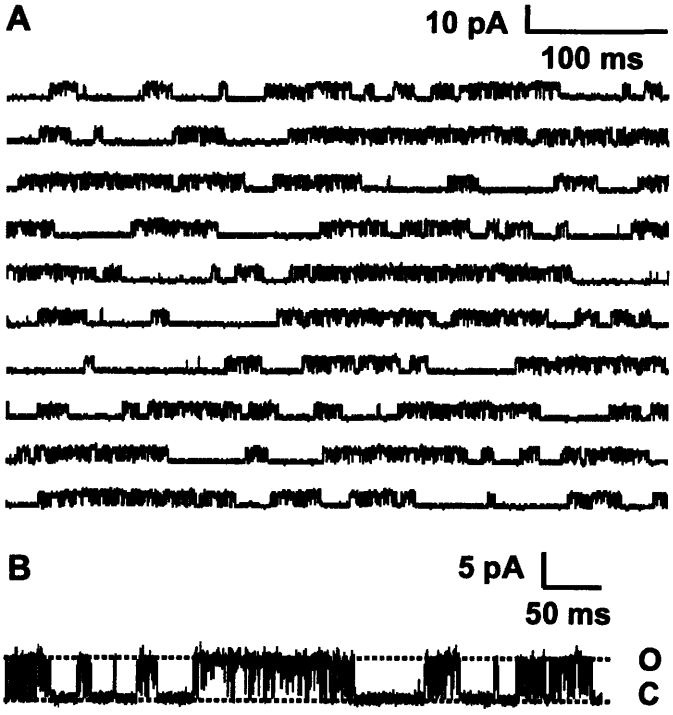

Figure 3.2. Dwell-time distribution analysis. Probability density function of the interburst closed time (A) and the burst length (B) distributions of K_{ATP} channels (~6.0 × 10^4 events with 1 ms critical time to define a burst; a bin size of 1 ms). A smaller bin size up to 0.1 ms (dead time) failed to detect any paucity of short events in the observed exponential distributions of the dwell times.

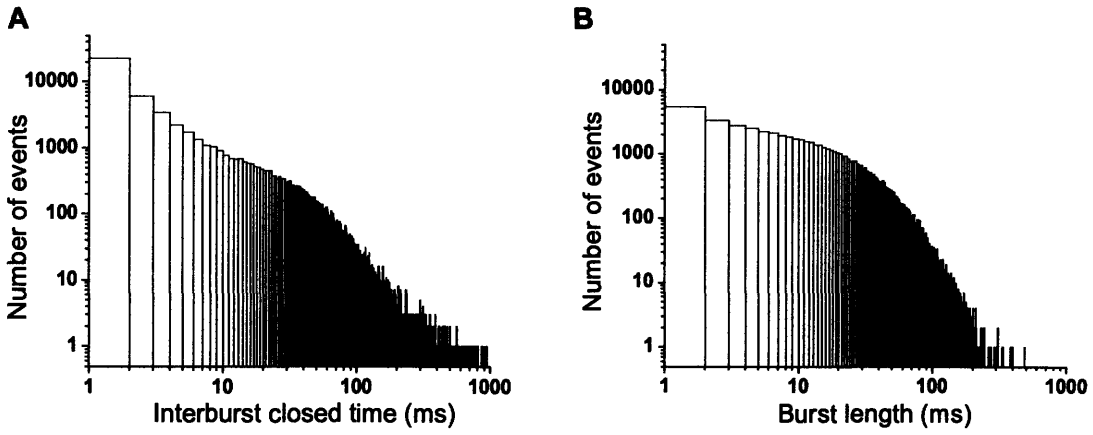

Figure 3.3. Maximum likelihood analysis. (A) A kinetic scheme contains the two open states (O_1 and O_4), the intraburst closed state (C_f) and the two interburst closed states (C_2 and C_3). (B) The open dwell-time histogram with the fit for a kinetic model (A) is composed of the sum (solid line) of two exponential components (dotted lines). (C) The distribution of closed times consists of the sum (solid line) of three exponential components (dotted lines). The difference in maximum log likelihoods obtained for the constrained ($O_1 \rightarrow C_2 \rightarrow C_3 \rightarrow O_4$) and unconstrained fitting is insignificant for all five recordings ($2\Delta LL$ of $0.1 \pm 0.1 < 3.84$). Each file has ~2.1×10^5 events and LL/event is 6.5 ± 0.1 (N = 5, S.D.) with absolute LLs of ~1.3×10^6.

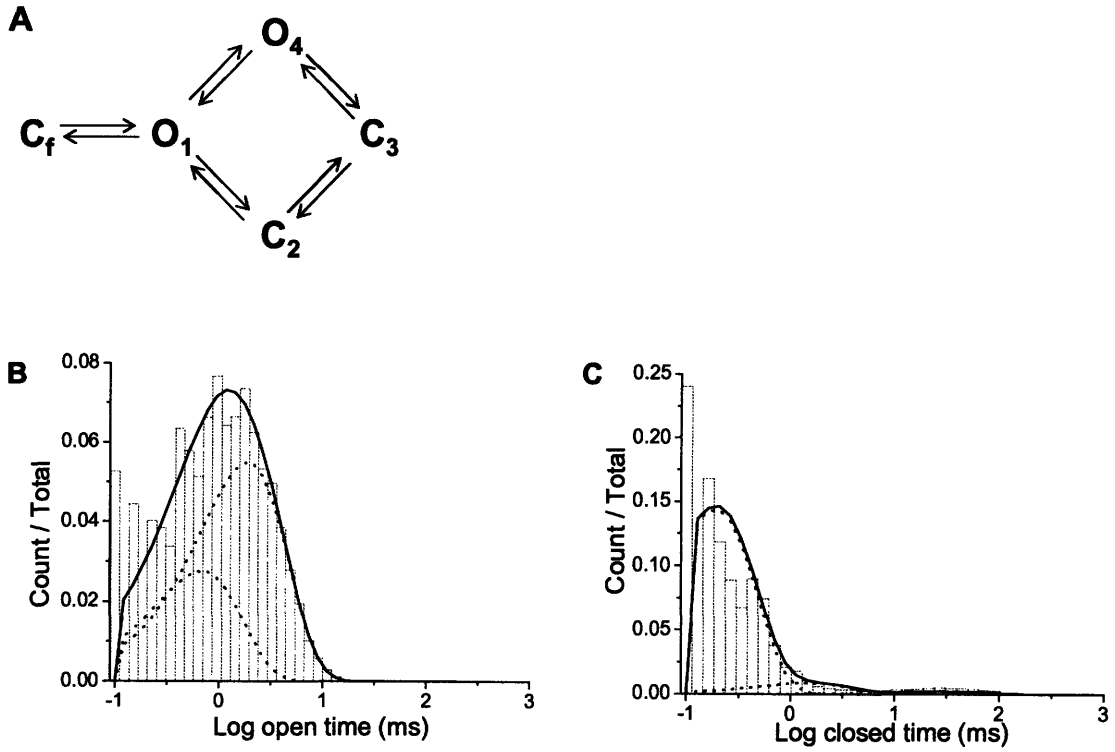

Figure 3.4. Two-dimensional dwell-time distribution analysis. The forward (A) and reverse (B) 2D dwell-time distributions from K_{ATP} single-channel recordings (> 10,000 events with 1 ms critical time to define a burst) has no statistical differences; Z-score of 1.7 ± 0.1 (N = 5, S.E.M.) with > 200 degrees of freedom. (C) The difference between the forward and reverse dwell-time distributions is not statistically significant; less than five events in each bin.

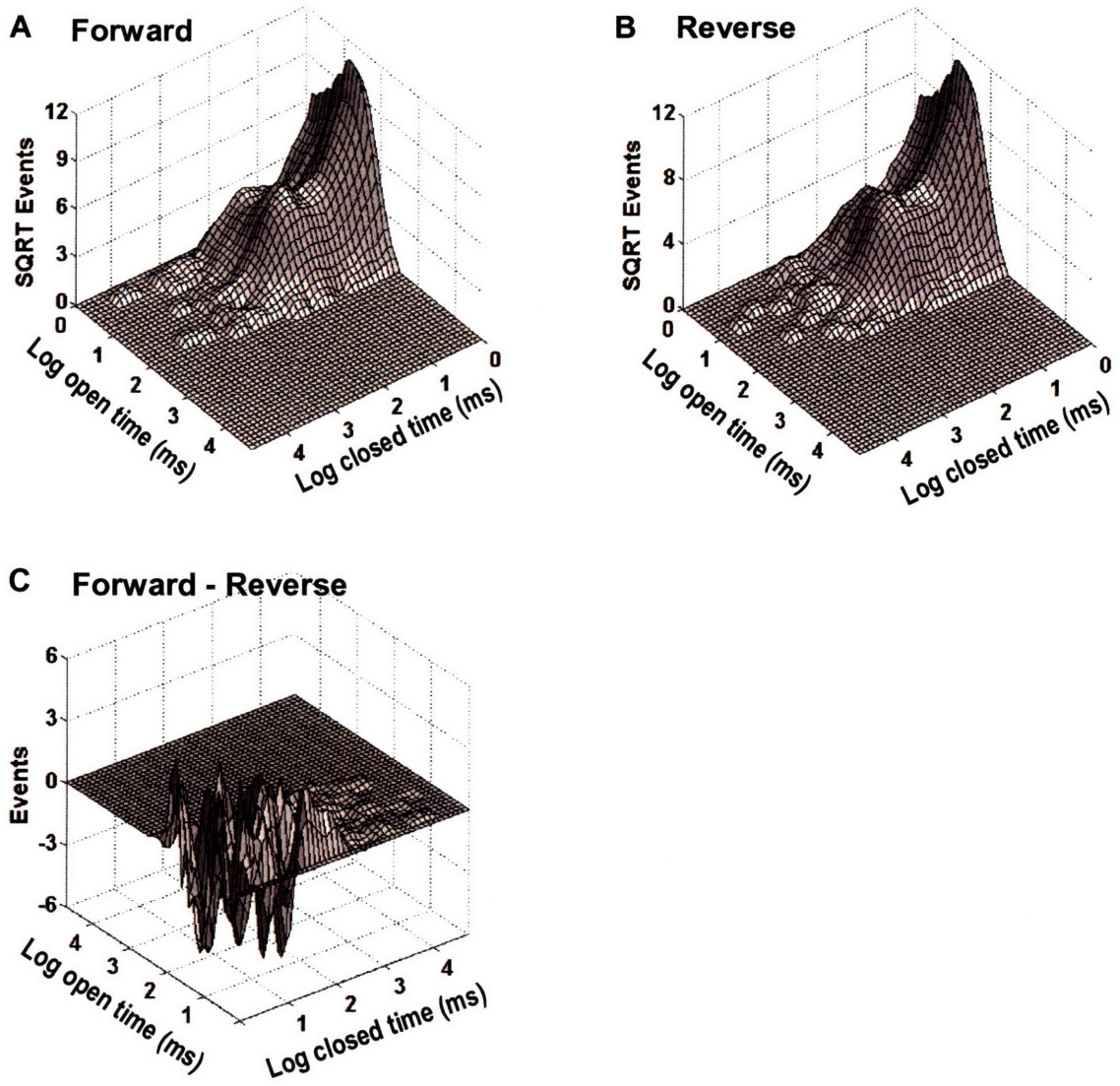

Figure 3.5. Cross-correlation function analysis. Cross-correlation functions (solid line for $G_{oc}(k)$ and dotted line for $G_{co}(k)$) derived from K_{ATP} single-channel recordings (~1.3×10^6 events from five different membrane patches) show a weak, negative cross-correlation.

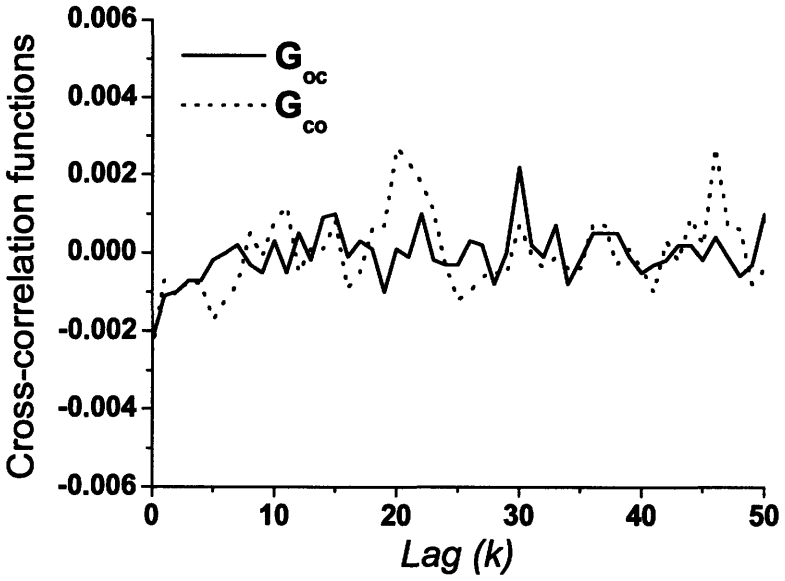

Figure 3.6. K_{ATP} undergoes changes in activity on longer timescales. (A) Channel activity changes substantially on the timescale of seconds and above; channel activity is shown as a record of idealized channel openings. (B) Channel activity (open probability, P_o) averaged over 100 ms.

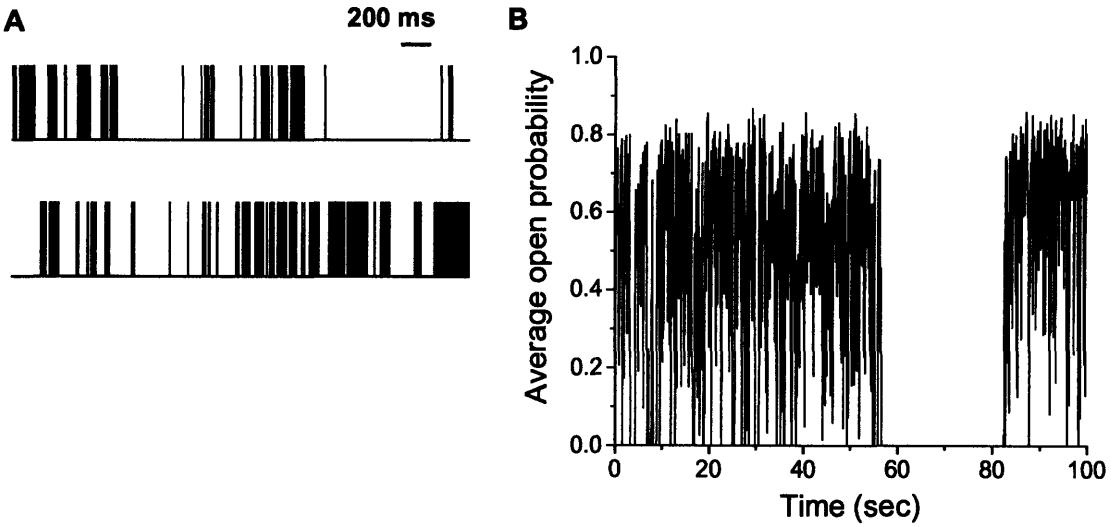

Figure 3.7. Third-order correlation functions. (A) The observed maximum relative asymmetry for average K_{ATP} activity was 0.015 ± 0.002 of $G_2 - G_2^T$. (B) Channel activity for a mutant Kir6.2 channel in the absence of SUR1 exhibits a symmetric third-order correlation function ($G_2 - G_2^T$ = 0.003 ± 0.001). (C) Recordings obtained from K_{ATP} channels in the absence of ATP exhibit asymmetric third-order correlation functions ($G_2 - G_2^T$ = 0.012 ± 0.002).

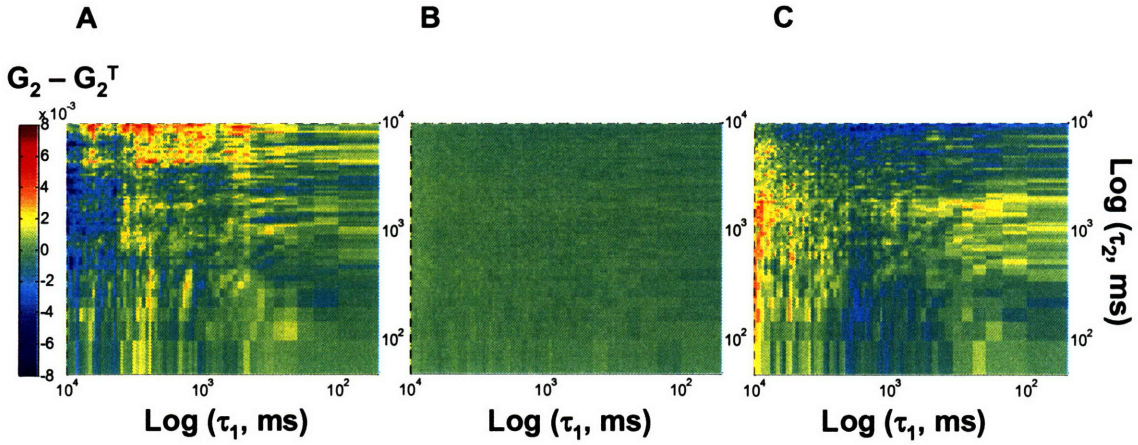

Figure 3.8. Third-order correlation functions from simulated records. (A) Cyclic mechanism for channels with bursting/non-bursting states. Detailed balance violations were introduced by changing the relative values of rate constants. Rate constants are as follows (sec^{-1}): k_{b1}, k_{1b}, k_{b3}, k_{3b} = 1000, k_{12}, k_{23} = 10, k_{34}, k_{41} = 1 and k_{14}, k_{43}, k_{32}, k_{21} = 0.001 for an irreversible mechanism, and k_{14}, k_{43} = 1 and k_{32}, k_{21} = 10 for a reversible mechanism. (B) Simulated records with the violations of detailed balance show $G_2 - G_2^T$ of 0.01 ± 0.001 (N = 5, S.E.M.). (C) Simulated records for a gating reaction at equilibrium have $G_2 - G_2^T$ of 0.006 ± 0.001 (N = 5, S.E.M.).

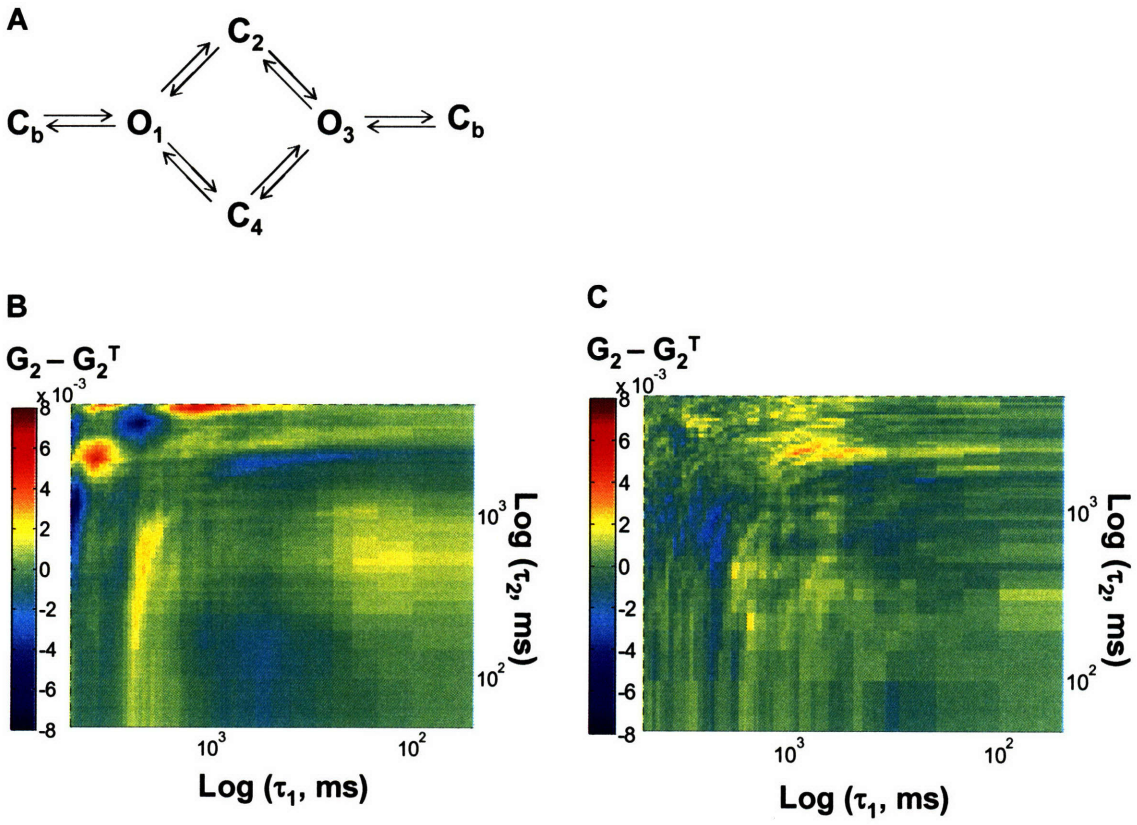

Figure 3.9. Third-order correlation function of experimental records from K_{ATP} channels. Numbers in the bar indicate the amplitude of third-order correlation functions.

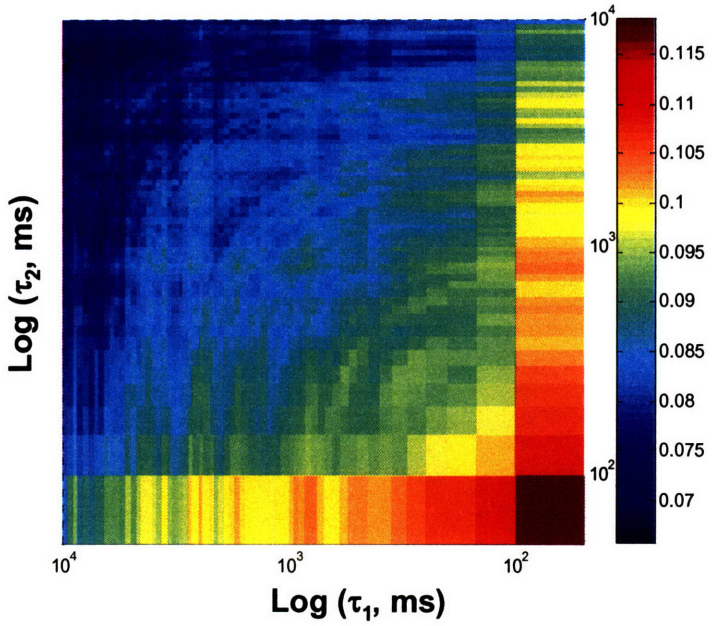

Figure 3.10. Kinetic identifiability in detection of microscopic reversibility violations. (A) A cyclic mechanism with three different bursting states. (B) The open probabilities shift from low to medium to high, and then back to low. (C) The third-order correlation function is asymmetric.

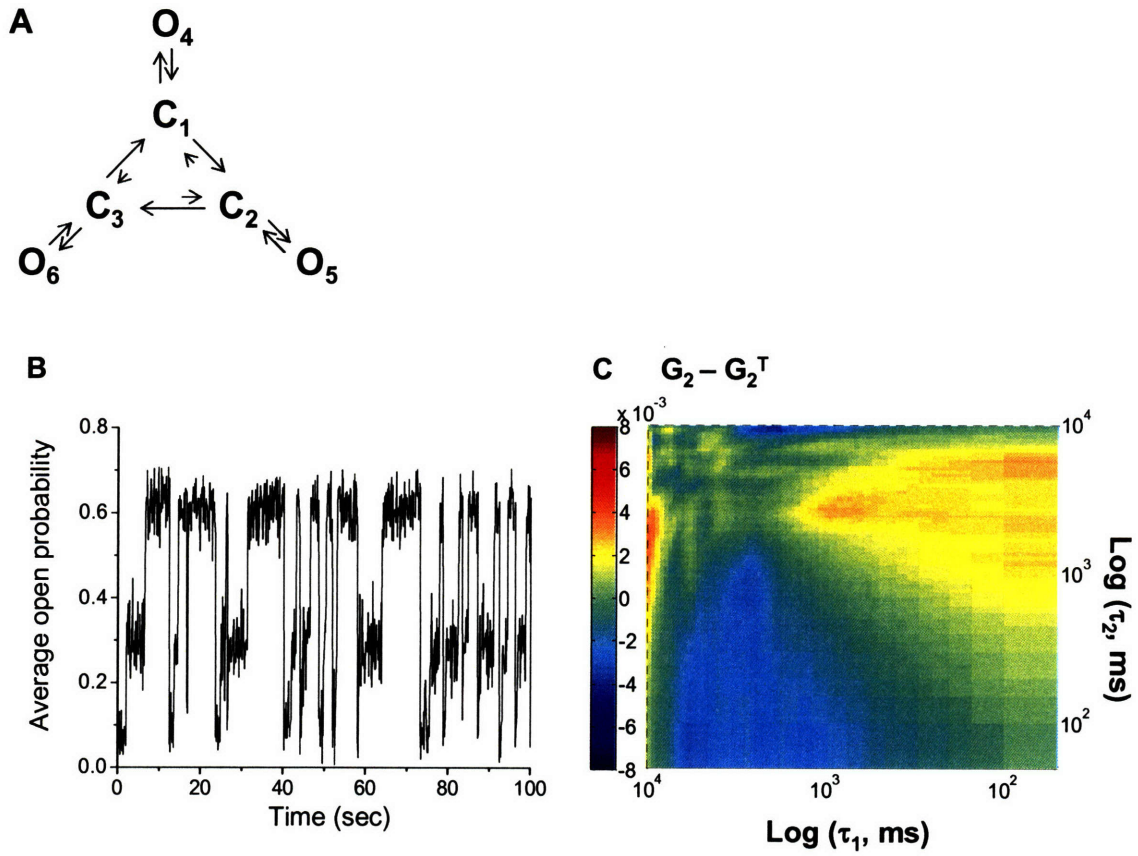

Figure 3.11. Only two kinetically identifiable bursting states. The asymmetric third-order correlation function is observed when only two of the bursting states exhibit different open probabilities.

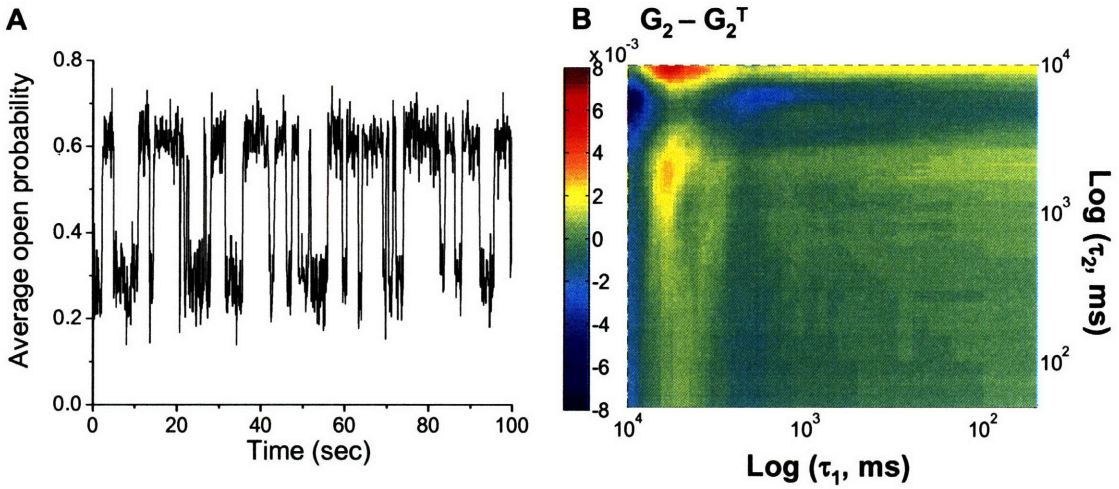

Figure 3.12. A kinetically non-identifiable and non-equilibrium cyclic mechanism. (A) The open probability does not vary with time. (B) The third-order correlation function is symmetric.

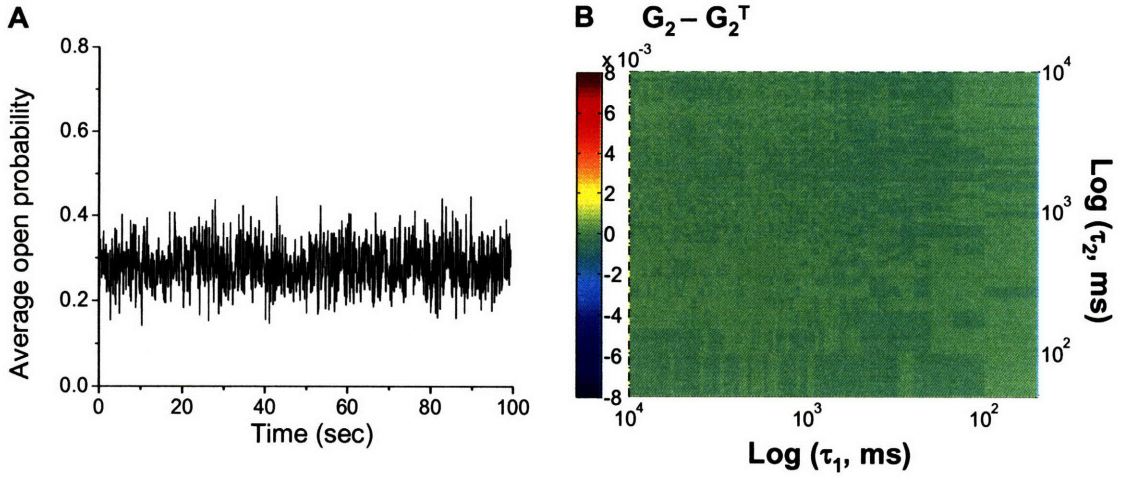

Figure 3.13. Proposed allosteric mechanism. Direct transitions between MgATP-bound and MgADP-bound states via ATP hydrolysis would be rare compared to indirect transitions via dissociation of one nucleotide and binding of the other nucleotide. Nucleotides would therefore act like allosteric inhibitors/activators of channel activity. (Different color in figure represents different microscopic rate constants.)

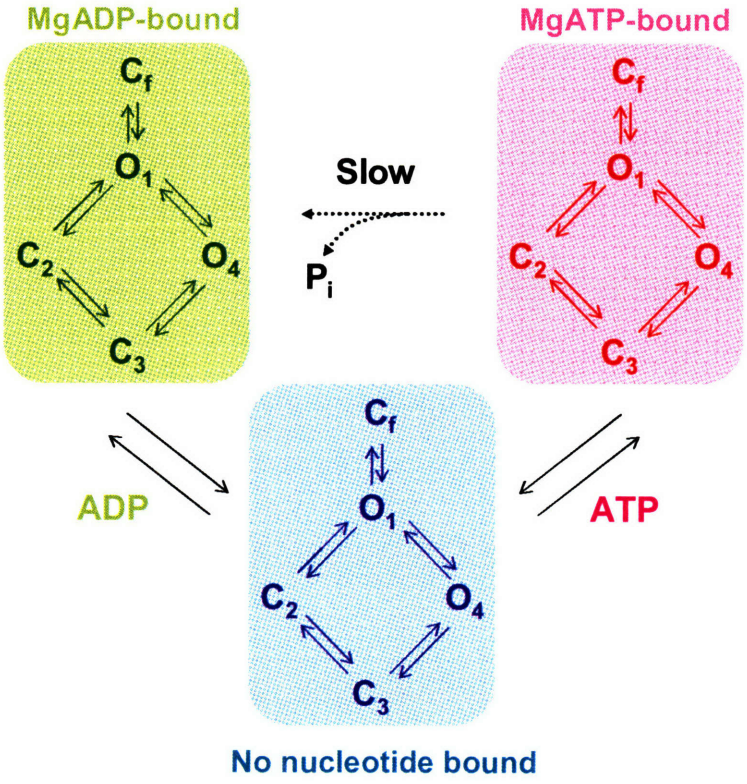

3.8. References

1. Nichols, C. G. 2006. K_{ATP} channels as molecular sensors of cellular metabolism. Nature 440:470-476.
2. Ashcroft, F. M. 2005. ATP-sensitive potassium channelopathies: focus on insulin secretion. J Clin Invest 115:2047-2058.
3. Seino, S., and T. Miki. 2003. Physiological and pathophysiological roles of ATP-sensitive K+ channels. Prog Biophys Mol Biol 81:133-176.
4. Ashcroft, F. M., and F. M. Gribble. 1998. Correlating structure and function in ATP-sensitive K+ channels. Trends Neurosci 21:288-294.
5. Jones, P. M., and A. M. George. 2000. Symmetry and structure in P-glycoprotein and ABC transporters what goes around comes around. Eur J Biochem 267:5298-5305.
6. Aguilar-Bryan, L., C. G. Nichols, S. W. Wechsler, J. P. t. Clement, A. E. Boyd, 3rd, G. Gonzalez, H. Herrera-Sosa, K. Nguy, J. Bryan, and D. A. Nelson. 1995. Cloning of the beta cell high-affinity sulfonylurea receptor: a regulator of insulin secretion. Science 268:423-426.
7. Gribble, F. M., S. J. Tucker, and F. M. Ashcroft. 1997. The essential role of the Walker A motifs of SUR1 in K_{ATP} channel activation by Mg-ADP and diazoxide. EMBO J 16:1145-1152.
8. Nichols, C. G., S. L. Shyng, A. Nestorowicz, B. Glaser, J. P. t. Clement, G. Gonzalez, L. Aguilar-Bryan, M. A. Permutt, and J. Bryan. 1996. Adenosine diphosphate as an intracellular regulator of insulin secretion. Science 272:1785-1787.
9. Shyng, S., T. Ferrigni, and C. G. Nichols. 1997. Regulation of K_{ATP} channel activity by diazoxide and MgADP. Distinct functions of the two nucleotide binding folds of the sulfonylurea receptor. J Gen Physiol 110:643-654.
10. Mikhailov, M. V., J. D. Campbell, H. de Wet, K. Shimomura, B. Zadek, R. F. Collins, M. S. P. Sansom, R. C. Ford, and F. M. Ashcroft. 2005. 3-D structural and functional characterization of the purified K_{ATP} channel complex Kir6.2-SUR1. EMBO J 24:4166-4175.
11. Zingman, L. V., A. E. Alekseev, M. Bienengraeber, D. Hodgson, A. B. Karger, P. P. Dzeja, and A. Terzic. 2001. Signaling in channel/enzyme multimers: ATPase transitions in SUR module gate ATP-sensitive K+ conductance. Neuron 31:233-245.
12. Masia, R., D. Enkvetchakul, and C. G. Nichols. 2005. Differential nucleotide regulation of K_{ATP} channels by SUR1 and SUR2A. J Mol Cell Cardiol 39:491-501.
13. Bienengraeber, M., A. E. Alekseev, M. R. Abraham, A. J. Carrasco, C. Moreau, M. Vivaudou, P. P. Dzeja, and A. Terzic. 2000. ATPase activity of the sulfonylurea receptor: a catalytic function for the K_{ATP} channel complex. FASEB J 14:1943-1952.
14. Rothberg, B. S., and K. L. Magleby. 2001. Testing for detailed balance (microscopic reversibility) in ion channel gating. Biophys J 80:3025-3026.
15. Wagner, M., and J. Timmer. 2001. Model selection in non-nested hidden Markov models for ion channel gating. J Theor Biol 208:439-450.

16. Colquhoun, D., and B. Sakmann. 1985. Fast events in single-channel currents activated by acetylcholine and its analogues at the frog muscle end-plate. J Physiol 369:501-557.
17. Gibb, A. J., and D. Colquhoun. 1992. Activation of N-methyl-D-aspartate receptors by L-glutamate in cells dissociated from adult rat hippocampus. J Physiol 456:143-179.
18. Stern, P., P. Behe, R. Schoepfer, and D. Colquhoun. 1992. Single-channel conductances of NMDA receptors expressed from cloned cDNAs: comparison with native receptors. Proc Biol Sci 250:271-277.
19. Song, L., and K. L. Magleby. 1994. Testing for microscopic reversibility in the gating of maxi K+ channels using two-dimensional dwell-time distributions. Biophys J 67:91-104.
20. Ball, F. G., C. J. Kerry, R. L. Ramsey, M. S. P. Sansom, and P. N. R. Usherwood. 1988. The use of dwell time cross-correlation functions to study single-ion channel gating kinetics. Biophys J 54:309-320.
21. Steinberg, I. Z. 1986. On the time reversal of noise signals. Biophys J 50:171-179.
22. Zeltwanger, S., F. Wang, G. T. Wang, K. D. Gillis, and T. C. Hwang. 1999. Gating of cystic fibrosis transmembrane conductance regulator chloride channels by adenosine triphosphate hydrolysis. Quantitative analysis of a cyclic gating scheme. J Gen Physiol 113:541-554.
23. Riordan, J. R., J. M. Rommens, B. Kerem, N. Alon, R. Rozmahel, Z. Grzelczak, J. Zielenski, S. Lok, N. Plavsic, J. L. Chou, and et al. 1989. Identification of the cystic fibrosis gene: cloning and characterization of complementary DNA. Science 245:1066-1073.
24. Colquhoun, D., and A. G. Hawkes. 1995. The principles of the stochastic interpretation of ion-channel mechanisms. In Single-channel recording. B. Sakmann, and E. Neher, editors. Plenum Press, New York, NY. 397-482.
25. Chen, T. Y., and C. Miller. 1996. Nonequilibrium gating and voltage dependence of the ClC-0 Cl- channel. J Gen Physiol 108:237-250.
26. Richard, E. A., and C. Miller. 1990. Steady-state coupling of ion-channel conformations to a transmembrane ion gradient. Science 247:1208-1210.
27. Hamill, O. P., and B. Sakmann. 1981. Multiple conductance states of single acetylcholine receptor channels in embryonic muscle cells. Nature 294:462-464.
28. Wyllie, D. J. A., P. Behe, M. Nassar, R. Schoepfer, and D. Colquhoun. 1996. Single-channel currents from recombinant NMDA NR1a/NR2D receptors expressed in Xenopus oocytes. Proc R Soc Lond B Biol Sci 263:1079-1086.
29. Momiyama, A., D. Feldmeyer, and S. G. Cull-Candy. 1996. Identification of a native low-conductance NMDA channel with reduced sensitivity to Mg2+ in rat central neurones. J Physiol 494:479-492.
30. Cull-Candy, S. G., and M. M. Usowicz. 1987. Multiple-conductance channels activated by excitatory amino acids in cerebellar neurons. Nature 325:525-528.
31. Schneggenburger, R., and P. Ascher. 1997. Coupling of permeation and gating in an NMDA-channel pore mutant. Neuron 18:167-177.
32. Trautmann, A. 1982. Curare can open and block ionic channels associated with cholinergic receptors. Nature 298:272-275.

33. Bello, R. A., and K. L. Magleby. 1998. Time-irreversible subconductance gating associated with Ba2+ block of large conductance Ca2+-activated K+ channels. J Gen Physiol 111:343-362.
34. Ribalet, B., S. A. John, L. H. Xie, and J. N. Weiss. 2006. ATP-sensitive K+ channels: regulation of bursting by the sulphonylurea receptor, PIP2 and regions of Kir6.2. J Physiol 571:303-317.
35. Lin, Y. W., T. Jia, A. M. Weinsoft, and S. L. Shyng. 2003. Stabilization of the activity of ATP-sensitive potassium channels by ion pairs formed between adjacent Kir6.2 subunits. J Gen Physiol 122:225-237.
36. Qin, F., A. Auerbach, and F. Sachs. 1997. Maximum likelihood estimation of aggregated Markov processes. Proc R Soc Lond B Biol Sci 264:375-383.
37. Qin, F., A. Auerbach, and F. Sachs. 2000. A direct optimization approach to hidden Markov modeling for single channel kinetics. Biophys J 79:1915-1927.
38. Shyng, S. L., and C. G. Nichols. 1998. Membrane phospholipid control of nucleotide sensitivity of K_{ATP} channels. Science 282:1138-1141.
39. Baukrowitz, T., U. Schulte, D. Oliver, S. Herlitze, T. Krauter, S. J. Tucker, J. P. Ruppersberg, and B. Fakler. 1998. PIP2 and PIP as determinants for ATP inhibition of K_{ATP} channels. Science 282:1141-1144.
40. Enkvetchakul, D., G. Loussouarn, E. Makhina, and C. G. Nichols. 2001. ATP interaction with the open state of the K_{ATP} channel. Biophys J 80:719-728.
41. Enkvetchakul, D., G. Loussouarn, E. Makhina, S. L. Shyng, and C. G. Nichols. 2000. The kinetic and physical basis of K_{ATP} channel gating: toward a unified molecular understanding. Biophys J 78:2334-2348.
42. Li, L., X. Geng, and P. Drain. 2002. Open state destabilization by ATP occupancy is mechanism speeding burst exit underlying K_{ATP} channel inhibition by ATP. J Gen Physiol 119:105-116.
43. Trapp, S., P. Proks, S. J. Tucker, and F. M. Ashcroft. 1998. Molecular analysis of ATP-sensitive K channel gating and implications for channel inhibition by ATP. J Gen Physiol 112:333-349.
44. Wagner, M., and J. Timmer. 2000. The effects of non-identifiability on testing for detailed balance in aggregated Markov models for ion-channel gating. Biophys J 79:2918-2924.
45. Enkvetchakul, D., and C. G. Nichols. 2003. Gating mechanism of K_{ATP} channels: function fits form. J Gen Physiol 122:471-480.
46. Proks, P., C. E. Capener, P. Jones, and F. M. Ashcroft. 2001. Mutations within the P-loop of Kir6.2 modulate the intraburst kinetics of the ATP-sensitive potassium channel. J Gen Physiol 118:341-353.
47. Rothberg, B. S., and K. L. Magleby. 1998. Investigating single-channel gating mechanisms through analysis of two-dimensional dwell-time distributions. Methods Enzymol 293:437-456.
48. Snedecor, G. W., and W. G. Cochran. 1989. Statistical methods. Iowa State University Press, Ames, IA. 468.
49. Qian, H., and E. L. Elson. 2004. Fluorescence correlation spectroscopy with high-order and dual-color correlation to probe nonequilibrium steady states. Proc Natl Acad Sci U S A 101:2828-2833.
50. Fredkin, D. R., M. Montal, and R. J. A. 1985. Identification of aggregated Markovian models: application to the nicotinic acetylcholine receptor. In

Proceedings of the Berkeley Conference in Honor of Jerzy Neyman and Jack Kiefer. L. M. Le Cam, and R. A. Olshen, editors. Wadsworth Press, Monterey, CA. 269-289.

51. Ball, F. G., and M. S. Sansom. 1988. Single-channel autocorrelation functions: the effects of time interval omission. Biophys J 53:819-832.
52. Colquhoun, D., and A. G. Hawkes. 1987. A note on correlations in single ion channel records. Proc R Soc Lond B Biol Sci 230:15-52.
53. Lauger, P. 1995. Conformational transitions of ionic channels. In Single-channel recording. B. Sakmann, and E. Neher, editors. Plenum Press, New York, NY. 651-662.
54. Colquhoun, D., and A. G. Hawkes. 1995. A Q-matrix cookbook. In Single-channel recording. B. Sakmann, and E. Neher, editors. Plenum Press, New York, NY. 589-633.
55. Drain, P., L. Li, and J. Wang. 1998. K_{ATP} channel inhibition by ATP requires distinct functional domains of the cytoplasmic C terminus of the pore-forming subunit. Proc Natl Acad Sci U S A 95:13953-13958.
56. Tucker, S. J., F. M. Gribble, C. Zhao, S. Trapp, and F. M. Ashcroft. 1997. Truncation of Kir6.2 produces ATP-sensitive K+ channels in the absence of the sulphonylurea receptor. Nature 387:179-183.
57. Singer, W. D., H. A. Brown, and P. C. Sternweis. 1997. Regulation of eukaryotic phosphatidylinositol-specific phospholipase C and phospholipase D. Annu Rev Biochem 66:475-509.
58. Pian, P., A. Bucchi, R. B. Robinson, and S. A. Siegelbaum. 2006. Regulation of gating and rundown of HCN hyperpolarization-activated channels by exogenous and endogenous PIP2. J Gen Physiol 128:593-604.

Chapter 4

Control of Peptide Product Sizes by the Energy-Dependent Protease ClpAP

4.1. Abstract

Processive proteases can unfold proteins and cleave them into fragments of a characteristic size. The detailed mechanism by which product sizes are controlled is still in question. One possible mechanism for the control of product sizes would be translocation of unfolded polypeptides to the protease active sites in units of defined length. We have investigated the mechanism by which ClpAP, an energy-dependent protease from *E. coli*, controls the sizes of its peptide products. We show that ClpAP generates peptide products with a distribution of sizes that has a pronounced peak at a peptide length of 6-8 amino acid residues. This product size distribution, which is similar to that observed previously for the proteasome, is robust to perturbations that interfere with translocation or proteolysis. To explain these results, we propose a mechanism in which translocation alternates with proteolysis, allowing peptides of more or less uniform length to be cleaved processively from a translocating substrate. In order to estimate the rate and energy efficiency of ClpAP-catalyzed measurements of product sizes, we apply information theory to quantify how precisely the product sizes are controlled. This analysis may also prove to be useful in characterizing the mechanisms of other proteases and nucleases, such as the proteasome and Dicer, which control the sizes of their products.

4.2. Introduction

In order to generate uniform product sizes, enzymes that hydrolyze polymeric substrates must be able to measure the length of a segment of substrate. Several enzymatic systems appear to carry out reasonably precise measurements. Mammalian and thermophilic proteasomes cleave protein substrates to small peptides of a characteristic size (1). In the case of the mammalian proteasome, controlling the size distribution of peptide products is likely to be important physiologically, since peptide products that are 8-10 amino residues long or longer can be processed further and presented as epitopes to MHC class I molecules (2). In fact, characterization of peptide product sizes (3-5) shows that proteasomes do control product sizes: the product peptides are log-normally distributed in size (5, 6), with peaks centered at 2-3, 9-10, and 20-30 residues (3). In their initial study, Goldberg and co-workers also commented on the implications of the peptide size distribution for the mechanism of peptide production (5), noting that the breadth of the observed distribution rules out a simple "molecular ruler" mechanism in which the spacing between protease active sites uniquely determines the peptide product size. They proposed that openings in the proteasome serve as a filter, trapping large products and allowing them to be cleaved to smaller ones. Subsequent studies showed that a mutant proteasome in which the central pore of the complex is constitutively open produces products that have a median length 40% greater than the wild-type due to both increased production of larger peptides (9-10 and 20-30 residues) and decreased production of smaller peptides (2-3 residues) (3). Interestingly, however, while the mutation changes the relative preference for generating peptides of different defined mean sizes, it does not change the mean sizes themselves. The mechanism by which the proteasome generates peptides of a defined mean size remains an open question.

The energy-dependent processive proteases of *E. coli* may also exert active control over product sizes. Structural (7-9) and biochemical studies indicate that in energy-dependent proteases such as ClpXP and ClpAP, the ATPase component (ClpX or ClpA) can unfold protein substrates and translocate them through an interior channel not much larger than a single polypeptide chain (10, 11). The translocation of protein substrates brings them to ClpP, which has a central proteolytic chamber 50 Å in diameter (9).

Openings in the chamber have been proposed to allow small peptide products to exit (9). However, when the protease active sites of ClpP are completely inactivated (through mutagenesis or chemical modification), the undigested protein substrate becomes trapped in ClpP (12, 13). While it is known that ClpAP makes ~20-30 cuts on average in casein (a natively unfolded substrate), suggesting that the average size of peptide products is 7-8 amino acid residues (14), the full distribution of peptide products has not previously been reported. Thus, the degree to which ClpAP can control its product sizes is unknown: the distribution of product sizes centered at 7-8 residues might be narrow or broad.

Unlike proteasomal products, the peptide products of ClpAP are believed not to have a biological function other than as a source of amino acids. It may nonetheless be important for ClpAP to control the sizes of its products. PepN, one of the major peptidases in *E. coli* (15), processes its substrates much faster than ClpAP (16), so that the overall breakdown of protein substrates to free amino acids might be fastest when ClpAP generates medium-sized products that can be rapidly hydrolyzed by PepN. Control of peptide product sizes might also be useful in smooth processing of large protein substrates, as accumulation of large peptide products in the central cavity of ClpP might hinder further proteolytic processing of the unfolded substrate. Coordination of the ClpX and ClpP activities has been proposed to prevent the translocating peptide from clogging the exit pores of the ClpP tetradecamer (17).

ClpAP might control product sizes by several mechanisms. As previously proposed for the proteasome (5), the exit of large peptides from ClpP might be hindered (9), thereby increasing the probability that these peptides will be cleaved again into smaller fragments. Binding requirements of the protease might also contribute to product size control. If binding of an extended region of polypeptide sequence around the cleavage site is required for efficient proteolysis, proteolysis will be disfavored when shorter segments of polypeptide substrate are bound, leading to preferential generation of longer products.

The interplay between translocation and proteolysis is another source of possible mechanisms for product size control. The relative rates of translocation and proteolysis might control product sizes. Proteolysis that was rapid compared to translocation would

allow many cleavage events while the polypeptide chain was translocating through ClpP, generating small products. Alternatively, allosteric coupling between the translocation and proteolytic activities might serve as the basis of a mechanism for control of product sizes. For both ClpA (18) and ClpX (17), there is allosteric coupling between the protease and the ATPase: binding of ClpP decreases the ATPase activity. If ClpP signals ClpA to stop translocation once a sufficiently large segment of polypeptide has entered the proteolytic chamber, ClpAP will be able to exert control over the range of product sizes.

In this study, we first investigate what product size distributions are predicted by four mechanistic alternatives for control of proteolysis. Each alternative mechanism makes a different prediction about the product size distribution and its sensitivity to biochemical perturbations of the protease. In the first mechanism (referred to hereafter as Mechanism 1), polypeptide translocation is independent of proteolysis (Figure 4.1.A), and both occur with constant probability per unit time. In Mechanisms 2 and 3, the rate of exit from the protease is dependent on the size of the peptide product, and peptides that do not exit the protease may be re-cleaved to smaller products (Figure 4.1.B). These mechanisms thus postulate that the protease acts as a filter, retaining large products but allowing smaller ones to escape. Mechanism 3 includes the additional feature that the rate of proteolytic cleavage is dependent on the size of the product. In Mechanism 4, translocation and proteolysis regulate each other reciprocally: activation of ClpA turns off ClpP, and vice versa (Figure 4.1.C). This mechanism also includes the feature that entry of the translocating polypeptide into ClpP triggers the conformational switch that controls reciprocal regulation.

While the form of the size distribution provides information about the mechanism of peptide product formation, the breadth of the size distribution of the products shows how precisely ClpAP can measure the sizes of its peptide products. To quantify the precision of product generation, we use Shannon information theory (19). This method of quantifying the precision of product size specification allows an estimation of the speed of measurement by the proteolytic machine, and addresses the question of how much energy the proteolytic machine requires to carry out its measurement.

The results of our study provide evidence that ClpAP does exert active control over the sizes of its peptide products. The size distribution is consistent with a mechanism in which a controlled cycle of allosteric activation and inactivation of ClpP by ClpA controls the sizes of peptide products and inconsistent with the other mechanisms we examine. We also find that ClpAP exerts this control efficiently, with a rate and energy cost comparable to a rationally designed enzyme-based information processing system (20).

4.3. Methods

ClpP-His$_6$ Purification. A plasmid for expression of *E. coli* ClpP with a C-terminal His$_6$ tag was kindly provided by Profs. Robert Sauer and Tania Baker (MIT). ClpP-His$_6$ was expressed in *E. coli* strain DH5α/QE704/KI175 and purified as described (13), except that cells were grown at 37°C and Tris buffers were replaced with HEPES buffers to avoid interference with the fluorescamine assay (see below).

ClpA Purification. The *clpA* gene in the overexpression vector pET9a was a generous gift from Profs. Robert Sauer and Tania Baker (MIT). The M169T mutation, which provides enhanced solubility and levels of full-length protein expression (21), was introduced into wild-type ClpA using the QuikChange™ Site-Directed Mutagenesis Kit protocol (Stratagene) and the sequence was confirmed.

ClpA M169T protein was expressed in *E. coli* strain BL21/DE3/pLysS. Cells were grown at 37°C in LB with kanamycin to an OD_{600} of 0.6. IPTG was then added to a final concentration of 1 mM, and cells were transferred to 25°C. After incubation for additional 3 hr at 25°C, cells were harvested by centrifugation for 15 min at 6,000×g and purified as described (22) with the following modifications. All Tris buffers were replaced with HEPES buffers. Cells were lysed by sonication. After ammonium sulfate precipitation, the pellets containing ClpA were resuspended and loaded onto a Macroprep High S support (Bio-Rad) cation exchange column. An 80 mL linear gradient from 0.1 M to 1 M KCl was applied. ClpA was eluted at approximately 0.6 M KCl.

GFP-ssrA Purification. A plasmid expressing GFP containing the S65G and S72A mutations that enhance the intensity of green fluorescence (23) and a C-terminal ssrA tag was kindly provided by Prof. Søren Molin (BioCentrum DTU, Denmark). Cells (*E. coli* JB401) expressing this protein were grown at 37°C in 2YT with ampicilin to an OD_{600} of 0.5. IPTG was added to a final concentration of 1 mg/L and cells were transferred to 25°C. After incubation for an additional 3 hr at 25°C, cells were harvested by centrifugation for 15 min at 6,000×g and purified using a published procedure (24), except that all Tris buffers were replaced with HEPES buffers.

Protease Assay. The rate of GFP-ssrA proteolysis by ClpAP was measured by monitoring the loss of GFP fluorescence (excitation at 467 nm and emission at 511 nm) using a microplate spectrofluorimeter (Molecular Devices Spectramax Gemini XS). Reactions were carried out at 37°C using 0.2 μM hexameric ClpA ($ClpA_6$) and 0.1 μM tetradecameric ClpP ($ClpP_{14}$). The reaction buffer contained 50 mM HEPES, pH 7.5, 300 mM NaCl, 30 mM $MgCl_2$, 0.5 mM DTT, 10% glycerol, 0.32 mg/mL creatine phosphokinase (from rabbit muscle, Sigma), 30 mM phosphocreatine, and 10 mM ATP. ClpA and ClpP were incubated with ATP and all other components for 1 min on ice to enable ClpA and ClpAP complexes to assemble before addition of GFP-ssrA.

ATPase Assay. The rate of ATP hydrolysis by ClpA during GFP-ssrA degradation was measured using the rate of NADH oxidation (monitored by absorbance at 340 nm) coupled via pyruvate kinase and lactate dehydrogenase (25). Reactions were performed at 37°C with 0.2 μM of $ClpA_6$, 0.1 μM of $ClpP_{14}$ and 10 μM GFP-ssrA in a buffer containing 50 mM HEPES, pH 7.5, 300 mM NaCl, 30 mM $MgCl_2$, 0.5 mM DTT, 10% glycerol, 0.23 mM NADH, 7.5 mM phosphoenolpyruvate, 19 U/mL pyruvate kinase (from rabbit muscle, Sigma) and 21 U/mL lactate dehydrogenase (from rabbit muscle, Sigma).

Partial Inactivation of ClpP. Partial inactivation of ClpP was performed by modification of the active site serine with DFP (14). ClpP (1.6 mg/mL) was incubated in 50 mM HEPES, pH 7.5, 200 mM KCl, 25 mM $MgCl_2$, 1 mM DTT, 0.1 mM EDTA, and 10% glycerol containing 4 mM DFP at room temperature for 90 min. Residual DFP was removed using size-exclusion chromatography (PD-10 column, Amersham Biosciences) equilibrated with the reaction buffer. The extent of labeling was determined by measuring peptidase activity with *N*-succinyl-Leu-Tyr-7-amido-4-methylcoumarin, a fluorogenic substrate. ClpP that was 72 ± 2% inactivated was used for further experiments.

Reductive Methylation of GFP-ssrA. Reductive methylation of GFP-ssrA was carried out as previously described (26) to prevent fluorescamine reaction with lysine residues (see "Fluorescamine Assay" section). GFP-ssrA that is completely alkylated (as determined by assay with 2,4,6-trinitrobenzenesulfonic acid (27)) has the same fluorescence properties and maximal degradation rate by ClpAP as unmodified GFP-ssrA.

Digestion of Methylated GFP-ssrA by ClpAP. Digestion of methylated GFP-ssrA by ClpAP was carried out under the same conditions used for the protease assays, except that the reaction mixture contained 0.1 μM $ClpA_6$, 0.05 μM $ClpP_{14}$ and 15 μM methylated GFP-ssrA. Similar experiments were carried out using α-casein (Sigma) (15 μM) as the substrate. Digestions of GFP-ssrA were also performed using sub-saturating (0.1 mM) ATP or using partially inactivated ClpP. All digestions were allowed to proceed for 2-3 hours. GFP-ssrA or casein degradation and ClpA auto-degradation were monitored by SDS-PAGE.

Size-Exclusion Chromatography of Peptide Products. Peptide products were desalted using a reverse-phase cartridge (Sep-Pak C18, Waters), and concentrated by centrifugal evaporation. Desalted products were submitted for MALDI mass spectrometric analysis (MIT Biopolymers Facility). Size-exclusion HPLC was performed using a polyhydroxyethyl aspartamide column (200 × 4.6 mm, PolyLC) (28). The mobile phase was 200 mM sodium sulfate, pH 3.0 (adjusted with phosphoric acid), 5 mM potassium phosphate and 25% acetonitrile. Peptide products were redissolved in the mobile phase and loaded onto the column. Fractions (0.5 min) were collected at a flow rate of 0.125 mL/min. To determine the apparent molecular weight of the peptides eluted, the column was calibrated with standard peptides in the 600-3500 Da range (5).

Fluorescamine Assay for Peptide Concentration. The relative amount of peptide in each fraction was measured using fluorescamine, which forms a fluorescent product on reaction with primary amines (29). 30 μL of each fraction from the polyhydroxyethyl aspartamide column was incubated with 15 μL of 100 mM sodium borate (pH 8.0), 15 μL of water, and 90 μL of 0.1% (w/v, in acetonitrile) fluorescamine for 5 min at room temperature. The fluorescamine solution was freshly prepared before use. The fluorescence emission was monitored at 510 nm at room temperature with an excitation wavelength of 380 nm.

4.4. Results

Simulations of Product Size Distributions for Four Mechanisms of Proteolysis. To simulate the generation of product peptides by Mechanism 1, both translocation and proteolysis were modeled as stochastic processes with constant probability of occurrence per unit time (the structurally identical (9) protease active sites are assumed to be catalytically identical as well). At each time step in the simulation, the system might translocate one monomer unit and/or cleave the translocating chain to generate a product. The histogram of product sizes derived from this simulation (Figure 4.2.A) shows an exponential distribution (more precisely, a geometric distribution with a large number of steps). Other variants of the independent mechanism also produce exponential product size distributions. Exponential product size distributions also result when translocation is deterministic (i.e., when a constant number of residues is translocated per unit time) but proteolysis is stochastic and when translocation and proteolysis are each partially rate-limiting.

Mechanism 2 assumes that the larger peptides exit the protease more slowly than smaller ones, and that peptide products that are retained in the protease can be re-cleaved to smaller products. The probability of retention in the protease is modeled as proportional to $\exp(\alpha L)$, where L is the length of the peptide product and α is a parameter representing the strength of the interaction between the peptide and the protease. Numerical simulations of the second model (Figure 4.2.B) generate product size histograms that, like those generated by the first model, have their maximum at the lowest molecular weights.

Mechanism 3 incorporates both a size-dependent rate of escape for products and a size-dependent rate of proteolytic cleavage. The product escape and proteolytic rates are modeled as proportional to $\exp(\alpha L)$ and $\exp(\beta L)$, respectively: L is the length of the peptide segment that has entered the protease, and α and β are parameters representing how product escape and proteolysis depend on the interaction of the peptide products/substrates with ClpAP. Numerical simulations of this model generate product

size histograms that, depending on the parameters α and β, can have a non-zero peak and are skew toward longer products (Figure 4.2.C).

To simulate the generation of product peptides by Mechanism 4, a switch between two states (ClpA active/ClpP inactive and ClpA inactive/ClpP active) is modeled as a stochastic process. The probability that the system will switch from the ClpA active/ClpP inactive state to the ClpA inactive/ClpP active state is modeled as proportional to $\exp(\gamma L)$, where L is the number of monomer units already translocated into ClpP and γ is a parameter representing the strength of the coupling. Numerical simulations of this model generate a product size distribution that has a non-zero peak and is skew toward longer products (Figure 4.2.D).

Size Distribution of Peptides Derived from ClpAP-Catalyzed Proteolysis. Peptide products derived from GFP-ssrA were separated using size-exclusion HPLC, and the amount of peptide in fractions corresponding to each size range was measured (5, 6). Carrying out the digestion with a large excess of GFP-ssrA over ClpAP ensured that the peptide products were derived predominantly (> 80%) from GFP-ssrA rather than auto-degradation (30, 31) of ClpA. The observed distribution (Figure 4.3) is non-exponential. It has a peak at 760-900 Da (6-8 amino acid residues, assuming an average molecular weight of 119 Da/residue), and is skew toward higher molecular weights.

Because the purification of the product peptides requires several chromatographic steps, it is possible that small peptides will be under-represented in the observed distribution. However, two lines of evidence indicate that this would be unlikely to cause an exponential distribution to appear to be non-exponential. First, studies on a variety of small peptides (three to four residues) have shown that solid phase extraction using a C18 sorbent affords average recoveries of 85-90% (32). In the GFP-ssrA product mixture, peptides of molecular weight 300-400 Da are present in amounts 30-45% of the amount of peptides at the peak molecular weight, suggesting that the observed peak is not due to differential recovery of smaller peptides. Second, MALDI mass spectrometric measurements (Figure 4.4) qualitatively suggest that peptides ~1000 Da dominate the product mixture, consistent with the quantitative measurement.

Sequence selectivity of proteolysis might contribute to the distribution of sizes. If sequence motifs that ClpP prefers are distributed non-uniformly throughout the sequence of the substrate, a non-uniform size distribution of products would result. To test the effect of sequence on size distribution, we measured the size distribution of peptide products derived from α-casein, a substrate unrelated to GFP-ssrA in primary sequence. The size distributions of both substrates were very similar (Figure 4.5), indicating that effects of primary sequence do not account for the size distributions.

Effects of Kinetic Perturbations on Product Size Distribution. The four mechanisms also make different predictions about the effects of artificially perturbing steps such as proteolytic cleavage or translocation. For Mechanisms 1-3, the size distribution of products depends on relative rates of steps in the mechanism. In the case of Mechanism 1, decreasing the rate of proteolysis relative to translocation would be expected to lead to larger products (Figure 4.6.A), while decreasing the rate of translocation relative to proteolysis would lead to smaller products. Similarly, for Mechanisms 2 and 3, the size distribution depends on the partitioning between proteolytic cleavage and escape of peptide products, so decreasing the rate of proteolysis relative to escape would be expected to generate larger products (Figure 4.6.B and 4.6.C). In contrast, Mechanism 4 predicts that the size distribution of products is solely determined by the strength of the interaction that activates ClpP and inactivates ClpA, so this mechanism predicts that decreasing the rate of proteolysis will not affect the size distribution of products.

Experimentally, it is possible to decrease the rate of proteolysis by partially inactivating ClpP with the active site-directed reagent DFP (14). Decreasing the rate of translocation is not as straightforward, but by decreasing the concentration of ATP below its K_m, it is possible to decrease the translocation rate by decreasing the ATPase rate. Because natively unfolded substrates such as casein require ATP-dependent translocation (12) but not unfolding, the observation that the rate of proteolysis of casein is dependent on the ATP concentration (18, 22) (apparent K_m of 0.18 mM (22)) indicates that translocation will occur at a sub-maximal rate at sub-saturating concentrations of ATP.

Neither of these experimental perturbations affects the product size distribution. Proteolysis in the presence of 0.1 mM ATP (the apparent K_m for ATP in GFP-ssrA degradation is 0.58 mM, as described in the next section) generates the same product size distribution as proteolysis in 10 mM ATP (Figure 4.7.A). The peak at 23.5 min (Figure 4.7.A) represents a small amount of contaminating adenine nucleotides, which control reactions showed to react with fluorescamine. The material in this peak was identified as nucleotide by its UV spectrum, which exhibits a peak at 260 nm. In addition, a chromatogram of authentic nucleotides (ATP and ADP) alone shows a peak at 23.5 min of retention time. Under conditions of sub-saturating ATP, the absolute amount of peptide products (~150 relative fluorescence units (RFU)) is about 1/8 of that under conditions of saturating ATP (~1200 RFU), making the contribution of contaminating adenine nucleotides apparent. In the complementary experiment using partially inactivated ClpP, ClpP in which 70% of the active sites have been modified with DFP generates the same product size distribution as that observed using fully active ClpP (Figure 4.7.B).

Kinetic Parameters for GFP-ssrA Proteolysis and ATP Hydrolysis. To help understand the rate and energy requirements for the measurement of product sizes, we measured steady-state kinetic parameters for two of the reactions that underlie this measurement: overall substrate proteolysis and ATP hydrolysis. Fitting the dependence of GFP-ssrA proteolysis rate on [GFP-ssrA] (Figure 4.8.A) to the Michaelis-Menten equation provided a K_m of 4.9 ± 0.6 μM and a k_{cat} (using $[ClpA_{12}P_{14}]$ as the enzyme concentration, corresponding to a complex of 2 $ClpA_6$ and 1 $ClpP_{14}$ (7)) of 15 ± 1 min^{-1}. These results are similar to recently published values (K_m of 5 ± 1 μM, k_{cat} of 10 ± 1 min^{-1}) (33). Fitting the dependence of the ATPase rate during proteolysis of GFP-ssrA on [ATP] (Figure 4.8.B) to the Hill equation (34) gave an apparent K_m of 0.58 ± 0.02 mM, a k_{cat} (using $[ClpA_{12}P_{14}]$ as the enzyme concentration) of 44 ± 1 sec^{-1}, and a Hill coefficient of 2.5 ± 0.2.

4.5. Discussion

We considered four mechanistic possibilities for processive proteolysis by ClpAP. In Mechanism 1, the translocation of unfolded polypeptide by ClpA is independent of proteolytic cleavage at the ClpP active sites, and size control comes from the relative rates of these processes. In Mechanism 2, size control comes from size-dependent escape of products. Physically, the parameter α corresponding to the probability of retention of the product might correspond to some non-specific hydrophobic interaction between the peptide product and the surface of the proteolytic chamber, where each residue of the peptide contributes a certain amount of free energy to the interaction. The relationship between αL and the retention probability is simulated as exponential because of the exponential relationship between activation energy and rate in activated rate theories such as Eyring or Kramers theories (35). In Mechanism 3, size control comes from both size-dependent escape of products and a size-dependent cleavage reaction. Size-dependent cleavage would be possible if, for example, catalysis of amide bond hydrolysis depended on the presence of binding of substrate residues extending well outside the site of cleavage. Finally, in Mechanism 4, allosteric communication between ClpA and ClpP allows translocation to alternate with proteolysis. This model thus assumes that each monomer unit reduces the barrier for the conformational switch by a certain amount of free energy. Physically, this might correspond to energy of binding of the unfolded polypeptide or strain energy that builds up as the unfolded polypeptide presses against the interior surface of the ClpP ring.

These mechanisms make distinct predictions about the nature of the size distribution of peptide products. The first mechanism predicts that the products will be exponentially distributed in size. If there is a single rate-limiting step in ClpAP-catalyzed proteolysis, the product size distribution would be expected to be a single exponential, because the waiting times between events are exponentially distributed for a process described by a single chemical step (36). Numerical simulations of this mechanism produce exponential product size distributions (Figure 4.2.A), as expected. This mechanism is thus inconsistent with the experimental size distribution.

Mechanism 2 predicts a distribution that, like the exponential distribution, has its maximum at the lowest size products (Figure 4.2.B). In this mechanism, size-dependent escape of products acts as a filter, preventing very large products from being formed. However, this filter does not prevent small products from escaping, so that nothing prevents the initial formation of small products due to random cleavages. This mechanism is thus, like the first mechanism, inconsistent with the observed product size distribution. The nature of any putative peptide filter is also somewhat problematic. Diffusion of even large polymers through narrow pores can occur on the timescale of milliseconds or less (37, 38), orders of magnitude faster than the overall rate of turnover for ClpAP (~10 min^{-1}). While a structural filter may contribute to size control in ClpAP, it is not likely to consist of a static pore. Non-specific binding of peptides to the inner surface of the protease might serve as an efficient filter, assuming that the residence time was dependent on hydrophobic interactions that would be larger for larger peptides. Access to the bulk solution that was gated by conformational changes (e.g., opening and closing of small apertures in the ClpP structure) might also serve as an effective filter.

In order to obtain a distribution of product sizes with a peak at a defined number of amino acid residues, ClpAP must have some way of cutting the polypeptide chain preferentially after translocation of a certain number of residues. One way to accomplish this would be to make the rate of proteolytic cleavage dependent on the size of the peptide segment bound to the protease active site, as postulated in Mechanism 3. This mechanism includes the feature that the substrate binding site can accommodate a large number of amino acid residues extending from the site of cleavage. Mechanism 3 further postulates that when more of this extended binding site is occupied, the efficiency of cleavage is higher. Thus, this mechanism predicts preferential generation of larger products. Simulations of Mechanism 3 show that preferential generation of larger products, in combination with a structural "filter," can lead to a product size distribution that, like the observed distribution, has a non-zero peak and is skew toward higher molecular weight products (Figure 4.2.C).

Mechanism 4 represents another way for ClpAP to control product sizes. This mechanism postulates that the active form of ClpA negatively regulates ClpP and vice

versa, so that translocation alternates with proteolysis. Mechanism 4 also postulates that it is the translocation of unfolded polypeptide by the active form of ClpA into the inactive form of ClpP that triggers activation of ClpP, causing ClpA to stop translocating the substrate. When the peptide product leaves the ClpP active site, ClpP becomes inactive and ClpA becomes active, starting the cycle again. In effect, this mechanism involves ClpAP first measuring the size of the product, then cutting it.

Numerical simulations of this mechanism showed that it generates a product size distribution that qualitatively reproduces the features of the observed distribution. It has a non-zero peak and is skew toward higher molecular weight products (Figure 4.2.D). In this mechanism, ClpP's ability to trigger the allosteric activation of ClpP/deactivation of ClpA determines the peak size of products. Increasing the parameter γ in the simulation, which represents ClpP's ability to trigger this allosteric activation/deactivation, leads to the formation of smaller products.

The form of the product size distribution thus allows Mechanisms 1 and 2 to be distinguished from Mechanisms 3 and 4. To distinguish Mechanism 4 from the other three mechanisms, we used sub-saturating concentrations of ATP to hinder translocation and partial inactivation of ClpP to hinder proteolytic cleavage. In the first three mechanisms, size control comes about through control of the relative rates of translocation and proteolysis (Mechanism 1) or the relative rates of proteolysis and product escape (Mechanisms 2 and 3). Hindering either translocation (Mechanism 1) or proteolysis (Mechanisms 1, 2, and 3) is thus expected to alter the size distributions for these mechanisms (Figure 4.6). In contrast, hindering translocation or proteolysis individually is not expected to alter the product size distribution in Mechanism 4, since the product sizes are not determined by the relative rates of translocation and proteolysis, but by the ability of bound peptide to trigger the conformational switch that activates proteolysis. Mechanism 4 predicts that once substrate binding to ClpP initiates the conformational switch, translocation stops and no additional substrate enters ClpP. In this case, the peptide product formed will be of the same size whether the proteolytic cleavage itself is slow or rapid.

Mechanism 4, unlike the simpler mechanisms considered, is consistent with all the available data. It is also consistent with previously reported results, such as the ability of ClpP to modulate the ATPase activity of ClpA (18) and ClpX (17) and the ability of active ClpA to translocate substrate into ClpP that has been inactivated by chemical modification or site-directed mutagenesis (7, 12). In the latter case, trapping of large unfolded substrates in inactivated ClpP would be interpreted as resulting from the inability of the modified ClpP to assume the active conformation. Of course, the ability of Mechanism 4 to account for the current experimental results does not preclude the ability of other mechanisms not considered here to do so. While Mechanism 4 provides a useful starting point for mechanistic studies, further experimental work will be required to test its predictions. For example, experiments to determine whether ClpA and ClpP actually alternate activation states in the course of a single enzymatic turnover and whether translocation exhibits controlled step sizes will be required. Transient-state or single-molecule kinetic approaches may prove to be necessary to address this question, as they are sensitive to microscopic steps that are averaged out using steady-state techniques. In particular, single-molecule experiments are likely to be useful, as Mechanism 4 predicts that the waiting time between proteolytic events will be non-exponentially distributed.

Quantitative Characterization of Product Size Control by ClpAP. ClpAP's ability to exercise control over the sizes of peptide products is analogous to carrying out a measurement. Any measurement carried out by a biomolecule will be subject to interference from thermal noise that reduces its precision (39). The effect of thermal noise might be reduced at the expense of slowing down the measurement by averaging it over a longer time. Expenditure of free energy is another way of reducing the effect of thermal noise (39). A molecular process with a sufficient number of irreversible steps can proceed in a regular, "clockwork"-like fashion (40). Mechanical precision of this kind could serve as the basis for the control of product sizes.

It would be thus informative to determine how ClpAP manages the compromise among precision, rate, and energy cost in controlling its product sizes. To address this question, we will need a way of quantifying the statistical uncertainty associated with a given size distribution. The amount of information required to specify the product size

distribution is a measure of the precision with which the enzyme controls the size of its products.

Information theory (19), which was introduced by Claude Shannon and others and has since been applied to problems in biology and bioinformatics (41, 42), provides a way to quantify information. The information content of a distribution expresses how much knowing the distribution reduces the uncertainty in knowing the measured quantity for an individual member of the ensemble. For example, if measurements of an experimental quantity are normally distributed with a mean of 50 and a standard deviation of 40, the distribution does not specify the value of an individual measurement precisely, while if the standard deviation is 2, the distribution contains sufficient information to specify the value of an individual measurement to a low level of uncertainty.

A decrease in uncertainty can be defined quantitatively as a decrease in statistical entropy (19). The uncertainty of a distribution can be defined as $\sum_i -p_i \ln(p_i)$, where p_i is the probability that an individual member of the ensemble belongs to bin i in a histogram (19). The statistical entropy of a distribution can be thus calculated as the difference between its uncertainty and that of a reference distribution. Here, we are interested in the statistical entropy of the observed size distribution compared to that of the size distribution that a completely random protease would be able to produce. We will therefore use as the reference distribution the exponential distribution, which random proteolysis would generate. The relative amount of peptide product in each bin of product sizes represents the probability of generating a product of that size, and the total uncertainty for a proteolytic cleavage is calculated by summing over all the bins in the experimental histogram. The specific reference distribution is an exponential distribution with the same mean as the experimental distribution, binned the same way as the experimental data. To quantify the uncertainty of the experimental size distribution, this distribution was fitted to a log-normal function, and the function numerically integrated (using the quadrature function in MATLAB) over a range of 1-5000 Da. The uncertainty of an exponential distribution with the same mean size as the experimental distribution was calculated in the same way.

Calculating the statistical entropy of the experimentally observed product size distribution compared to an exponential distribution with the same mean provides a value of ~0.1 bits for the decrease in statistical entropy associated with specifying the observed distribution. The estimate of the statistical entropy of the product size distribution allows calculation of an order-of-magnitude estimate for the rate of information processing in product formation. Since the distribution of products is centered at 6-8 amino acid residues, and GFP-ssrA is 251 amino acid residues long, a typical turnover will comprise about 30 proteolytic cleavages (in accord with previous estimates (14)). Assuming that the distribution of product sizes does not vary within a single turnover, the value of ~0.1 bits represents the information required to specify each proteolytic cleavage. Therefore, about 3 bits are required to specify the outcome of all the proteolytic cleavages in one turnover. The turnover number for GFP-ssrA is 15 min^{-1}, meaning that ClpAP can perform its size specification at a rate of ~1 bit/sec. This estimate represents a lower limit: while a greater decrease in statistical entropy may be required to define the process that leads to product formation, a decrease of at least that magnitude is required in order to account for the observed product size distribution.

We can also ask how much free energy is dissipated in the course of specifying the product size distribution. The total free energy dissipated is an upper limit on the energetic cost of controlling product sizes. The maximal rate of ATP hydrolysis under turnover conditions is about 2×10^3 min^{-1} (Figure 4.8.B). Since hydrolysis of ATP under physiological conditions is exergonic by about 20 kT (43), ClpAP dissipates about 5×10^4 kT/min (hydrolysis of protein amides, which is much slower and is less exergonic, contributes a relatively small amount to the total energy dissipation). The value of ~0.5 bits/sec estimated above provides an estimate of 10^3 kT/bit as a lower limit for the energy efficiency of product size specification. It is likely that the value of approximately 10^3 kT/bit does not represent the minimum energy required for specifying the product size distribution, as mechanical steps such as unfolding will certainly consume an appreciable fraction of this energy without contributing directly to information processing.

Biological Implications of Control of Sizes of Proteolytic Fragments. While eukaryotic proteasomes need to control peptide product sizes because peptides below a

certain length cannot be presented as antigens (2), there is not an obvious disadvantage to the production of very short peptides in *E. coli*. The question thus arises of whether there actually exists a selective pressure for control of peptide product sizes in *E. coli*. One possible explanation for the function of the observed size distribution of ClpAP products is that it optimizes the overall rate of degradation of misfolded proteins to free amino acids. The aminopeptidase PepN hydrolyzes short peptides to free amino acids and is responsible for most of the aminopeptidase activity in *E. coli* (15, 16). Its steady-state rate of proteolysis is much greater than ClpP's for roughly comparable substrates (k_{cat} of 370 sec^{-1} for hydrolysis of a para-nitroanilide substrate (16), compared to 2.5 min^{-1} for ClpP's hydrolysis of a somewhat less activated aminomethylcoumarin substrate (44)). However, PepN degrades unfolded proteins very slowly (a half-time on the order of hours (16)). Thus, use of the slower peptidase ClpAP to digest misfolded proteins into peptides small enough for the faster peptidase PepN to accept would optimize the overall rate of processing.

It is also possible that control of product sizes is required to keep the translocating substrate from clogging the central pore of ClpAP. ClpXP (45) and the proteasome (46) can process substrates that are larger than their central pores. This ability suggests that smooth processing of large substrates will require energy-dependent proteases to have a way of preventing translocation of more unfolded polypeptide than can be productively accommodated into the central chamber of the protease. Translocation of only small segments of substrate before proteolysis and clearance of the ClpP active sites might help ClpAP avoid non-productive binding of large segments of substrate to the interior surface of ClpP.

General Mechanistic Features of Enzymes that Measure Product Sizes. Other enzymes in a variety of organisms can also be thought of as "measuring" their substrates. In addition to the proteasome, which produces products with a size distribution similar to that observed for ClpAP, the nuclease Dicer also produces products with a very narrow size distribution (20-22 nucleotide residues) (47), and tripeptidylpeptidases cleave the first three amino acid residues from peptides (48). The mechanism for generation of a narrow size distribution of products may at first seem to follow trivially from the existence of

multiple active sites in the enzyme structure. Dicer, for example, has two distinct nuclease active sites (49), suggesting that the physical spacing between them might determine the product size. Such a mechanism would be an oversimplification. Even when there is a defined spacing between active sites, the microscopic steps in the enzymatic mechanism must also be ordered in a way that allows control of product sizes. For example, a mechanism where an enzyme binds the substrate at two active sites, cleaves it at each of the sites sequentially, and releases the product will allow generation of uniformly-sized products from a polymeric substrate. However, if the enzyme can deviate from the correct order of steps (e.g., if partially cleaved product can diffuse from the enzyme and re-bind at random), random cleavages will occur, decreasing the uniformity of product sizes.

One way to ensure a defined order of conformational changes is to drive them using dissipation of free energy; that is, to make each conformational change effectively irreversible. In the limit where every step is very far from equilibrium (i.e., irreversible), the enzyme always traverses the cycle in order (40). This would allow a complex algorithmic task to be carried out: first the enzyme does A, then B, then C, etc. The price paid for carrying out a complex task with high fidelity is thus the irreversible consumption of chemical energy. For proteases and nucleases, the irreversibility of the hydrolytic step may suffice to provide the free energy needed to determine the size distribution.

The phenotype of peptide product formation in ClpAP is remarkably similar to that observed for mammalian and thermophilic proteasomes (4, 5). The product sizes for those enzymatic systems have a similar skew distribution, and are similarly unaffected by partial inactivation of protease active sites (4). The proteasome may therefore have a similar mechanism of peptide product formation, in which translocation of polypeptide substrate alternates with proteolysis. There is evidence for allosteric coupling between chymotryptic sites and caspase sites in the 20S proteasome (6). The "measure and cut" and "bite-chew" (6) mechanisms are not mutually exclusive, and both may contribute to production of epitopes of the proper size and sequence.

It may be that, for proteasomes, the ability to measure product sizes serves as an integral part of the generation of epitope-like peptides from protein substrates. A protease that initiated proteolysis at one end of the substrate polypeptide and processively cleaved off peptides of a constant size from that end would generate a unique set of products even without being able to cleave specific sequences preferentially. For such an enzyme, the mechanical precision of product size measurement, combined with the ability to cleave processively without slipping, would allow preferential generation of a small subset of possible peptide products.

4.6. Figures

Figure 4.1. Possible mechanisms for control of product sizes by ClpAP. (A) Size control through modulation of relative rates of translocation and proteolysis (Mechanism 1). ClpA and ClpP are active (gray) simultaneously, so translocation and proteolysis occur simultaneously. (B) Size control through use of a structural "filter." Small products escape from ClpP more readily than larger ones, which may be re-cleaved. Proteolysis may be random (Mechanism 2) or biased toward longer products (Mechanism 3). (C) Size control through allosteric coupling between translocation and proteolysis (Mechanism 4). ClpA and ClpP reciprocally regulate each other's activity, so that when ClpA is active, ClpP is inactive (white). Translocation and proteolysis alternate.

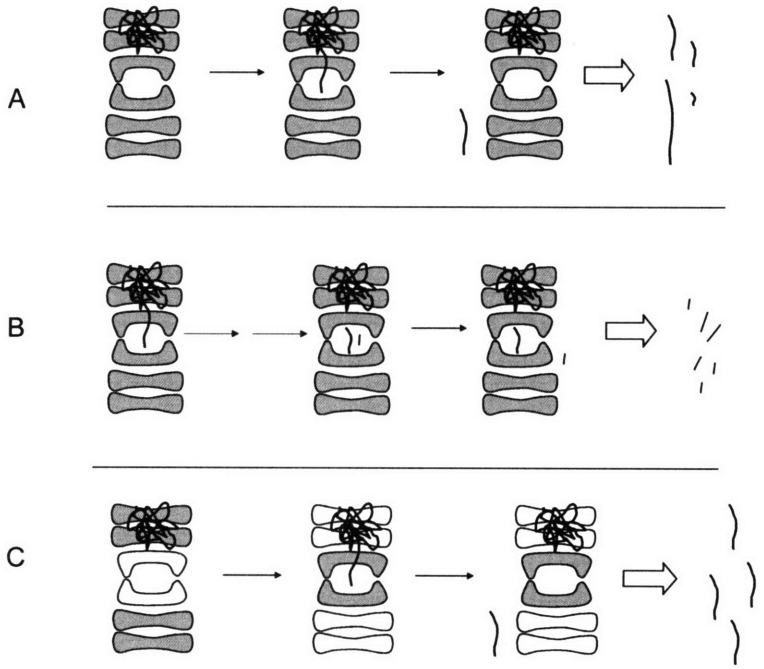

Figure 4.2. Simulations of the four mechanisms in Figure 4.1. In each case, ~1000 product-forming events were simulated. (A) Simulated product size distribution using Mechanism 1 (translocation 10-fold faster than proteolysis). (B) Simulated product size distribution using Mechanism 2 (interaction parameter α = 0.08). (C) Simulated product size distribution using Mechanism 3 (interaction parameter α = 0.08, interaction parameter β = 0.008). (D) Simulated product size distribution using Mechanism 4 (coupling parameter γ = 80).

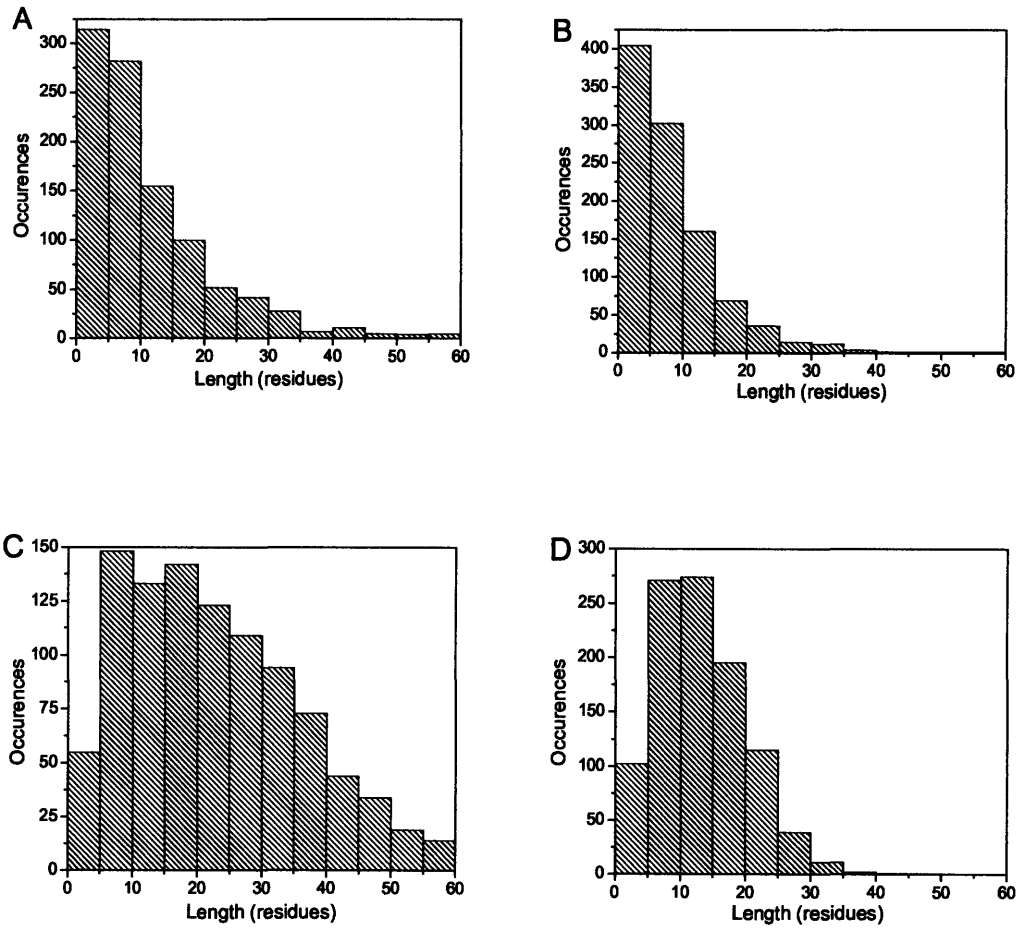

Figure 4.3. Size distribution of peptides derived from ClpAP-catalyzed proteolysis of GFP-ssrA.

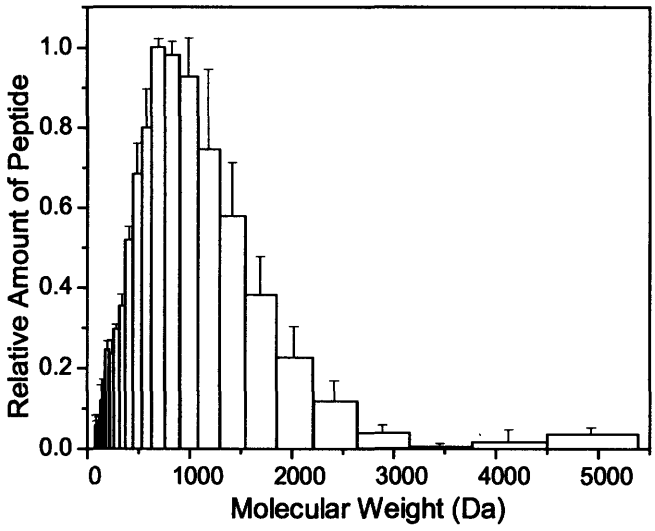

Figure 4.4. MALDI mass spectrum of peptide products.

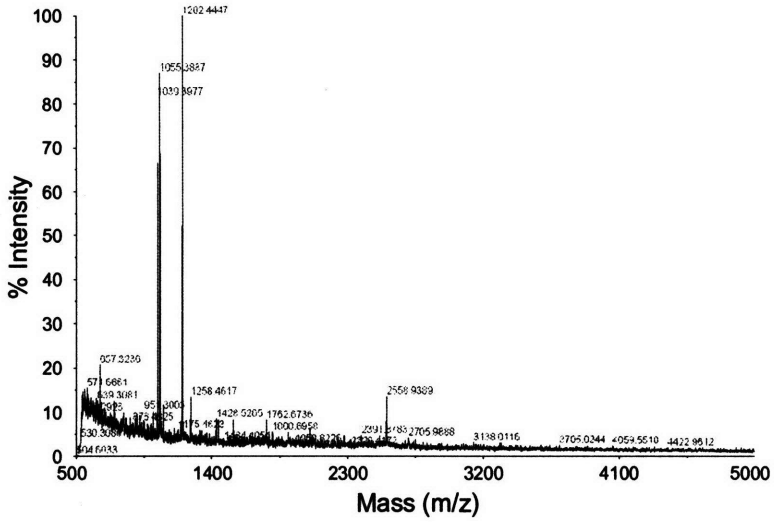

Figure 4.5. Effects of primary sequence of substrates on product size distribution. Comparison of product size distributions obtaining using GFP-ssrA as substrate (filled squares) and using α-casein as substrate (open circles).

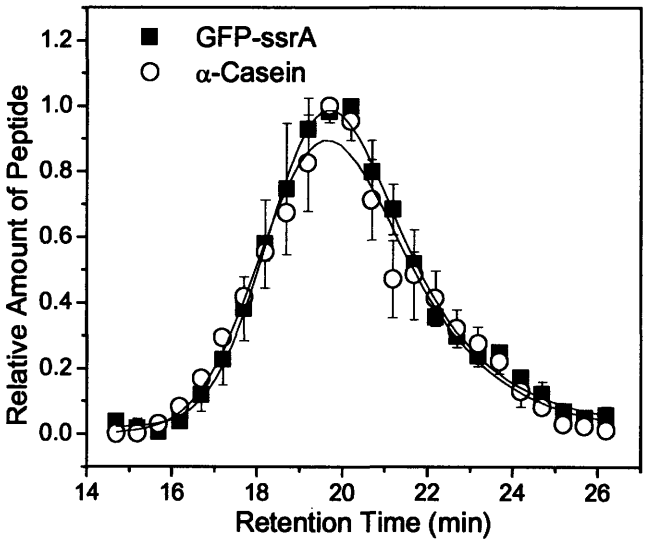

Figure 4.6. Simulated effects of decreasing proteolytic rate on the product size distribution. The rate of proteolysis is set at a reference value (0.05 per time step, histograms in black) or one-third of the reference value (histograms in gray). (A) Simulation using Mechanism 1. (B) Simulation using Mechanism 2. (C) Simulation using Mechanism 3. Arrows point to the maxima of the distributions.

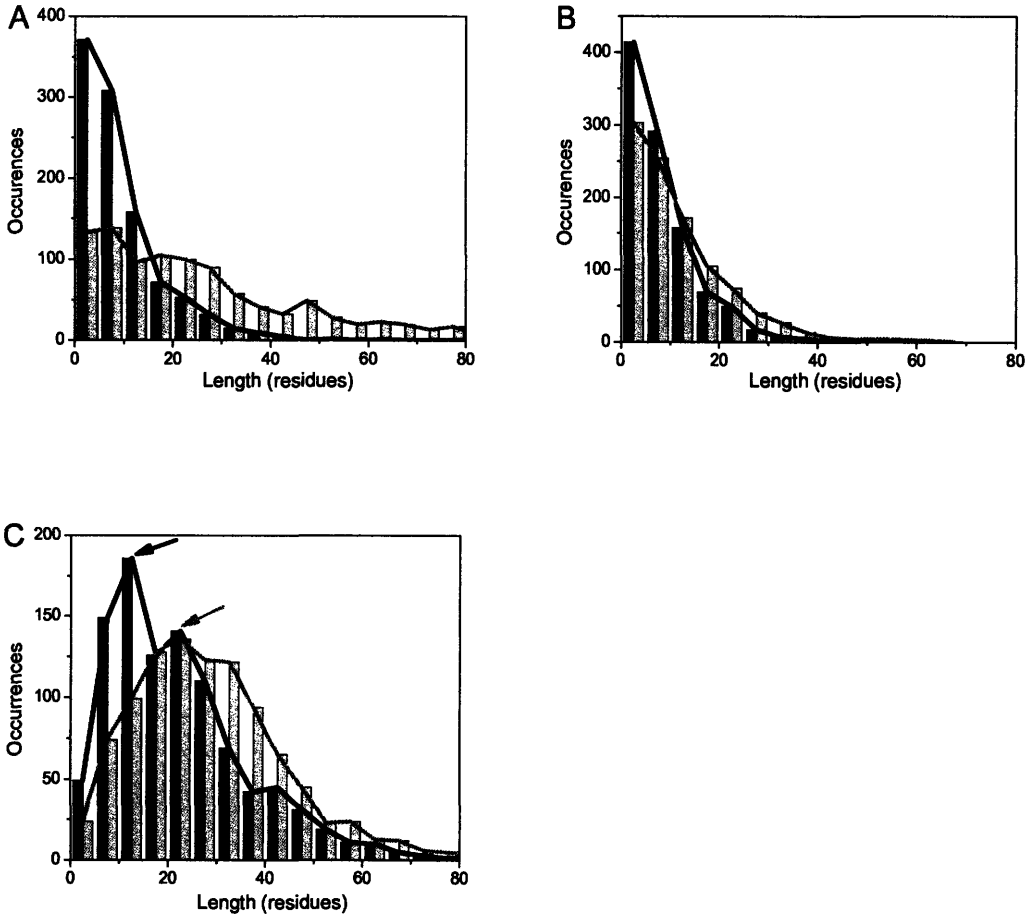

Figure 4.7. Effects of kinetic perturbations on product size distribution. (A) Comparison of product size distributions with saturating (10 mM) ATP (filled squares) and sub-saturating (0.1 mM) ATP (open circles). The peak at 23.5 min retention time (arrow) is mostly contributed by nucleotides (ATP and ADP), not by the peptide products. (B) Comparison of product size distributions with fully active ClpP (filled squares) and partially inactivated ClpP (open circles).

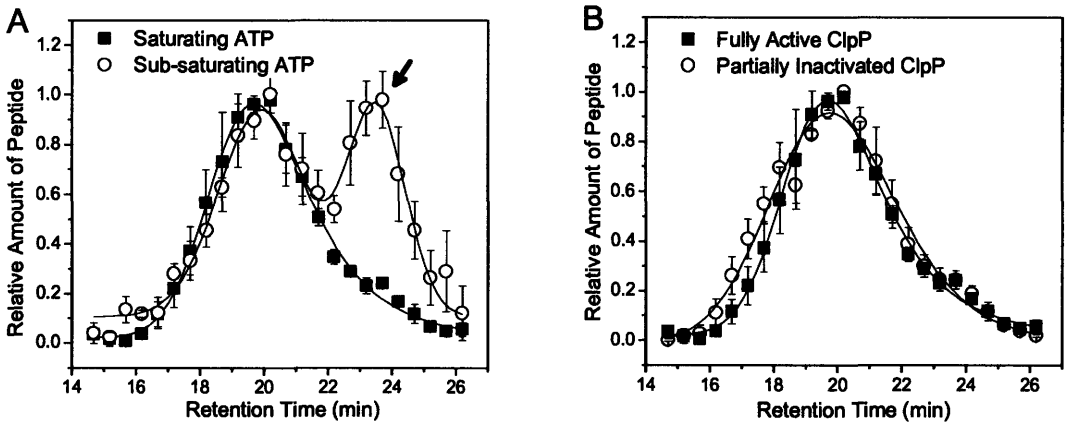

Figure 4.8. Kinetic parameters for GFP-ssrA proteolysis and ATP hydrolysis. (A) The dependence of the GFP-ssrA proteolysis rate on [GFP-ssrA]. The rate of GFP-ssrA proteolysis by ClpAP was measured by monitoring the loss of GFP fluorescence. (B) The [ATP]-dependence of the ATPase rate during proteolysis of GFP-ssrA. The rate of ATP hydrolysis by ClpA during GFP-ssrA degradation was measured via the loss of NADH in a coupled reaction.

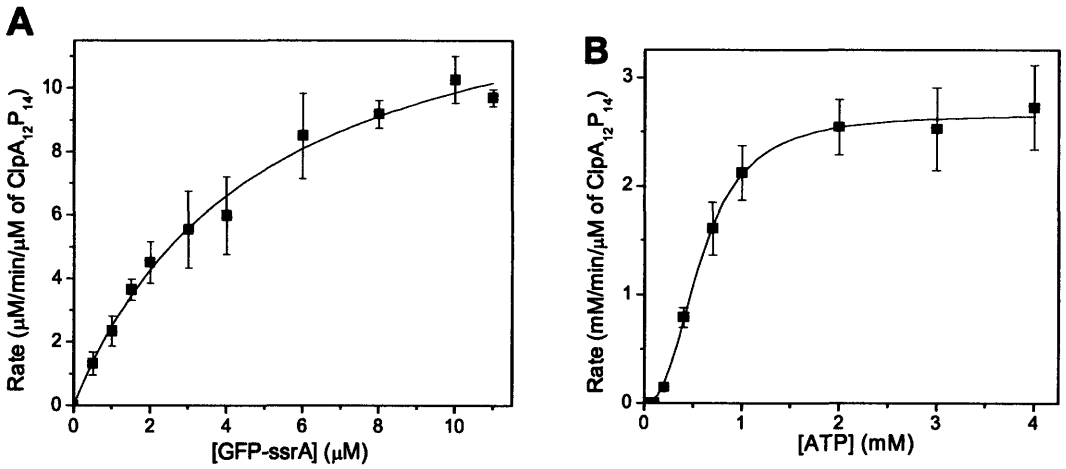

4.7. Numerical Simulations

The following script for MATLAB (version 6.5.1, The Mathworks) was used for simulation of Mechanism 1, as described in the text.

```
% Model for peptide sizes
A=[1 0.99]
P=[1 0.1]
L=0
C=1
X=1
O=zeros(1000,1);
while L<=1000
    while X<237
        r1=rand;
        adv=A(1,1)*A(1,2);
        if r1<=adv
            X=X+1;
            C=C+1;
        end
        r2=rand;
        cut=P(1,1)*P(1,2);
        if C>0 & r2<=cut
            L=L+1;
            O(L,1)=C;
            C=0;
        end
    end
X=1;
C=1;
end
dlmwrite('proteolysis1output.txt',O,' ')
```

The following script was used for simulation of Mechanism 2:

```
% Model for peptide sizes:  random proteolysis + a
% "filter" to exclude large products
%probability of cleavage
cut=0.015
%counter for product peptides
L=1
%counter for seq. position
X=1
%counter for # of rounds of proteolysis before all peptides diffuse out
q=0
%S=matrix representing sequence positions; (bound/unbound, +/- a
%cut at this position, length of the peptide that includes this residue,
%position of last N-terminal cut)
S=zeros(237,4);
%set all positions as "bound" (to ClpAP)
S(:,1)=1;
%O = output peptide lengths
O=zeros(1000,1);
%Nterm=position of last N-terminal cleavage
Nterm=0;
Nterm2=0;
```

```
%G=constant representing binding affinity of a residue to ClpP active
site
G=0.08;
while L<1000
    while nnz(S(:,1))>0
        for X=1:237
            S(X,4)=Nterm;
            r1=rand;
            if S(X,1)>0 & r1<=cut
                %incorporate a cleavage at the residue
                S(X,2)=1;
                %calculate length of peptide that includes this residue
                S(X,3)=X-Nterm;
                %set next position of last N-terminal cleavage
                Nterm=X;
            end
        end
        Nterm=0;
        %calculate whether peptide diffuses out of active site
         for X2=1:237
            r2=rand;
            length=S(X2,3);
            Nterm2=S(X2,4);
            if S(X2,2)==1 & r2<=exp((-1)*G*length)
                O(L)=length;
                L=L+1;
                S((Nterm2+1):X,1)=0;
            end
          end
        Nterm2=0;
    end
%reset sequence variables
S=zeros(237,4);
S(:,1)=1;
Nterm=0;
end
dlmwrite('proteolysis10output.txt',O,' ')
```

The following script was used for simulation of Mechanism 3:

```
% Model for peptide sizes:  random proteolysis + a
% "filter" to exclude large products + coupling of binding
% to proteolysis
%probability of cleavage
cut=0.05
%counter for product peptides
L=1
%counter for seq. position
X=1
%S=matrix representing sequence positions; (bound/unbound, +/- a
%cut at this position, length of the peptide that includes this residue,
%position of last N-terminal cut)
S=zeros(237,4);
%set all positions as "bound" (to ClpAP)
S(:,1)=1;
%O = output peptide lengths
O=zeros(1000,1);
%Nterm=position of last N-terminal cleavage
```

```
Nterm=0;
Nterm2=0;
%G=constant representing binding affinity of a residue to ClpP active
site
G=0.08;
%F=constant representing coupling of binding affinity to proteolytic
rate
F=0.1;
while L<1000
    while nnz(S(:,1))>0
        %C = counter for number of residues translocated
        C=0;
        for X=1:237
            S(X,4)=Nterm;
            r1=rand;
            C=C+1;
            if S(X,1)>0 & r1<=cut*(1-exp((-1)*G*F*C))
                %incorporate a cleavage at the residue
                S(X,2)=1;
                %calculate length of peptide that includes this residue
                S(X,3)=X-Nterm;
                %set next position of last N-terminal cleavage
                Nterm=X;
                C=0;
            end
        end
        Nterm=0;
        %calculate whether peptide diffuses out of active site
         for X2=1:237
            r2=rand;
            length=S(X2,3);
            Nterm2=S(X2,4);
            if S(X2,2)==1 & r2<=exp((-1)*G*length)
                O(L)=length;
                L=L+1
                S((Nterm2+1):X,1)=0;
            end
          end
        Nterm2=0;
    end
%reset sequence variables
S=zeros(237,4);
S(:,1)=1;
Nterm=0;
end
dlmwrite('proteolysis11output.txt',O,' ')
```

The following script was used for simulation of Mechanism 4:

```
% Model for peptide sizes:  both translocation and proteolysis
% probabilities controlled by amt. of peptide translocated
%A[conformational state, prob. of translocation]
A=[1 1]
%P[conformational state, prob. of trapping]
P=[0 1]
%L = length of peptide product
L=0
%C = counter for length of peptide product
```

```
C=0
%X = counter for position in protein
X=1
%O = array of peptide product sizes
O=zeros(1000,1);
fillfactor=100
time=0;
transcount=0;
protcount=0;
turnover=0;
while L<=1000
      while X<237
            r1=rand;
            r2=rand;
        time=time+1;
        fillP=exp(-C/fillfactor);

  %trapping the translocating chain
        trap=(1-fillP);
        if r1<=trap
            A(1,1)=0;
            P(1,1)=1;
        else
            A(1,1)=1;
            P(1,1)=0;
        end

   %translocation
            transloc=A(1,1)*A(1,2);
            if r2<=transloc
                        X=X+1;
                        C=C+1
                transcount=transcount+1;
            end

     %cutting the translocating chain
            if P(1,1)==1 & C>0
                  L=L+1
            O(L,1)=C;
                  C=0;
            A(1,1)=1;
            P(1,1)=0;
            protcount=protcount+1;
            end
      end
X=1;
C=0;
turnover=turnover+1;
end
transrate=transcount/time
protrate=protcount/time
steady=turnover/time
mean(O)
dlmwrite('proteolysis8output.txt',O,' ')
```

4.8. References

1. Pickart, C. M., and R. E. Cohen. 2004. Proteasomes and their kin: proteases in the machine age. Nat Rev Mol Cell Biol 5:177-187.
2. Rock, K. L., I. A. York, T. Saric, and A. L. Goldberg. 2002. Protein degradation and the generation of MHC class I-presented peptides. Adv Immunol 80:1-70.
3. Kohler, A., P. Cascio, D. S. Leggett, K. M. Woo, A. L. Goldberg, and D. Finley. 2001. The axial channel of the proteasome core particle is gated by the Rpt2 ATPase and controls both substrate entry and product release. Mol Cell 7:1143-1152.
4. Kisselev, A. F., T. N. Akopian, K. M. Woo, and A. L. Goldberg. 1999. The sizes of peptides generated from protein by mammalian 26 and 20 S proteasomes. Implications for understanding the degradative mechanism and antigen presentation. J Biol Chem 274:3363-3371.
5. Kisselev, A. F., T. N. Akopian, and A. L. Goldberg. 1998. Range of sizes of peptide products generated during degradation of different proteins by archaeal proteasomes. J Biol Chem 273:1982-1989.
6. Kisselev, A. F., T. N. Akopian, V. Castillo, and A. L. Goldberg. 1999. Proteasome active sites allosterically regulate each other, suggesting a cyclical bite-chew mechanism for protein breakdown. Mol Cell 4:395-402.
7. Ishikawa, T., F. Beuron, M. Kessel, S. Wickner, M. R. Maurizi, and A. C. Steven. 2001. Translocation pathway of protein substrates in ClpAP protease. Proc Natl Acad Sci U S A 98:4328-4333.
8. Guo, F. S., M. R. Maurizi, L. Esser, and D. Xia. 2002. Crystal structure of ClpA, an Hsp100 chaperone and regulator of ClpAP protease. J Biol Chem 277:46743-46752.
9. Wang, J. M., J. A. Hartling, and J. M. Flanagan. 1997. The structure of ClpP at 2.3 angstrom resolution suggests a model for ATP-dependent proteolysis. Cell 91:447-456.
10. Hoskins, J. R., K. Yanagihara, K. Mizuuchi, and S. Wickner. 2002. ClpAP and ClpXP degrade proteins with tags located in the interior of the primary sequence. Proc Natl Acad Sci U S A 99:11037-11042.
11. Sauer, R. T., D. N. Bolon, B. M. Burton, R. E. Burton, J. M. Flynn, R. A. Grant, G. L. Hersch, S. A. Joshi, J. A. Kenniston, I. Levchenko, S. B. Neher, E. S. C. Oakes, S. M. Siddiqui, D. A. Wah, and T. A. Baker. 2004. Sculpting the proteome with AAA+ proteases and disassembly machines. Cell 119:9-18.
12. Singh, S. K., R. Grimaud, J. R. Hoskins, S. Wickner, and M. R. Maurizi. 2000. Unfolding and internalization of proteins by the ATP-dependent proteases ClpXP and ClpAP. Proc Natl Acad Sci U S A 97:8898-8903.
13. Kim, Y. I., R. E. Burton, B. M. Burton, R. T. Sauer, and T. A. Baker. 2000. Dynamics of substrate denaturation and translocation by the ClpXP degradation machine. Mol Cell 5:639-648.
14. Thompson, M. W., S. K. Singh, and M. R. Maurizi. 1994. Processive degradation of proteins by the ATP-dependent Clp protease from Escherichia coli. Requirement for the multiple array of active sites in ClpP but not ATP hydrolysis. J Biol Chem 269:18209-18215.

15. Chandu, D., and D. Nandi. 2003. PepN is the major aminopeptidase in Escherichia coli: insights on substrate specificity and role during sodium-salicylate-induced stress. Microbiol 149:3437-3447.
16. Chandu, D., A. Kumar, and D. Nandi. 2003. PepN, the major Suc-LLVY-AMC-hydrolyzing enzyme in Escherichia coli, displays functional similarity with downstream processing enzymes in archaea and eukarya. Implications in cytosolic protein degradation. J Biol Chem 278:5548-5556.
17. Joshi, S. A., G. L. Hersch, T. A. Baker, and R. T. Sauer. 2004. Communication between ClpX and ClpP during substrate processing and degradation. Nat Struct Mol Biol 11:404-411.
18. Hwang, B. J., K. M. Woo, A. L. Goldberg, and C. H. Chung. 1988. Protease Ti, a new ATP-dependent protease in Escherichia coli, contains protein-activated ATPase and proteolytic functions in distinct subunits. J Biol Chem 263:8727-8734.
19. Cover, T. M., and J. A. Thomas. 1991. Elements of information theory. Wiley, New York, NY.
20. Benenson, Y., T. Paz-Elizur, R. Adar, E. Keinan, Z. Livneh, and E. Shapiro. 2001. Programmable and autonomous computing machine made of biomolecules. Nature 414:430-434.
21. Seol, J. H., S. H. Baek, M. S. Kang, D. B. Ha, and C. H. Chung. 1995. Distinctive roles of the two ATP-binding sites in ClpA, the ATPase component of protease Ti in Escherichia coli. J Biol Chem 270:8087-8092.
22. Maurizi, M. R., M. W. Thompson, S. K. Singh, and S. H. Kim. 1994. Endopeptidase Clp: ATP-dependent Clp protease from Escherichia coli. Method Enzymol 244:314-331.
23. Delagrave, S., R. E. Hawtin, C. M. Silva, M. M. Yang, and D. C. Youvan. 1995. Red-shifted excitation mutants of the green fluorescent protein. Biotechnology (NY) 13:151-154.
24. Yakhnin, A. V., L. M. Vinokurov, A. K. Surin, and Y. B. Alakhov. 1998. Green fluorescent protein purification by organic extraction. Protein Expr Purif 14:382-386.
25. Nørby, J. G. 1988. Coupled assay of Na+,K+-ATPase activity. Method Enzymol 156:116-119.
26. Rypniewski, W. R., H. M. Holden, and I. Rayment. 1993. Structural consequences of reductive methylation of lysine residues in hen egg white lysozyme: an X-ray analysis at 1.8-A resolution. Biochemistry 32:9851-9858.
27. Habeeb, A. F. 1966. Determination of free amino groups in proteins by trinitrobenzenesulfonic acid. Anal Biochem 14:328-336.
28. Silvestre, M. P. C., M. Hamon, and M. Yvon. 1994. Analysis of protein hydrolysates. 1. Use of poly(2-hydroxyethylaspartamide)-silica column in size-exclusion chromatography for the fractionation of casein hydrolysates. J Agric Food Chem 42:2778-2782.
29. Udenfriend, S., S. Stein, P. Bohlen, W. Dairman, W. Leimgruber, and M. Weigele. 1972. Fluorescamine: a reagent for assay of amino acids, peptides, proteins, and primary amines in the picomole range. Science 178:871-872.
30. Gottesman, S., W. P. Clark, and M. R. Maurizi. 1990. The ATP-dependent Clp protease of Escherichia coli. Sequence of ClpA and identification of a Clp-specific substrate. J Biol Chem 265:7886-7893.

31. Dougan, D. A., B. G. Reid, A. L. Horwich, and B. Bukau. 2002. ClpS, a substrate modulator of the ClpAP machine. Mol Cell 9:673-683.
32. Herraiz, T., and V. Casal. 1995. Evaluation of solid-phase extraction procedures in peptide analysis. J Chromatogr A 708:209-221.
33. Xia, D., L. Esser, S. K. Singh, F. S. Guo, and M. R. Maurizi. 2004. Crystallographic investigation of peptide binding sites in the N-domain of the ClpA chaperone. J Struct Biol 146:166-179.
34. Cantor, C. R., and P. R. Schimmel. 1980. Biophysical chemistry. W. H. Freeman, San Francisco, CA.
35. Hänggi, P., P. Talkner, and M. Borkovec. 1990. Reaction-rate theory. 50 years after Kramers. Rev Mod Phys 62:251-341.
36. Colquhoun, D., and A. G. Hawkes. 1995. The principles of the stochastic interpretation of ion-channel mechanisms. In Single-channel recording. B. Sakmann, and E. Neher, editors. Plenum Press, New York, NY. 397-482.
37. Kasianowicz, J. J., E. Brandin, D. Branton, and D. W. Deamer. 1996. Characterization of individual polynucleotide molecules using a membrane channel. Proc Natl Acad Sci U S A 93:13770-13773.
38. Movileanu, L., and H. Bayley. 2001. Partitioning of a polymer into a nanoscopic protein pore obeys a simple scaling law. Proc Natl Acad Sci U S A 98:10137-10141.
39. Bennett, C. H. 1982. The thermodynamics of computation. Int J Theor Phys 21:905-940.
40. Svoboda, K., P. P. Mitra, and S. M. Block. 1994. Fluctuation analysis of motor protein movement and single enzyme kinetics. Proc Natl Acad Sci U S A 91:11782-11786.
41. Carothers, J. M., S. C. Oestreich, J. H. Davis, and J. W. Szostak. 2004. Informational complexity and functional activity of RNA structures. J Am Chem Soc 126:5130-5137.
42. Schneider, T. D. 1994. Sequence logos, machine/channel capacity, Maxwell's demon, and molecular computers: a review of the theory of molecular machines. Nanotechnology 5:1-18.
43. Voet, D., and J. Voet. 2004. Biochemistry. Wiley, Hoboken, NJ.
44. Thompson, M. W., and M. R. Maurizi. 1994. Activity and specificity of Escherichia coli ClpAP protease in cleaving model peptide substrates. J Biol Chem 269:18201-18208.
45. Burton, R. E., S. M. Siddiqui, Y. I. Kim, T. A. Baker, and R. T. Sauer. 2001. Effects of protein stability and structure on substrate processing by the ClpXP unfolding and degradation machine. EMBO J 20:3092-3100.
46. Lee, C., S. Prakash, and A. Matouschek. 2002. Concurrent translocation of multiple polypeptide chains through the proteasomal degradation channel. J Biol Chem 277:34760-34765.
47. Zamore, P. D. 2001. RNA interference: listening to the sound of silence. Nat Struct Biol 8:746-750.
48. Tomkinson, B. 1999. Tripeptidyl peptidases: enzymes that count. Trends Biochem Sci 24:355-359.

49. Zhang, H. D., F. A. Kolb, L. Jaskiewicz, E. Westhof, and W. Filipowicz. 2004. Single processing center models for human dicer and bacterial RNase III. Cell 118:57-68.

ACKNOWLEDGEMENTS

I would like to thank my thesis advisor, Professor Stuart Licht. Stuart is a kind and inspiring advisor as well as a brilliant and enthusiastic scientist. I thank Stuart for accepting me into his laboratory and supporting me consistently throughout my doctoral period at MIT. I could not have imagined having a better advisor for my Ph.D.

I would also like to say a big 'thank-you' to all of the members in the Licht Laboratory, past and present – Amy Weeks, Dina Volfson, Hyunna Song, Jiejin Chen, Laura Jennings, Mary Farbman, Mathew Tantama, Melva James, Monica Guo, Shaunna Stanton, Steve Fredette, Wan-Chen Lin. Thanks to you all!

Finally, my family deserves my sincere gratitude for all their support. I would like to thank my sister, Ki-Eun, her husband, Hee-Sub, and their son, my beloved nephew, Hyun-Bin. Most importantly, I am very grateful to my parents, Ohk-Ran Kim and Dong-Soo Choi for their unconditional love and absolute confidence in me. I LOVE you two so much!

Kee-Hyun Choi

Massachusetts Institute of Technology
Cambridge, Massachusetts
November 2007

KEE-HYUN CHOI

Education

Massachusetts Institute of Technology, Cambridge, MA
Ph.D. in Biological Chemistry, February 2008
Ph.D. research advisor: Professor Stuart Licht
Dissertation: Mechanistic investigation of coordinated conformational changes in multisubunit ion channels and enzymes

Korea University, Seoul, Korea
M.S. in Physical Chemistry, February 2001
M.S. research advisor: Professor Young-Sang Choi
Thesis: Hydrogen-bonding interaction of methyl-substituted pyridines with thioacetamide: steric hindrance of methyl group

Korea University, Seoul, Korea
B.S. in Chemistry, February 1999

Publications

1. **K.-H. Choi** and S. Licht, **Control of peptide product sizes by the energy-dependent protease ClpAP.** *Biochemistry, 44,* 13921-13931 **(2005)**
2. **K.-H. Choi**, H.-J. Lee, A. Karpfen, C.-J. Yoon, J. Park, and Y.-S. Choi, **Hydrogen-bonding interaction of methyl-substituted pyridines with thioacetamide: Steric hindrance of methyl group.** *Chemical Physics Letters, 345,* 338-344 **(2001)**
3. H.-J. Lee, **K.-H. Choi**, I.-A. Ahn, S. Ro, H.G. Jang, Y.-S. Choi, and K.-B. Lee, **The β-turn preferential solution conformation of a tetrapeptide containing an azaamino acid residue.** *Journal of Molecular Structure, 569,* 43-54 **(2001)**
4. N.-K. Kim, H.-J. Lee, **K.-H. Choi**, J.-A. Yu, C.-J. Yoon, J. Park, and Y.-S. Choi, **Substituent effect of N,N-dialkylamides on the intermolecular hydrogen bonding with thioacetamide.** *Journal of Physical Chemistry A, 104,* 5572-5578 **(2000)**
5. H.-J. Lee, I.-A. Ahn, S. Ro, **K.-H. Choi**, Y.-S. Choi, and K.-B. Lee, **Role of azaamino acid residue in β-turn formation and stability in designed peptide.** *Journal of Peptide Research, 56,* 35-46 **(2000)**

Selected Presentations

1. **K.-H. Choi**, M. Tantama, and S. Licht, **Reversible gating of the ATP-sensitive potassium channel.** *The American Chemical Society 234th National Meeting & Exposition,* Boston, MA, August **2007**
2. **K.-H. Choi**, M. Tantama, and S. Licht, **The role of ATPase in ATP-sensitive potassium channel gating.** *Gordon Research Conference on Enzymes, Coenzymes & Metabolic Pathways,* Biddeford, ME, July **2007**
3. **K.-H. Choi** and S. Licht, **Control of stochastic fluctuations in ATP-sensitive potassium channel gating.** *Gordon Research Conference on Membrane Transport Proteins,* Biddeford, ME, August **2006**
4. **K.-H. Choi** and S. Licht, **Mechanism of control of product sizes by the energy-dependent protease ClpAP.** *The Biophysical Society 49th Annual Meeting,* Long Beach, CA, February **2005**
5. **K.-H. Choi** and S. Licht, **ClpAP-catalyzed proteolysis forms peptide products of a defined size: How does ClpAP use energy to make a measurement?** *Gordon Research Conference on Biocatalysis,* Meriden, NH, July **2004**

Awards/Honors

2007	Morse Travel Grant, MIT
2003 – 2004	Lester Wolfe Predoctoral Fellowship, MIT
1998	The First Collegiate Honor, Korea University
1997 – 1998	General Scholarship for Scholastic Achievements, Korea University
1995	Special Scholarship for Academic Excellence as a Freshman, Korea University